Development of a Compact Sound Source for the Active Control of Turbofan Inlet Noise

by

Mary Elizabeth Dungan

Thesis submitted to the Faculty of the
Virginia Polytechnic Institute and State University
in partial fulfillment of the requirements for the degree of

MASTER OF SCIENCE
in
Mechanical Engineering

APPROVED:

W.F. O'Brien, Co-Chairman

C.R. Fuller, Co-Chairman

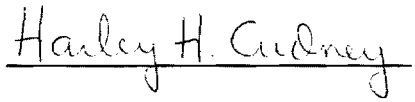

H.H. Cudney

April, 1992

Blacksburg, Virginia

C.2

LD
5655
V855
1992
D865

Development of a Compact Sound Source for the Active Control of Turbofan Inlet Noise

by Mary Elizabeth Dungan

W.F. O'Brien and C. R. Fuller, Co-Chairmen

Abstract

The concept of a compact sound source driven by piezoactuators is experimentally investigated, and analytical design tools are developed. The sound source, consisting of a thin, cylindrically curved aluminum panel and a pair of collocated, surface-bonded piezoceramic actuators, was developed with the objective of employing it as a secondary sound source in the active control of turbofan blade-interaction inlet noise.

The sound source was fitted in an experimental duct representative of an aircraft engine inlet, and the interior and exterior sound pressure levels generated by the source were measured. The effects of excitation voltage, excitation frequency, duct length, and downstream termination of the duct were investigated. It was found that the source is capable of generating relatively high acoustic levels at its fundamental frequency (over 130 dB at maximum voltage input).

Techniques for analytically predicting the acoustic levels are investigated. A commercial code for numerical modelling of structural - acoustic radiation was utilized. Results show generally good agreement with experimental measurements for the case of the short duct. It is believed that the model accuracy can be further improved through additional refinements in the modelling techniques.

Acknowledgements

I would like to thank my committee members, Drs. Walter O'Brien, Chris Fuller, and Harley Cudney, for working with me on this very interesting project. It has certainly been a worthwhile experience.

The support of the Langley Research Center of the National Aeronautics and Space Administation is gratefully acknowledged. Langley sponsored this research and generously provided the use of laboratory resources . Special thanks go to Vern Metcalf of the Structural Acoustics Branch for his insights and assistance throughout this project.

Thanks also to fellow student Allan Kelly for all his help with the finite element software. His assistance in this project was invaluable, and his infinite patience was greatly appreciated.

I also wish to thank Dr. Larry Mitchell for his assistance with the modal analysis and dynamic modelling portions of the project. His insights and advice were timely and much needed.

Thanks to John Harvell and Frank Wilder for all their help in generating this thesis document.

And of course, thanks to Milton for all the support and encouragement throughout this experience, and for taking such good care of Poohcat in my absence.

Table of Contents

Table of Figures

Table of Tables

Nomenclature

B	number of rotor blades
C	nondimensional parameter
I_{ref}	reference intensity
J_m	Bessel function of the first kind of order m
K	nondimensional parameter
M	wall Mach number
M_z	axial mean flow Mach number
M_x	actuator moment about the x axis
M_z	actuator moment about the z axis
P_x	actuator force in the x-direction
P_z	actuator force in the z-direction
$Q_{m\mu}$	eigenvalue for m, μ mode and a particular hub-to-tip ratio
R	acoustic resistance
$R_{i,f}$	voltage ratio of the i^{th} microphone at a frequency of f Hz
S	number of stator blades
V	voltage
Y_m	Bessel function of the second kind of order m
b	actuator width
c	sonic velocity
d	honeycomb backing depth
d_{31}	piezoelectric strain coefficient
f	frequency (cycles/second, Hz)
k	spatial harmonic of the distortion
$k_{m\mu}$	radial wavenumber of (m,μ) mode

k_z axial wavenumber

l_{max} maximum element dimension

m circumferential order

n harmonic of blade passage frequency

p pressure

p_{ref} reference pressure

r duct radius

r_o radius of duct inner wall

s_{if} sensitivity factor for the i^{th} microphone at frequency f

t_a actuator thickness

t_b panel thickness

v number of half-waves in the panel's circumferential direction

w number of half-waves in the panel's axial direction

z specific acoustic impedance

Ω rotor shaft angular velocity (rad/s)

Ω_p interaction pattern angular velocity (rad/s)

δ panel displacement

ε induced strain in the piezoactuator

ϕ angle of wavefront propagation relative to duct axis

ϕ_m phase angle of the m^{th} mode

λ wavelength

λ_z axial wavelength

λ_θ circumferential wavelength

μ radial order

θ angle measured around the circumference

σ hub-to-tip ratio

ω circular frequency (rad/s)

ψ nondimensional ratio of physical properties of substructure and actuator

Subscripts:

p-p peak-to-peak

rms root mean square

Chapter 1 Introduction

1.1 Background

With the advent in the 1960's of the jet engine, noise levels in the vicinity of airports increased dramatically. The unprecedented noise levels associated with these engines provoked strong community reaction and led to federal regulation of aircraft noise levels. Subsequent aircraft engine development has been increasingly characterized by reduction in noise levels. In fact, the high bypass ratio civil aviation engines have restored conditions to the lower levels associated with propeller aircraft. However, in situations requiring a low bypass ratio and a high jet velocity the noise levels remain excessive [1].

Since 1969, federal regulations have set noise limits on new passenger aircraft. FAR Part 36 regulations first put compelling pressure on manufacturers to reduce civil aircraft noise, specifying maximum EPNL (effective perceived noise level) for sideline, takeoff, and approach as a function of gross takeoff weight. The more recent and internationally agreed-upon ICAO/FAA regulations further reduced the noise limits. Satisfying the takeoff and approach requirements has historically presented the greatest challenge. Figure 1 summarizes the requirements for takeoff and approach as a function of gross takeoff weight. Superimposed on Figure 1.1 are measured sound levels by aircraft body type. The improvement in noise levels of the newer wide body jets over the older narrow body type is readily apparent. Essentially it has been changes in the engines, and not the aircraft, that have made possible the improvements to date.

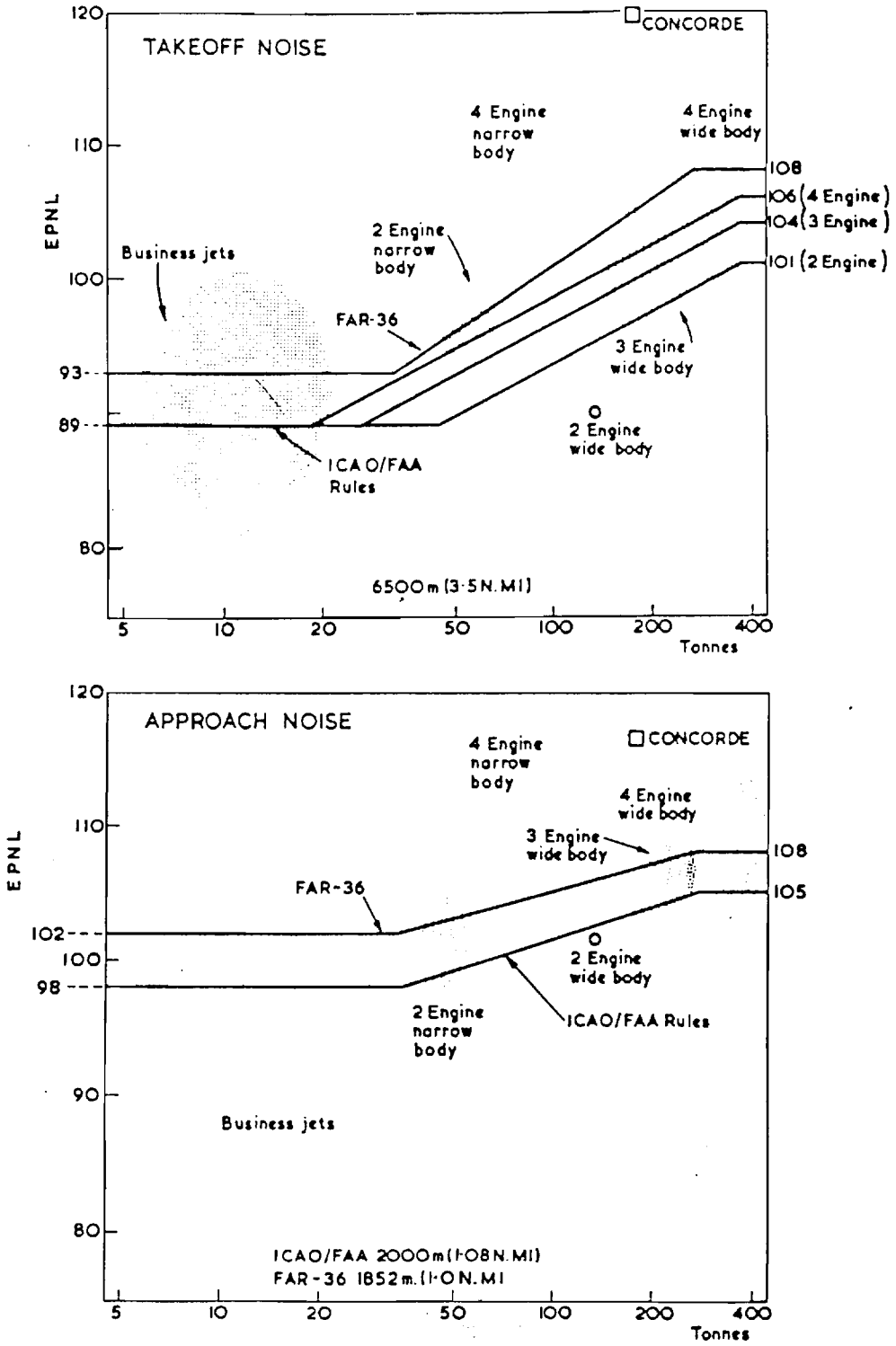

Figure 1.1 -- Takeoff and approach noise levels -- regulations and typical measurements (abscissa shows gross takeoff weight). Reprinted from [1].

Much of this improvement in noise is associated with the development of the high bypass ratio turbofan engine. As a means of increasing propulsive efficiency, a larger mass flow rate is combined with a lower jet velocity in the design of these engines. Since exhaust noise is proportional to the eighth power of jet velocity, reduction in exhaust noise is an inherent feature of these engines. However, this reduction in exhaust noise, which is broad band in nature, tends to unmask the fan and compressor noise by lowering the background level against which it is heard. The discrete-frequency inlet noise is actually more irritating than the broad band exhaust noise. Thus, although the reduction in exhaust noise is beneficial for take-off, it provokes a stronger community reaction as the aircraft approaches [2].

The development of the high-bypass engine in the late 1960's together with the international recognition of the need to limit noise led to a surge of interest in noise research. Comprehensive reviews of the literature are given by Mugridge and Morfey [3] and by Cumpsty [4], among others. This body of research has resulted in such standard design practices as the selection of rotor and stator blade numbers and the specification of axial spacing as a means of reducing the noise generated. Research has also led to improvements in blade design, increasing the aerodynamic performance and thus decreasing the noise generated. However, despite the progress that has been made, many noise sources are still not well understood. For instance, the basic mechanisms of broad band noise from the fan, compressor, and engine core have yet to be identified conclusively [1]. Moreover, most of the research has focused on the high bypass ratio civil transport. Many of the improvements in noise generation associated with these engines cannot offer solutions to the problems posed by high-speed aircraft, where jet velocities are necessarily high. Neither can they be applied to the older propeller-driven aircraft, which are finding increasing commercial aviation use. Although acoustic

treatment in the form of engine liners and cabin wall treatment does offer some reduction in noise, it is at the expense of added weight and reduced fuel efficiency.

Rising fuel costs have created interest in more fuel-efficient aircraft engines. Two such engines currently in development are the advanced turbo-prop (ATP) and the ultra-high-bypass (UHB) engines. Although attractive from the standpoint of fuel efficiency, a major drawback of these engines is the high noise levels associated with them. In order for these engines to be accepted by a public that has become accustomed to the relative quiet of modern turbofan engines, it will be necessary to reduce the noise generated by these engines to acceptable levels. If passive means of acoustic treatment, e.g., liners, are used as the sole means of noise reduction, the associated weight penalty can be expected to offset the increase in fuel efficiency. Thus, while research continues in such areas as improving acoustic liners in engines and cabins, attention is also being turned to alternative means of noise reduction.

Active control is an area that shows potential for reducing noise radiation from aircraft engines and cabin interior noise levels. The basic mechanism of active control is the generation of an antiphase noise field of equal amplitude and spectral content to cancel the primary sound field. The technique has been successfully utilized in the automotive industry [5]. Recent work has shown active control to be a viable method of reducing noise levels in aircraft cabins by employing distributed vibration sources attached to a fuselage model to generate the control field [6]. Similarly, experiment has shown that loudspeakers mounted around the circumference of an aircraft engine inlet to generate a control field are effective in reducing the primary noise field created by the fan [7, 8]. However, the loudspeakers used to generate the control field in these experiments were large, bulky, and thus unsuitable for aeronautical application. Nonetheless, these experiments were successful in demonstrating that such an active

control scheme is a promising method of reducing engine noise radiating from the inlet duct and could find immediate application in quieting existing engines. Perhaps more importantly, the technique also represents a possible means of quieting the next-generation ATP and UHB engines without incurring the weight penalty associated with passive means of acoustic treatment. In order to make active control of fan noise a viable technology, however, it is necessary to replace the loudspeakers used in previous work with an acoustic source suitable for aeronautical application. Such a source must be powerful enough to effectively reduce the primary noise field, yet impose no prohibitive penalty in terms of size, weight, or aerodynamic loss. Thus, a compact, lightweight sound source is needed for this application, and such a sound source is not currently believed to exist. It is necessary to not only develop such a source, but also to develop or identify the analytical tools needed to support detailed design work.

1.2 Purpose and Scope

In order to make active control of turbofan inlet noise a viable technology, it is necessary to develop a suitable sound source to generate the control field. One proposal for designing a compact sound source suitable for active control of aircraft engine inlet noise is to create an array of thin, curved panels, flush mounted inside the inlet housing and driven by one of more force transducers attached to the panel. The purpose of this work is threefold: 1) to experimentally investigate the potential of this concept, 2) to measure the performance of an actual source, and 3) to develop or identify the analytical tools needed to design such a sound source. The scope of this work includes the design and analysis of a compact sound source using the finite element method, the experimental investigation of its characteristics and capabilities, and the development of analytical tools to support further development work. This research is a logical extension

of previous work using loudspeakers to generate the control field [7, 8]. Although the application here is inlet noise, specifically the tone interaction noise associated with the fan, the technique of active control is also a potential mechanism for reducing other discrete-frequency components in the inlet, bypass, and exhaust ducts.

Chapter 2 Literature Review

There exists a large body of literature on the subject of aircraft engine noise, reflecting the extensive research activity in this area. Several comprehensive reviews of the literature have been published, covering a wide range of topics. However, this literature review will focus only on those areas pertaining to this thesis work.

This section is organized as follows. First, because several components of an aircraft engine can be treated as a cylindrical duct, a brief summary of duct acoustics will be presented. This will lay the necessary foundation for discussion of several noise control techniques. Next, an overview of noise sources in turbomachinery will be presented, followed by a review of noise control techniques in existing arcraft engines. A discussion of the noise problems associated with future-generation aircraft engines will follow, leading naturally to a review of current research areas in aircraft noise. Next, the concept and application of active control will be discussed. Finally, because piezoelectric actuators are utilized in this study, a review of the analytical models for predicting piezoelectric actuator-induced structural loads will be presented.

2.1 Duct Acoustics

To study turbomachinery noise, it is necessary to understand the processes by which sound waves propagate through the machine. The presence of the duct has a strong effect on the acoustics of the machine. In general, there is a circumferential and a radial variation in pressure amplitude and phase, and the wave fronts spiral along the duct. The relationship between pressure, power, and intensity for such a wave is not

simple and is further complicated by the addition of acoustic liners, for which the normal velocity perturbations at the wall do not vanish.

Upstream of the fan the duct is generally a circular cylinder, while downstream it is usually annular. The circular nature of the problem dictates the form of the equation describing the pressure wave propagation. When the hub-to-tip ratio becomes high enough the circular annulus may be unwrapped into an equivalent rectangular duct. The first comprehensive description of the nature of the pressure field in both rectangular and circular ducts was given by Tyler and Sofrin in 1962 [2]. They introduced the notion of modal analysis into the study of turbomachinery acoustics. Another account was given by Morfey in 1964 [9]. These results are briefly summarized here and are reviewed in greater detail in Appendix A. Tyler and Sofrin tabulated the radial patterns as a function of hub-to-tip ratio. Figure 2.1 displays some of their results for a hub-to-tip ratio of 0.5 and various values of circumferential and radial order.

For a circular duct with no mean flow, the axial wavenumber is given by

$$k_z = \sqrt{\frac{\omega^2}{c^2} - k_{m\mu}^2} \tag{1}$$

where m denotes the circumferential order (m cycles or lobes around the circumference), and μ denotes the radial order (μ nodes or zero crossings in the radial direction). The eigenvalue, $k_{m\mu}$, denotes the radial wavenumber for the (m,μ) mode. When $\frac{\omega}{c} < k_{m\mu}$, the wave decays exponentially in the axial direction. When $\frac{\omega}{c} = k_{m\mu}$, k_Z is zero; this is known as the cutoff condition. When $\frac{\omega}{c} > k_{m\mu}$, the wave propagates unattenuated.

Equation (1) can be given more physical significance for turbomachinery by rewriting it as

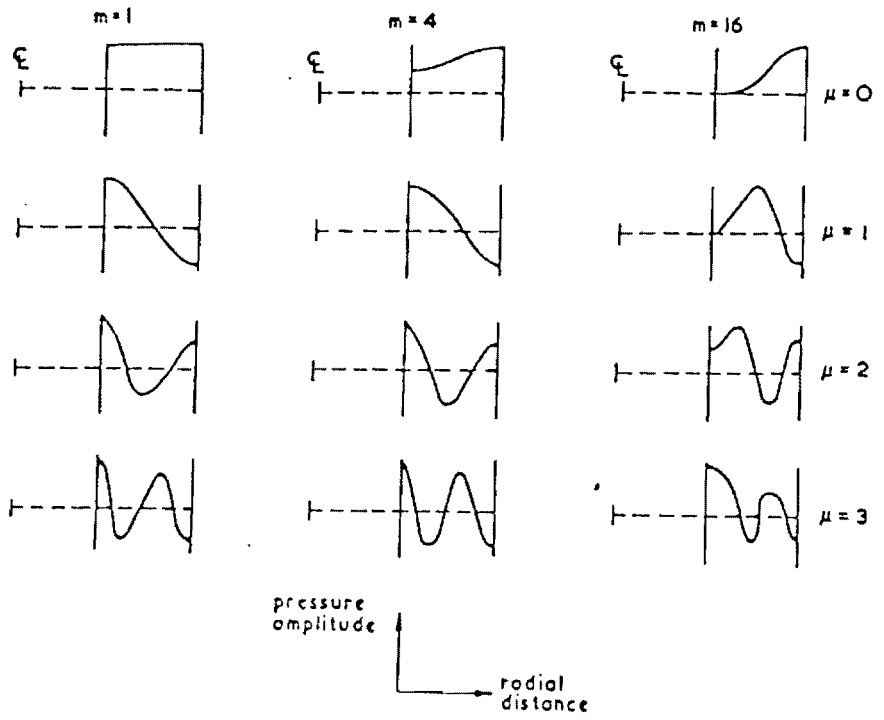

Figure 2.1 -- Radial variation in pressure amplitude in a cylindrical duct with 0.5 hub-to-tip ratio. Reprinted from [1].

$$k_z = \sqrt{\frac{M^2 m^2}{r_o^2} - k_{m\mu}^2} \tag{2}$$

Here,

$$M = \frac{\Omega r_0}{c}\ , \tag{3}$$

and $\omega = m\Omega$, (4)

where M=wall Mach number,

Ω = pattern speed in rad/s, and

r_0=wall outer radius.

The cutoff condition can then be written as $M = \frac{r_o k_{m\mu}}{m}$. The cutoff Mach number is slightly greater than one for large values of m and much greater than one for small values of m. Thus, when the rotating pressure pattern Mach number is subsonic, the wave decays exponentially and is cut off.

The axial wavelength λ_Z and the circumferential wavelength λ_θ can be written as

$$\lambda_z = \frac{2\pi}{k_z} \tag{5}$$

and $$\lambda_\theta = \frac{2\pi r}{m}\ . \tag{6}$$

The angle of wavefront propagation, ϕ, relative to the duct axis is

$$\Phi = \tan^{-1}\frac{\lambda_z}{\lambda_\theta} \tag{7}$$

or $$\Phi = \tan^{-1}\frac{m}{k_z r}\ . \tag{8}$$

Thus, at cutoff, k_z=0 and the wave fronts are axial and move in a circumferential direction. For k_z real and nonzero, the wave fronts (surfaces of constant phase) spiral along the duct.

In aircraft engines, the flow Mach numbers are generally not negligible. Sofrin and McCann [10] extended their analysis to include the effect of uniform axial flow. The circumferential and radial form of the solution is unchanged and the axial wavenumber becomes

$$k_z = \frac{1}{1-M_z^2}\left(M_z \frac{\omega}{c} \pm \sqrt{\left(\frac{\omega}{c}\right)^2 - (1-M_z^2)k_{m\mu}^2} \right) \tag{9}$$

where M_Z is the axial mean flow Mach number and z is taken positive in the direction of M_Z. The + and - signs denote the downstream and upstream directions of propagation, respectively. At cutoff, the argument inside the square root becomes zero, and the axial wavenumber is not zero as in the case of no flow but becomes

$$k_z = \left(\frac{M_z}{1-M_z^2}\right)\left(\frac{\omega}{c}\right) \tag{10}$$

At cutoff, the wave fronts are convected downstream and are not aligned with the duct axis.

These results have assumed constant-diameter circular or annular ducts. In most cases, the duct diameter or shape varies. Propagation in ducts of varying shape has been reviewed by Nayfeh, et al [11]. In many cases, however, the principal characteristics of a duct can be determined without considering the effect of varying shape (geometry) because the attenuation following cutoff is generally so rapid that the pressure amplitudes become negligible before the variation in shape becomes significant.

In addition to the modal structure inside the duct, the radiated field outside the duct is also of interest because the sound field inside the duct becomes a nuisance only

when it is radiated to the free field. The inlet and exhaust pipes are terminated with an open end, leading to little reflection of propagating modes provided the smallest opening dimension exceeds one quarter wavelength [12]. One approach to determining this radiation field is that adopted originally by Tyler and Sofrin [2]. Here, the mean flow is neglected and the duct exit is surrounded by a large baffle. Another approach, undertaken by Lansing [13], is to model the duct as an unflanged pipe. This method has shown very close agreement with the flanged method at high frequencies. Still another approach is that of Lowson [14] who modeled components such as fans as unducted. The effects of flow and soft duct walls were considered by Candel [15], who found that the resulting radiation patterns obtained are affected very little at frequencies significantly above cutoff.

In these analyses, refraction effects at the inlet due to velocity gradients, and at the exit due to velocity and temperature gradients in the exhaust, have been ignored.

2.2 Noise Sources in Turbomachinery

The field of axial turbomachinery noise has been the subject of several thorough reviews. Two notable references are Morfey [12] and Cumpsty [4]. Cumpsty points out some of the difficulties associated with turbomachinery noise research. For instance, the experimental study of high-speed turbomachinery noise is complicated by the following factors: 1) velocities of rotating components are typically close to sonic, complicating the description of the acoustic processes; 2) acoustic wavelengths are typically of the same order as blade chord; 3) sound is refracted by the high Mach number flows; 4) inserting a probe into the flow can generate sound through interaction with adjacent moving blades. Insight into noise sources has gradually accrued through altering various parameters and noting the results.

Theoretical study of turbomachinery noise also presents problems because of the same factors -- Mach numbers close to unity complicate the analytical characterization of the acoustic processes, as do wavelengths comparable to blade chord. Another approach, known as aeroacoustics, generally requires a range of information that is typically unavailable, and quantitative results may be obtained only by adopting sweeping assumptions [1].

Despite these difficulties, one mitigating factor is that the amplitudes of the pressure fluctuations of interest are very small, and a linear analytic treatment is usually justified. Thus, the field of turbomachinery noise has generated considerable interest among researchers.

The study of turbomachinery noise can be divided into three major areas: 1) fan and compressor noise, 2) turbine noise, and 3) core noise. The relative magnitudes and directivity patterns of the various noise sources are shown in Figure 2.2 for both low-bypass and high-bypass engines. Each of these noise sources will be briefly discussed, with more attention devoted to fan and compressor noise as it is the subject of this thesis.

1) Fan and Compressor Noise. The subject of fan and compressor noise can be divided into three areas: 1) interaction tone noise, 2) multiple pure tone noise, and 3) broad band noise. Of these, interaction tone noise has been the most widely studied type of compressor noise. Interaction tone noise is the term given to the noise produced by rotating blades interacting with stationary nonuniformities, such as the wakes of stators. Tyler and Sofrin showed that this interaction produces an interference pattern for which the circumferential Mach number of a point on the wave exceeds the cutoff value. This is the mechanism by which rotors with subsonic tip speeds produce pressure fields rotating with a Mach number greater than one. Tyler and Sofrin showed that the interaction pattern set up by B rotor blades and S stator vanes can be described as

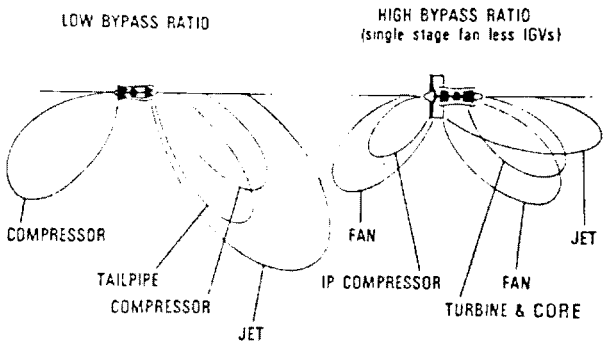

Figure 2.2 -- Comparative noise sources for low- and high-bypass engines. Reprinted from [1].

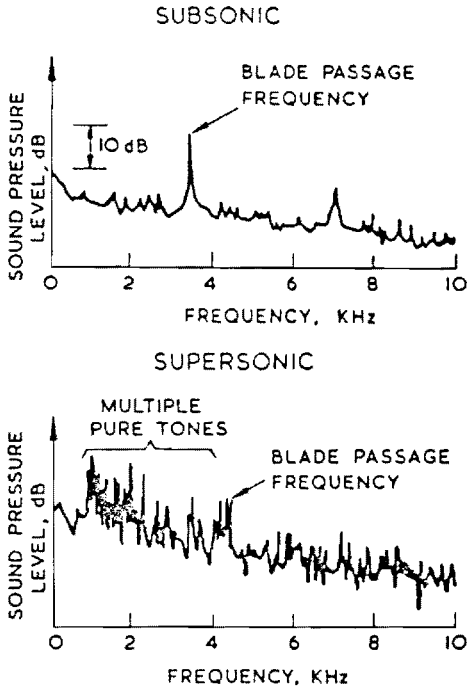

Figure 2.3 -- Typical forward arc spectra. Reprinted from [1].

$$m = nB \pm KS \quad (11),$$

where m = circumferential order of the pattern,

n = harmonic of blade passing frequency,

K = spatial harmonic of the distortion.

The angular velocity of the interaction pattern, Ω_p, is then given by

$$\Omega_p = \Omega \frac{nB}{nB \pm KS} \quad (12)$$

where Ω = rotor shaft angular velocity.

Typical spectra of the noise radiating from the inlet show that the lower frequencies dominate [16]. The noise at these frequencies corresponds to harmonics of blade passage frequency, $B\Omega/60$ x an integer. Typical forward arc spectra are shown in Figure 2.3. In addition to rotor-stator interaction, interaction tone noise is generated by interaction between the rotor and unsteady, turbulent distortions in the inlet flow. This effect is described in more detail in [1] and [3].

Multiple pure tone noise, also termed "buzz-saw noise", is a phenomenon associated with supersonic tip speeds in which the shock waves ahead of the rotor create sound waves. Multiple pure tone noise is well understood because it is inherently simpler than other types of turbomachinery noise. Crucial work in this area was done by Sofrin and Pickett [17], who demonstrated the processes of decay and evolution of the sound waves ahead of several rotors. They showed the rates of decay to be predictable by one-dimensional shock theory. Work in this area was also done by Morfey and Fisher [18], who showed that there is a worst case Mach number for which decay is minimized. Work has been done in the area of altering the blade profile in order to reduce the multiple pure tone noise [1]. However, acoustic treatment of the inlet has proven successful in attenuating multiple pure tone noise and so interest in eliminating it at the source through blade design has diminished.

In contrast to multiple pure tone noise, broad band noise is not well understood, due in part to the difficulty of determining the source of the noise experimentally. The progress that has been made in understanding broad band noise has come from making such changes as altering the pressure ratio and observing the effect on the noise. Sources of broad band noise in fans and compressors include interaction between incident turbulence and the blade rows, random unsteadiness in the blade rows, and separated flow. Another source, proposed by Smith and House [19], is the interaction between the turbulence in the wakes of one blade row and the downstream blade row. Work has been done to characterize such effects as throttling, blade loading, and stall on broad band noise generation. While general observations have been noted, such as the increase in broad band noise as the machine is throttled, the underlying processes of noise generation are not well understood. The cause of broad band noise can vary with design, type of machine, and mode of operation. Cumpsty [4] presents a thorough review of broad band noise research and concludes that "the overall position with broad band noise from compressors and fans can only be summarized as highly confused".

Turbine Noise. Compared to the research activity in the area of fan and compressor noise, relatively little work has been done in the area of turbine noise. One reason is that, for low bypass engines, the jet noise has been the main problem in rear-arc noise. For high-bypass engines, turbine noise is typically small compared to fan or compressor noise. In addition, turbine blading does not lend itself to theoretical treatment, whereas the small camber of compressor blades allows them to be modeled as flat plates. Also, turbines create considerable problems in the experimental measurement of noise, as the far-field signal is contaminated by turbulent flow downstream of the turbine, making the characterization of broad band noise difficult and distorting the tone spectrum.

It is known, however, that some of the mechanisms underlying compressor noise apply to turbines as well, including the interaction between rotor and stator blades. As in the case of compressors, it is possible to choose blade numbers for turbines in such a manner as to utilize cutoff.

Because of the difficulties involved in both experimental and analytical work on turbine noise, relatively few accounts exist in the literature. Cumpsty [4] provides one review.

Core noise originates with the hot stream of the engine, excluding the noise from the turbine and the jet, although this definition is somewhat arbitrary. Because both core noise and jet noise are broad band, it is difficult to separate them in practice. Research has been done to study the effects of engine speed, strut incidence, nozzle lip, and the combustion system on engine noise. Bushell [20] has reviewed the subject.

The noise generated by aircraft engine components propagates through ducts and is affected by geometry changes. However, these changes are generally gradual, smooth, and relatively small in order to keep the mean flow attached. Moreover, the duct boundary layers are generally thin, and regions of separated flow are negligible, further simplifying the study of sound propagation. Other factors affecting sound propagation in turbomachinery ducts are flow direction, flow Mach number, temperature gradients, and swirl. The ducts are often short, especially the intake, and the radiation pattern is important. Modes radiating to the side are much more troublesome than those radiating straight ahead.

2.3 Noise Control in Aircraft Engines

Some of the earliest work in aircraft engine noise control dealt with noise from multistage compressors in low (or zero) bypass ratio engines. These compressors almost

always used inlet guide vanes and noise was not considered in the design. In the development of the high-bypass engine, noise was considered from design inception. Inlet guide vanes were done away with, but a new source of noise was introduced by supersonic fan blade tips. Sound generation in a high-bypass engine differs from that in a low-bypass engine due to the absence of inlet guide vanes and a lower hub-tip ratio, but also because larger spacing between the rotating and outward guide vanes is included to reduce interaction. In addition, high-bypass engines are designed for much lower jet velocity than low-bypass engines. Therefore, the jet or exhaust noise, which is proportional to the eighth power of jet velocity, is greatly reduced in a high-bypass turbofan. Turbofans are typically 10 - 15 dB quieter than earlier jet engines due to the lower jet velocity. However, this reduction of the broad band exhaust noise tends to unmask the more tonal fan noise, resulting in a noise pattern that is much quieter overall but may be more objectionable in the forward arc [2].

Thus, the large reductions in engine noise associated with the high-bypass engine are an inherent benefit of lower exhaust velocity, but can also be attributed in part to such design practices as larger axial spacing to reduce interaction, selection of blade numbers to utilize cutoff, and improvements in aerodynamic design. These practices are now standard in aircraft engine design.

Where possible engine designers incorporate the available knowledge of noise generation and propagation from design inception to eliminate the sound at its source. For instance, Kaji and Okazaki's [21] conclusion that modes rotating in the same direction as the rotor are much more likely to propagate through the rotor than modes rotating in the opposite direction has direct application in engine design. However, where it is not possible to eliminate or reduce the noise at the source, acoustic liners are widely used to attenuate the sound levels.

Acoustic liners are typically one of two types: 1) honeycomb, and 2) bulk absorber. Figure 2.4 shows a schematic of a honeycomb type acoustic liner and where the lining can be used in a bypass engine. Acoustic liners have a finite impedance defined by

$$z = \frac{p}{u} \tag{13}$$

where pressure, p, and velocity, u, are normal to the surface. For a rigid wall, the normal velocity is zero, and $z \to \infty$. For a perforate honeycomb liner with a thin perforate sheet,

$$z = R + i\left(\frac{\omega m}{c} - \cot\frac{\omega d}{c}\right) \tag{14}$$

where resistance R = ratio of in-phase pressure and velocity,

d = honeycomb backing depth

and c = sonic velocity.

The liner resistance R is determined primarily by the porosity of the facing material. When the wall impedance is finite (i.e., the wall is not rigid) the eigenvalues $k_{m\mu}$ and $Q_{m\mu}$ are dependent on the values of resistance and reactance. Once the eigenvalues are known, axial attenuation by the liner can be determined. Cumpsty [1] notes that in evaluating the effect of liners, certain assumptions about the input sound field must be made. One of the principal limitations to the accurate prediction of attenuation is specifying the strengths of all the modes generated by the engine.

The use of liners has proven effective in reducing engine noise. With lining extending over an axial length of one radius, it is possible to reduce the multiple pure tones until they essentially vanish, reducing the overall intake noise of a high-bypass ratio engine by about 5 PNdB. Lining the bypass duct may result in an 8 PNdB reduction in rear arc peak noise, while lining the exhaust pipe provides about 3 PNdB

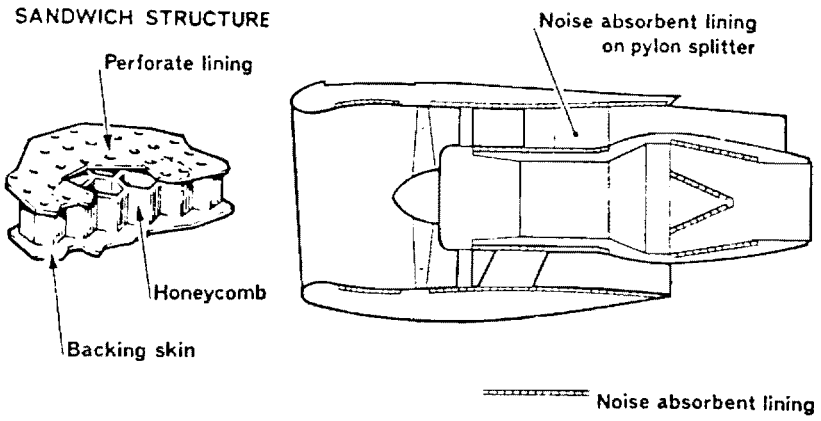

(a)

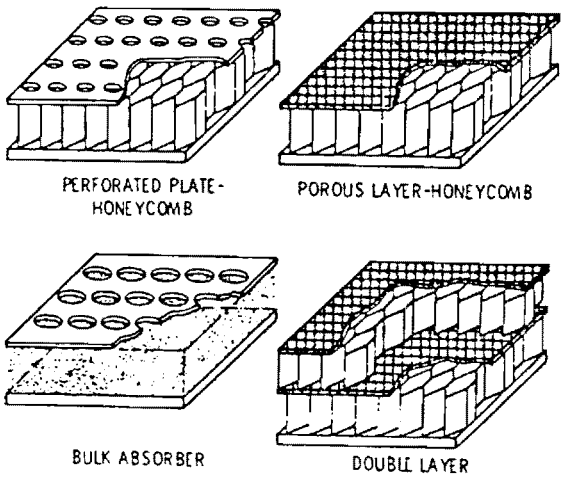

(b)

Figure 2.4 -- a) Schematic of installation of linings in a high-bypass-ratio engine; b) Types of acoustic liners. Reprinted from [1].

reduction. (Noise rating scales are described in Appendix B.) Acoustic liners are reviewed in more detail in Nayfeh, et al [11].

Reduction in engine noise has directly translated into quieter airliner cabins. Interior noise levels in early jet aircraft could be very high. Development of the high-bypass engine resulted in quieter cabins and led manufacturers to quiet many of the older engines. However, interior noise levels of propeller-driven passenger aircraft remain very high in some cases. Acoustic treatment of cabin walls is commonly used, but low-frequency noise can remain a problem. The topic of cabin noise is reviewed by several sources [16]. In addition to acoustic treatment of cabin interiors, noise reduction techniques include propeller modification to improve airfoil performance, placement of baggage compartments and service areas near the plane of propeller rotation, and synchrophasing, or the automatic control of the phase relationship of propellers rotating at different angular velocities.

2.4 Next-Generation Aircraft Engines

The role of the turbofan engine in reducing aircraft engine noise is well known. Although propeller-driven aircraft are more fuel efficient up to about Mach 0.6, the speed and comfort of turbofans outweighed the disadvantage of the turbofan's lower fuel efficiency, and development of propeller technology ceased in the mid-1950's. However, when the Middle East oil embargo of 1973 drove fuel costs from about one quarter of airline direct operating costs to about one half, fuel efficiency became a major concern. Interest in propeller-driven aircraft was renewed, and in 1978, NASA launched its Advanced Turboprop Program (ATP).

The ATP, of propfan, can improve upon the fuel consumption of the older narrow-body passenger airline turbofans by up to 50%. It can save up to 30% compared with the latest advanced turbofans used on such aircraft as the Boeing 757.

The propfan has eight or more thin, highly swept blades, compared to conventional turboprops with up to four straight, large-diameter blades. The propfan's blading minimizes both compressibility losses and propeller noise during high-speed cruise.

Early research verified the propfan's potential but identified several technical concerns, including propeller and aircraft interior noise. One objective of the ATP program is reduction of cabin noise and vibration to the point where passenger comfort levels are comparable to those of turbofan-powered aircraft. Another is verification that the propfan meets FAR Part 36 regulations. Testing has shown that in order for these requirements to be met, high fore and aft harmonics must be dealt with, and cabin acoustic treatment must improve upon bare walls by 25-30 dB for wing mounted engines.

Ducted propellers known as ultra-high bypass engines (UHB) are also in development. With bypass ratios of forty to eighty (compared to four to six for high-bypass engines), these engines are advantageous on long-range high-speed aircraft with wing-mounted engines. However, technical concerns including far-field community noise at takeoff and approach must be resolved. Like the ATP, this engine's fan is very large in diameter, leading to high blade tip velocities and acoustic pressures. Because this engine is ducted, it is a potential candidate for application of the active noise control system considered in this thesis work.

Propfans and ducted propellers show great potential for improving fuel efficiency and increasing cruise Mach number. However, further progress in noise control is

needed, both to reduce community and airport noise, and to decrease the weight due to acoustic treatment. The subject is reviewed in greater detail by several sources [22-24].

2.5 Current Research in Aircraft Noise

Most of the aircraft engine noise research to date has focused on civil air transport and the high bypass engine. Of the various factors that contribute to the reduction in noise associated with these engines, low jet velocity has had the greatest effect on noise reduction. Unfortunately, low jet velocity does not offer a solution to the noise problems of high-speed aircraft, where bypass ratios are necessarily low and jet velocities high. Neither can many of the high-bypass solutions be applied to existing turbojets and turboprops still in use. Furthermore, the next-generation ATP and UHB engines present noise problems that are as yet unresolved. Because of the large propellers (9-12 feet in diameter) of these engines, tone interaction fan noise is one area that must be addressed for these engines to gain acceptance.

Current research toward quieting existing engines has focused mostly on improving acoustic liners [1]. In the past, very good results have been obtained using very simple, single-layer perforate-honeycomb liners. Research in this area includes double-layer lining and bulk absorber types of liners.

Other current areas of research include blade sweep, counter rotation, and fuselage wall modification to increase cabin sound absorption. Blade sweep and counter rotation in particular are research areas generally associated with the prop-fan engines, but appear to offer potential for more conventional engines as well. Metzger [16] presents a thorough review of propeller aircraft noise control strategies.

A relatively recent area of noise control research is active control. In a typical active control scheme, a control sound source generates a sound field that interacts with

the primary sound field in such a manner as to cancel it. The control sound field is of equal amplitude and frequency content as the primary field, but has a 180° phase shift so that the pressure waves from the two sources cancel when superimposed. The technique has been the subject of much research in vibration control and structural acoustics, and has proven to be a viable concept in automotive muffler design [5] and in the control of aircraft cabin noise [6]. The field of active control is reviewed in detail in Section 2.6.

As Metzger noted [16], the best solution to the problem of aircraft engine noise is that which provides the largest reduction in noise with the least possible weight penalty. Towards this end, active control may prove to offer significant reductions in engine noise, provided a lightweight, compact control source can be developed which offers sufficient acoustic output. The subject of this thesis, then, is the application of active control to inlet noise, specifically the interaction tone noise associated with the fan and compressor on engines with ducted inlets. This application could potentially be used to quiet not only the next-generation engines, but also to improve upon the existing turbofan and turbojet engines.

2.6 Active Control

The concept of active control was first described almost sixty years ago, when, in 1934, the German physicist Paul Lueg received a patent for his "Process of Silencing Sound Oscillations" [25]. The underlying principle of active control is straightforward: because sound waves propagate linearly, the net effect of two or more sound waves is the superposition of each wave acting individually. Thus, if a secondary sound source generates a sound wave that is identical and coherent to some primary sound wave, but with a 180° phase shift, the result will be silence. The implementation of an active control scheme thus involves the introduction of one or more secondary, or control,

sources that will destructively interfere with some primary source, thereby reducing or (ideally) eliminating the overall sound field.

At the time of Lueg's work, the state of the art in electronic technology was insufficient to support experimental work. Thus, further development of active control was not undertaken until the 1950's, when Olson and May published their work describing an "electronic sound absorber" [26]. Olson first identified automobile and aircraft noise as possible applications of active control technology in 1956 [27]. Notable contributions during this time period were also made by Conover, who applied the concept of active control to sound radiation from large transformers [28]. However, he realized only limited success, and interest in active control waned. Advances in computer technology in the 1960's and 1970's prompted a renewed interest in active control, with work focusing mainly on transformer noise and duct noise. Relatively recent advances in digital signal processing technology have spurred further development in the area of active control, and the past decade has seen much research activity in the area.

An active control system is composed of three basic components: 1) a control system, typically a digital signal processing system, which determines the control signal needed to interact with the primary sound source; 2) error sensors to provide electrical feedback to the control system, and 3) one or more control sources, which generate the secondary sound field needed to destructively interfere with the primary sound field [29]. In general, in order for a system of secondary sources to destructively interfere with some primary sound field over a significant volume of space, two requirements must be met: 1) the waveform of the secondary source must be the mirror image of the primary source, and 2) the sound field generated by the secondary source must match that of the primary source. Thus, both temporal and spatial constraints are imposed on the

secondary sound source. In order to meet this second requirement of spatial matching, multiple secondary sources are generally required [25].

Active control of duct noise has received a considerable amount of attention in recent years. While many accounts describe the active control mechanisim as cancellation of the primary field by a secondary field, other descriptions do exist. One such suggestion is that the cancellation is more accurately described as a reflection of the primary source wave at the secondary source [30, 31]. More recently, it has been suggested that the secondary source changes the radiation impedance "seen" by the primary source, unloading and thus reducing the overall sound power output [32]. Many of the analytical models published represent the primary source as radiation from the plane of the duct wall. A more typical configuration in turbomachinery applications would locate the primary source in the plane of the duct cross section. Such a model was presented by Snyder and Hansen for the case of a semi-infinite rectangular duct [33].

Quite recently, experimental work has demonstrated the applicability of active control technology to aircraft engine duct noise. In these experiments, a research rig built around a Pratt and Whitney JT15D turbofan engine was fitted with an array of horn drivers located around the inlet circumference a short distance upstream of the fan. This array of loudspeakers served as the secondary source while the primary source was the fundamental blade passage tone of the fan, generated in this case by the fan's interaction with stationary upstream rods. Under near-idle operating conditions, a significant decrease in the overall sound field was realized when control was actuated. This experiment is believed to be the first of its kind in that it has demonstrated the effectiveness of active control in an operational aircraft engine [7,8].

This thesis work is a natural extension of the JT15D experimental work. In order to make active control of aircraft engine inlet noise a practical application, it is necessary

to develop a compact, lightweight sound source which can replace the large, bulky horn drivers used in the JT15D research. Such a compact sound source must generate enough acoustic output to effectively reduce the primary sound field, while imposing no prohibitive penalty in terms of weight and aerodynamic losses.

2.7 Piezoelectric Actuators

The piezoelectric effect has been known for over a century. Since its discovery in 1880, the effect has been discovered in numerous materials, including such crystals as quartz, boracite, and Rochelle salt. Other piezoelectric materials include polyvinyldene fluoride (PVDF), a polymer, and lithium niobate ($LiNbO_3$), a crystal. A piezoceramic material of lead zirconate titanate composition, known as PZT, was used in this thesis work.

The piezoelectric effect can be described as the generation of a voltage in response to an applied strain in the piezoelectric material. The converse effect also occurs: applying a voltage across a piezoelectric material will generate strain in the material. (The relationship between voltage and strain is known and is discussed further in a later section.) Due to the dual nature of the piezoelectric effect, transducers made of piezoelectric material can act as both actuators and sensors. Piezoelectric materials are commonly used in sonar transducers, audio speakers, microphones, and accelerometers [34].

Recently, piezoelectric materials have begun to be extensively used in a variety of research applications to excite structures, measure structural motion, and control the motion of a structure. Piezoelectric transducers are finding increasing usage in these applications because they offer several advantages over the commonly-used point shaker. They are compact and lightweight by nature, they can be imbedded in a structure, and

they do not require additional structural support, as does a shaker. In addition, they provide a distributed, rather than a point, type of actuation and sensing, which can be very beneficial in terms of control of structural vibration modes. All of these characteristics make piezoelectric materials a suitable choice for the development of a compact sound source. In particular, utilizing a piezoceramic material, such as PZT, as the actuator for a sound source provides the capability to excite a large response in the sound source substructure with negligible weight penalty.

For these reasons, piezoelectric patches are utilized in this study as the actuators which drive the sound source. The sound source consists of a thin aluminum panel, curved to fit flush with the inlet duct wall, with two surface-bonded piezoelectric patches. In order to model the effect of the actuators on the panel, it is necessary to determine the induced loads on the panel for a given voltage input.

Analytical models of piezoelectric actuators are available in the literature, including models derived from beam theory and plate theory. These include the one-dimensional models of Crawley and de Luis [35] and Lazarus and Crawley [36], and the two-dimensional models of Wang and Rogers [37] and Dimitriadis, Fuller, and Rogers [38]. In the one-dimensional case, Crawley and de Luis [35] showed that a collocated pair of piezoelectric patches perfectly bonded results in two equivalent concentrated moments acting at the edges of the actuator patch. In the two-dimensional case, Dimitriadis, et al [38] showed that the resultant moments induced by the collocated piezoceramic patches are applied along the four edges of the patches and result in spherical pure bending. The three models considered in this study are detailed in Appendix C.

Relatively recently, attention has begun to focus on optimizing the actuator-substructure coupling in order to maximize the performance of piezoceramics as

actuators. In one study, Kim and Jones [39] studied the effect of actuator thickness on the actuator-substructure coupling and found that, for the piezoelectric materials considered (PZT and PVDF), an optimal actuator thickness exists. Another recent study focused on the effects of adhesive layer stiffness and thickness on actuator-substructure coupling in a two-dimensional beam model [34]. In this study, it was found that 1) modal amplitudes decrease with increasing adhesive stiffness, and 2) modal amplitude either increased or decreased with adhesive layer thickness, depending on the stiffness of the adhesive. As piezoelectric actuators and sensors find increasing experimental and industrial application, interest in performance optimization will undoubtedly continue.

Chapter 3 Design of the Acoustic Source

3.1 Description of the Source

The control field sound source consists of an array of identical thin, cylindrically curved panels with an inner radius of curvature corresponding to that of the engine inlet. These panels are flush mounted inside the inlet duct and sealed on all edges to prevent leakage around the panel and to minimize the aerodynamic losses created by the addition of the panels. Each panel is driven by one or more piezoelectric force transducers mounted on the surface of the panel. When the panel is driven in its fundamental, or (1,1), mode the radiation efficiency of the panel is maximized. In addition, the response of the panel to excitation is maximized when it is driven at its resonance. Therefore, the panel is designed such that its fundamental frequency is near the tone to be cancelled, e.g., the fundamental blade passage frequency, typically 2000 - 4000 Hz. In addition to driving the panel at its fundamental frequency, maximization of the acoustic output is achieved by maximizing the input voltage to the piezoelectric actuator. It is known that above a certain voltage level, the piezoelectric properties of the actuator will begin to deteriorate. This maximum safe input voltage is a function of the piezoelectric material, thickness of the actuator, and the manner in which the actuator is driven.

In order to generate sufficiently high levels of acoustic output to cancel the primary sound field, it will generally be necessary to utilize a number of these panels. Several panels can be mounted in an array around the circumference of the inlet and driven in-phase to produce the overall sound pressure level required for a particular application. The maximum number of panels that can be used depends on the physical

dimensions of the panel, the circumference and available axial length of the inlet, and the method of securing the panel to the inlet wall.

3.1.1 Mechanical Design

In designing the source, there are actually very few physical constraints, thus allowing for a great deal of flexibility and creativity in the design. One constraint is that the inner radius of the panel must correspond to the inner radius of the engine's inlet duct at the locations where the source panels will be installed. This requirement is imposed so that the sound source may be mounted flush inside the inlet to minimize any aerodynamic losses or disturbances as the air flows through the inlet. Another constraint that was adopted for this particular design was the size of the force transducer. The sources utilized piezoceramic (PZT) patches as the actuator. Since a large supply of 2.5" x 1.5" x 0.0075" (0.0635 x 0.0381 x .0001905 m) PZT patches was readily available, these were used in this work. Thus, the size of the patches imposed a constraint on the physical dimensions of the panel, because the panel must be large enough to accommodate the patch. These two parameters -- inner radius and patch dimensions -- were the only physical constraints in the mechanical design of the panel. However, there were several other factors that were considered in an attempt to optimize the sound source to maximize the sound pressure level (SPL) generated while minimizing the total weight of the source. These additional considerations include the following.

1. Material. Because of the need to minimize the weight of the source, it was desired to choose a low density material for the source. For the initial design, 6061 aluminum was chosen. Its low mass density makes aluminum a frequent choice in aeronautical design.

2. Circumferential length. An attempt was made to minimize the length of the source in the circumferential direction, because this would maximize the number of sources that could be installed in a circumferential array. Because the overall sound level generated is directly proportional to the number of sound sources, this in turn maximizes the overall sound output for a given panel design.

3. Mounting the panel. The manner in which the panel is mounted in the engine inlet, or the effective boundary conditions on the panel, has a profound effect on the dynamic characteristics of the panel. In general, the more rigid the boundary conditions for a given panel geometry, the higher the natural frequencies of the panel. The natural frequencies of a given structure are maximized by rigidly clamped boundary conditions. The effect of boundary conditions on the dynamic characteristics of the panel can thus be used as a means to minimize the panel weight because as the boundary conditions on the panel approach a rigidly clamped condition, the overall size of the panel, and therefore the weight required to produce the desired frequency, decreases. In other words, a relatively smaller, lighter panel with rigidly clamped edges can have higher resonances than a thicker and heavier panel with less rigidly clamped boundaries. The effect of boundary conditions on the resonant frequencies of the panel will be discussed further in a later section of this paper.

These design considerations -- choice of material, circumferential length of the source, and the manner in which the panel is mounted in the duct -- were not considered rigid design constraints. Rather, they were viewed as general design guidelines, but would be necessary input parameters in any deterministic optimization of the source design.

3.1.2 Acoustic Design

The mechanical design constraint of panel curvature is fundamentally linked to the design of the panel as an acoustic source. Because of the curvature of the panel, the in-plane displacement induced by the piezoactuators is coupled to the out-of-plane motion of the panel, which generates the desired acoustic waves. This coupling of the in-plane to the out-of-plane motion is a basic principle of shell theory [40].

The curvature of the panel also has the effect of increasing the resonant frequencies of the panel over those of an analogous flat plate. This effect is advantageous in the design of the sound source because a relatively smaller, lighter panel of curved geometry can have the same resonant frequencies as a larger, heavier, flat plate. In other words, the relatively high frequency range required of the sound source can be obtained with a lower weight penalty using a curved panel as opposed to using a flat plate of similar dynamic characteristics. This effect of curvature on the resonant frequencies of the panel is caused by the added stiffness of a curved structure versus a flat plate.

3.1.3 Excitation of the Panel

Excitation of the panel is accomplished by applying a sinusoidal input voltage to one or more piezoelectric force transducers bonded to the panel surface. It is a characteristic of piezoelectric materials that an applied voltage induces strain in the material. The amplitude of the panel's response to this induced strain is determined by the input voltage to the transducer, while the frequency of the response corresponds to that of the sinusoidal input signal to the piezoactuator. In order to maximize the acoustic response of the panel, the piezoactuators must be positioned and driven in such a manner as to excite the fundamental, or (1,1), mode of the panel. As previously discussed,

vibration of the panel at its fundamental resonant frequency will maximize the amplitude of the response.

3.1.4 Placement of the Actuators

Through careful positioning of the actuators on the panel surface, the (1,1) mode can be selectively excited while minimizing the contribution, or spillover, from unwanted modes.

For this design, the optimal configuration was to position the actuator on the panel surface such that the actuator was centered on the panel surface with the actuator edges parallel to the panel edges. In those configurations involving actuators on both sides of the panel, the actuators were symmetrically bonded to the top and bottom surfaces of the panel.

Because the actuators are centered on the panel's surface, the (1,1) mode of the panel couples well to the motion of the actuator, since all points on the panel beneath the actuator are in-phase with one another. In contrast, the next three modes contain nodal lines centered beneath the actuators. These modes are the (1,2), (2,1), and (2,2) modes, where the (v,w) notation represents v half-waves in the circumferential direction and w half-waves in the axial direction of the panel. These three modes are dipole-type modes, which are inherently inefficient acoustic radiators. Because these modes have nodal lines centered beneath the actuators, half of the area under the actuator is 180° out of phase with the other half, and thus these modes do not couple well to the motion of the actuator. It follows that the modal participation of these three modes will be minimized by placement of the actuators as previously described, and the participation of the (1,1) mode will be dominant.

3.1.5 Securing the Panel

The effect of the boundary conditions, i.e., the manner in which the panel is mounted, has already been discussed from the standpoint of mechanical design. Here the effect of boundary conditions on the acoustic output of the panel will be considered.

For this design, the most desirable method of mounting the panel in the inlet is to secure all four edges of the panel to the inlet wall, thus preventing communication between the fluid inside the duct with the fluid on the other side of the panel. Mounting the panel to the inlet wall in this manner is similar to mounting the panel in a finite baffle, which has the effect of increasing the acoustic radiation into the duct. Thus, the attachment of all four panel edges to the duct wall is advantageous with respect to the acoustic output of the source. This mounting configuration is also advantageous with regard to the dynamic properties of the panel, as previously discussed.

3.2 Finite Element Analysis

A finite element method was used to design the sound source. The software package used was SDRC I-DEAS Version 4.1, and the solution method chosen was SVI (Simultaneous Vector Iteration). The model was constructed using thin shell elements. Two types of analyses were performed: 1) a Normal Modes analysis was performed to obtain natural frequencies and mode shapes, and 2) a Forced Response analysis was run to obtain displacements. The solution methods are discussed in detail in [41].

3.2.1 Assumptions and Geometry

The assumptions included in the finite element analysis are as follows:

1. isotropic material

2. linearity
3. elasticity
4. homogeneous material
5. no residual stresses in the panel from fabrication.

The assumption of isotropic material properties is a reasonable one for the types of materials considered in this study. The assumptions of linearity, elasticity, and homogeneity are embodied in the finite element code. Residual stresses always result from machining and fabrication processes, but were assumed negligible for this study.

The finite element model used in this study is shown in Figure 3.1, and the material properties used are given in Table 3.1. In addition to the thin shell elements which comprise the panel structure itself, the model also contains two other types of element: 1) spring elements to represent the effect of the test duct and the adhesive layer securing the panel to the test duct, and 2) lumped mass elements to account for such added masses as actuators and accelerometers. These spring and lumped mass elements will be discussed in greater detail in a later section.

The panel is 6.5" (0.1651 m) in the axial direction, 5.5" (0.1397 m) in the circumferential direction, and 0.063" (0.0016 m) thick, with an inner radius of 9.0" (0.2286 m) corresponding to the outer radius of the test duct. The active, or unconstrained, area of the panel is 4.0" (0.1016 m) long axially by 3.0" (0.0762 m) long circumferentially, leaving a 1.25" (0.03175 m) wide band around the perimeter of the active area. This band represents the surface area that is secured to the test duct with adhesive. This adhesive bond is represented by spring elements in the finite element model. The panel is shown in Figure 3.2.

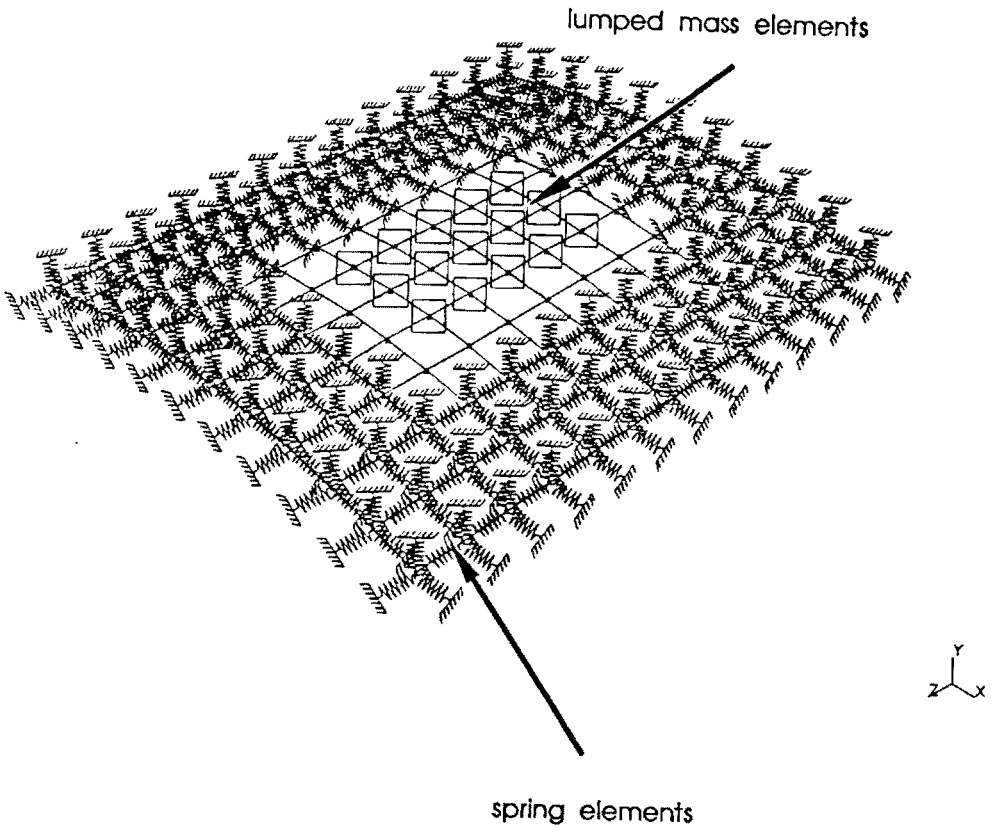

Figure 3.1 -- Finite element model of panel.

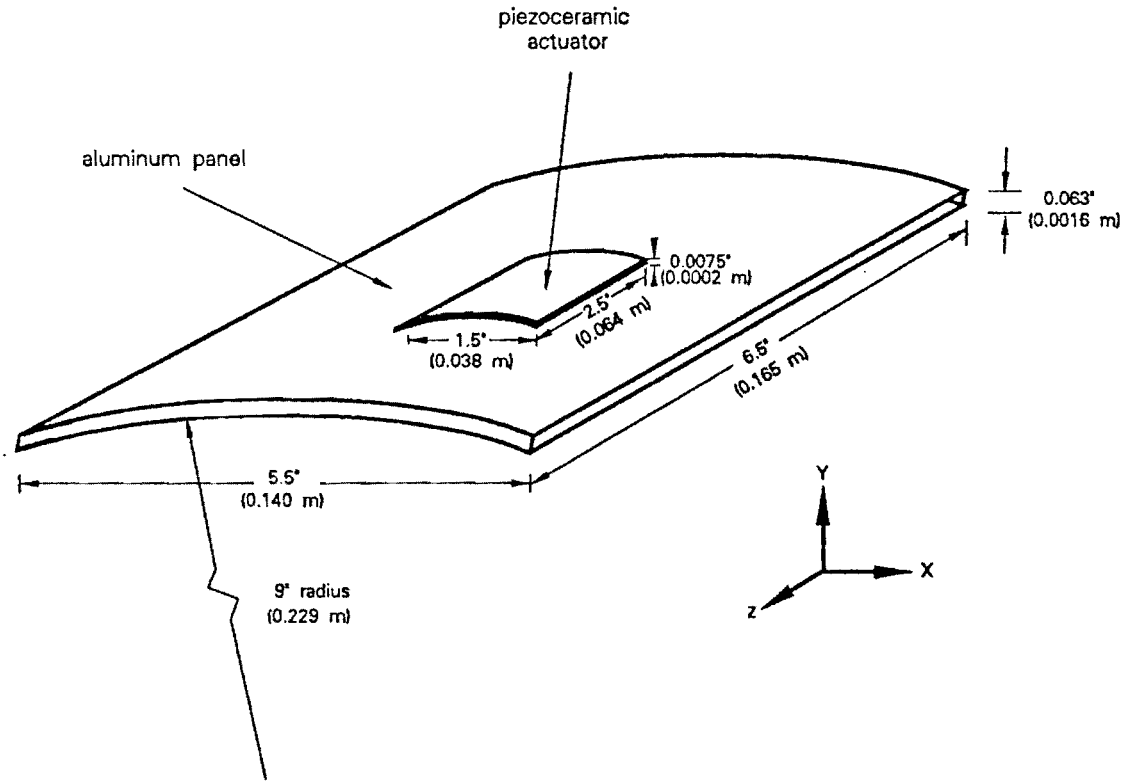

Figure 3.2 -- Schematic of panel.

Table 3.1 -- Material properties of aluminum.

Property	English units	SI units
mass density	0.10107 lbm/in.^{3}	2800 kg/m^3
Young's modulus	10.4 x 10^6 psi	72 x 10^9 Pa
Poisson's ratio	0.32	0.32

Table 3.2 -- Undamped natural frequencies of the panel.

mode	FEM simply supported	FEM clamped	experimental
1,1	1245	3594	1708
1,2	2698	4436	3196
2,1	3066	4700	2324

3.2.2 Boundary Conditions

The dynamic characteristics of the source panel are greatly influenced by the boundary conditions imposed on the structure. Thus, a critical step in the finite element analysis is the characterization of the physical boundary conditions of the system. The finite element model was used to calculate the undamped natural frequencies for the cases of simply supported and clamped boundary conditions. These results were then compared to experimental results. Particular attention was given to the fundamental, or (1,1), frequency, as this vibration mode is of special interest in this study. Table 3.2 summarizes these results for the first three modes. The (1,1), (1,2), and (2,1) modes are shown in Figures 3.3 - 3.5.

These results indicate that the actual physical boundary conditions are somewhat more rigid than the simply supported case, in which only the out-of-plane motion is restrained. However, the experimental results are much closer to the simply supported case than to the clamped case in terms of natural frequency, indicating that any restraint in the in-plane directions is considerably less than that implied by a clamped boundary condition, in which the in-plane as well as the out-of-plane motion is fully restrained. Thus, a flexible, yet not totally free, boundary condition is appropriate for this model, and this is accomplished using translational spring elements for which stiffness values in three directions may be specified. These spring stiffnesses may either be determined by trial and error, or they may be estimated from beam theory. A combination of these approaches was undertaken in this study.

Another factor influencing the undamped natural frequencies of the panel is the mass loading effect of the actuators, adhesive, electrical leads, and any other added mass such as accelerometers and wax. Using the value for mass density given in Table 3.1, the mass of the entire panel is 99.7 grams, while the mass of the active, or unconstrained area

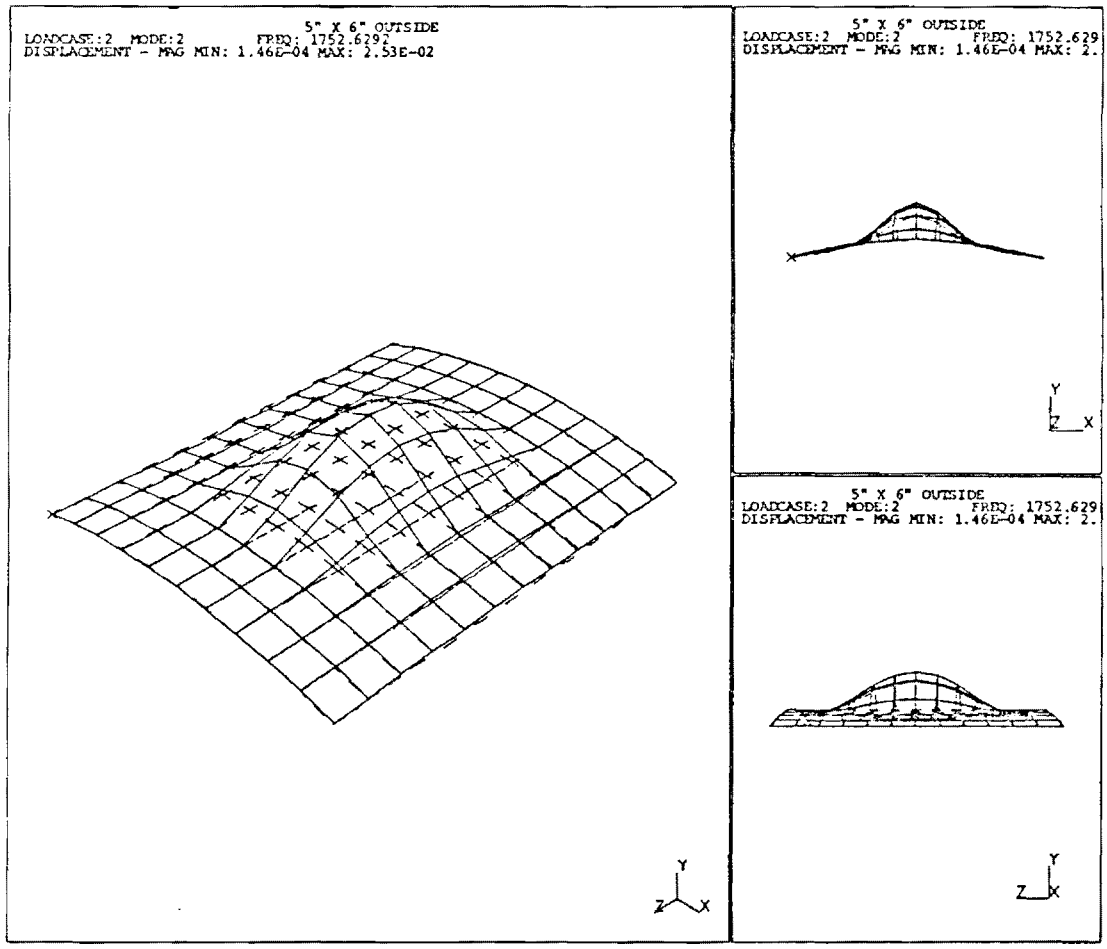

Figure 3.3 -- (1,1) vibrational mode.

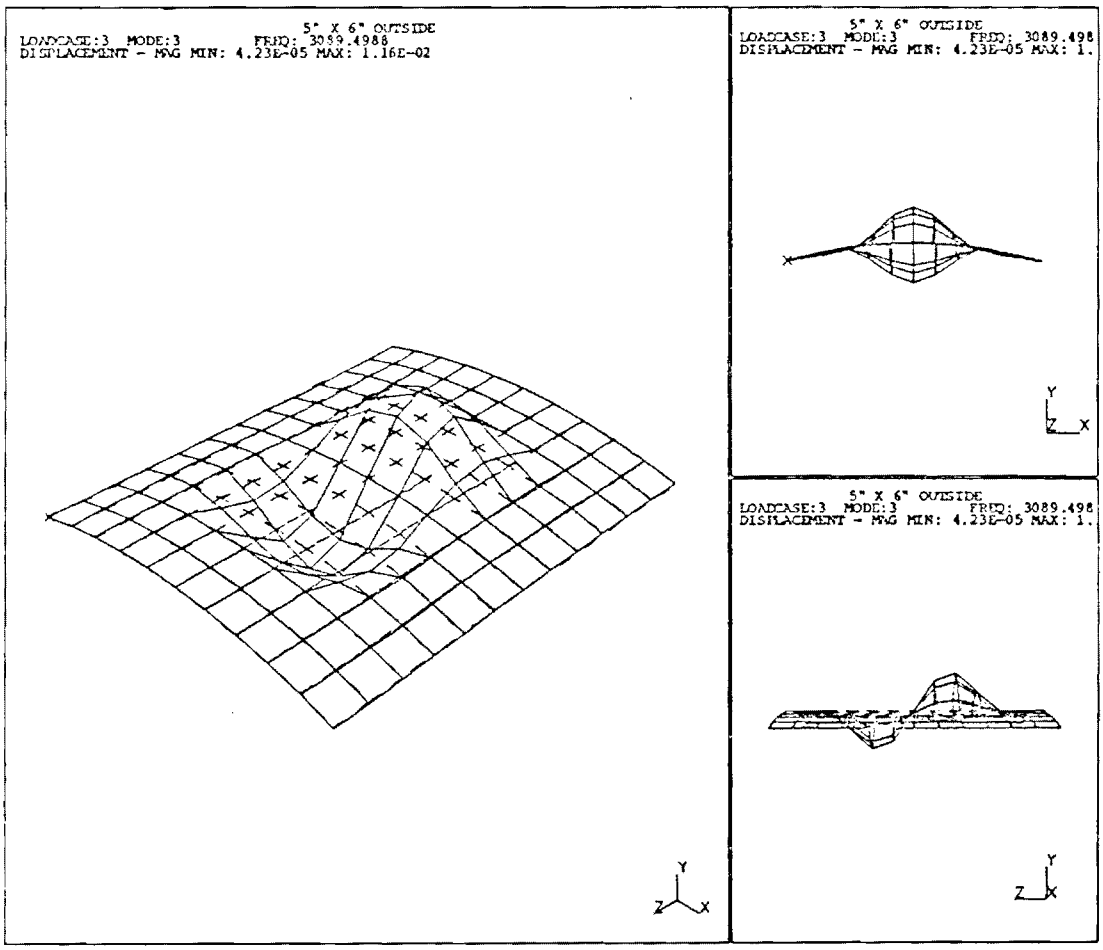

Figure 3.4 -- (1,2) vibrational mode.

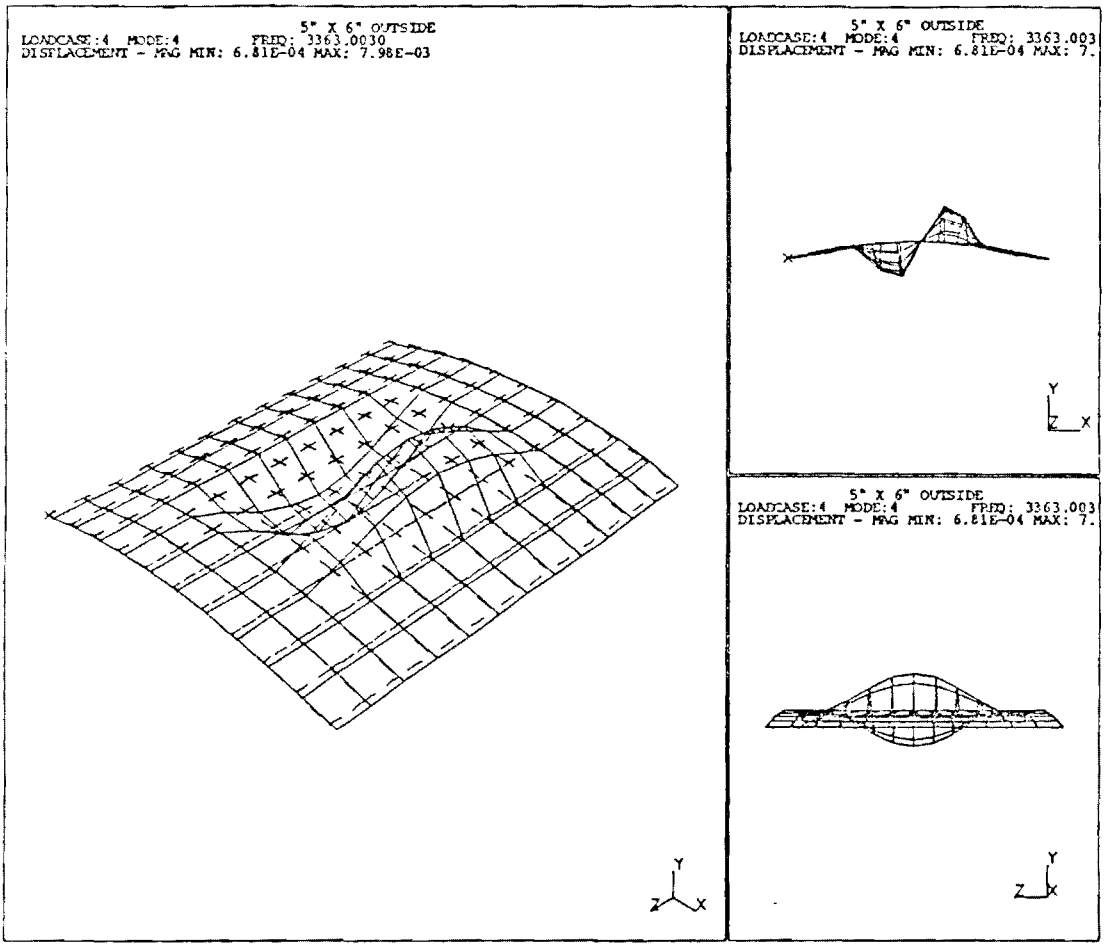

Figure 3.5 -- (2,1) vibrational mode.

of the panel is 33.5 grams. The mass of one actuator is 3.5 grams, which implies that the mass of an actuator pair is about 21% of the panel's mass, neglecting the mass of the adhesive layers. This mass loading due to the actuators can be expected to lower the resonant frequencies somewhat. Indeed, the finite element model predicts a decrease in undamped natural frequency of up to 18% for the simply supported case, depending on mode, when the mass of the two actuators is applied as a distributed load among the nodes lying beneath the actuator pair. The effect is even more pronounced for the clamped boundary condition case. The model was also solved for the case of the actuator pair modeled as a point mass applied at a single node. As expected, this case predicts no change in natural frequency for those modes containing nodal lines lying beneath the point mass, because the point mass offers no resistance to a nodal point and thus does not have any mass loading effect on those modes. However, this case does demonstrate the mass loading effect on the (1,1), (1,3), and (3,1) modes, which have antinodes, or points of maximum displacement, lying beneath the node where the point mass is applied. These results are tabulated in Table 3.3.

Based on these results, the mass of the actuator pair was included in the finite element model. This mass was distributed uniformly over the nodes lying beneath the actuator pair.

3.2.3 Modeling the Actuator

The mass loading effect of the actuator pair was discussed in a previous section. In this section, the modeling of the actuator's dynamic loading on the panel will be reviewed.

Table 3.3 -- Mass loading effect of actuator pair on undamped natural frequency, a) simply supported, and b) clamped boundaries.

a) Simply supported

mode	panel alone (no added mass)	actuator point mass included	% change	actuator pair distributed mass included	% change
1,1	1245	919	-26	1019	-18
1,2	2698	2698	0	2285	-15
2,1	3066	3066	0	2684	-12
2,2	4304	4304	0	3848	-11
1,3	4623	3489	-25	4035	-13
3,1	6393	5641	-12	5883	-8
2,3	6298	6285	0	5750	-9
1,4	7155	7155	0	6334	-11
3,2	7558	7558	0	7069	-6

b) Clamped

mode	panel alone (no added mass)	actuator point mass included	% change	actuator pair distributed mass included	% change
1,1	3594	2109	-41	2841	-21
1,2	4436	4435	0	3575	-19
2,1	4700	4684	0	3921	-17
2,2	6111	6111	0	5181	-15
1,3	6205	5213	-16	5161	-17
3,1	8723	7765	-11	7821	-10
2,3	8201	8197	0	7125	-13
1,4	8924	8924	0	7691	-14
3,2	9896	9892	0	8950	-10

Table 3.4 -- Actuator-induced loads on the panel.

Configuration	Dimitriadis, et al	Wang & Rogers	Lazarus & Crawley
1) pure bending	M_x = 0.0861N-m M_z = 0.1435 N-m	M_x = 0.0600 N-m M_z = 0.1000 N-m	M_x = 0.0600 N-m M_z = 0.1000 N-m
2) pure extension	P_x = 179.36 N P_z = 107.62 N	P_x = 124.96 N P_z = 74.98 N	P_x = 168.06 N P_z = 100.83 N
3) one actuator	M_x = 0.0431 N-m M_z = 0.0718 N-m P_x = 89.68 N-m P_z = 53.81 N-m	M_x = 0.0300 N-m M_z = 0.0500 N-m P_x = 62.49 N-m P_z = 37.49 N-m	M_x = 0.0441 N-m Mz = 0.0736 N-m P_x = 91.96 N P_z = 55.17 N

Note: The subscripts x and z refer to moments about, and forces in the direction of, the x and z axes, respectively (see Figure 3.2).

Four actuator configurations were studied experimentally: a) the two actuators acting in-phase, b) the two actuators acting 180° out of phase, c) the actuator on the inside surface acting alone, and d) the actuator on the outside surface acting alone. To determine the loads exerted on the panel by the actuator(s), an analytical model developed by Dimitriadis, et al [38] was used to calculate the equivalent loads applied along the actuator edges. The results of this model are given in Table 3.4 for an excitation voltage of 100 V_{rms}. This model assumes 1) perfect bonding between the actuator and the panel, implying strain continuity across the bond interface, and 2) collocation (symmetric bonding) of the actuator patches. While neither of these assumptions is realized in practice, both are reasonable for this analysis. The analytical model used was developed for a flat plate for which in-plane and out-of-plane motion are uncoupled. Since the results are being applied to a curved panel, in which in-plane motion is coupled to out-of-plane motion, the results may be expected to deviate from analytical prediction. Indeed, some deviation from theory was observed in the experimental results. However, without an analytical actuator model derived from cylindrical shell theory, the model used is the most appropriate one available. Two other analytical models were considered as well [36, 37] and the results of these models are also tabulated in Table 3.4. Because these models were derived from beam theory, it was decided to use the plate-based model instead, as it includes two-dimensional effects.

The results in Table 3.4 are for three actuator configurations. In configuration 1, the actuator pair driven 180° out-of-phase is modeled by bending moments at the edges of the actuator, since pure bending results from two symmetrically bonded actuators driven in this manner. In configuration 2, the actuator pair driven in-phase is modeled by forces applied at the edges of the actuators. Since the two symmetrically bonded actuators are driven in-phase, the resulting load applied to the plate is in-plane tension

alternating with in-plane compression. In configuration 3, a single actuator is modeled by a combination of forces and moments along the edges of the actuator. Because the actuator is off the neutral surface of the panel, the motion of the actuator creates a bending moment in addition to the in-plane force generated.

Because experiment shows the maximum panel response when the outside panel is driven alone, this case (configuration 3) was used in the finite element analysis. From the standpoint of aerodynamics, also, it is desirable to avoid using an actuator on the inside, or airflow, surface of the panel.

Although the actuator model used was derived from flat plate theory, the displacements predicted are of the same order of magnitude as experimental results. This will be discussed in more detail in a later section.

3.2.4 Forced Response Analysis

A forced response analysis of the finite element model was used to determine the displacement, and thus velocity, at each panel node in response to the piezoactuator. The results were then compared to experimental results measured with an accelerometer. These finite element results were used to specify velocity boundary conditions in SYSNOISE.

The first task in this process was to obtain the normal modes of the panel. The effects of boundary conditions and actuator mass has been discussed in a previous section, and these effects were included in the forced response analysis. Because the experimental results used for comparison were obtained using an accelerometer attached to the antinode, or center point, of the panel, it was necessary to determine the effect of the accelerometer mass on the panel response. This was analyzed in a similar manner as the mass of the actuators. A lumped mass element of 0.002 kg representing the

accelerometer was attached to the center node of the panel, and the natural frequencies were calculated. The distributed mass of the actuator pair was included in the analysis, and the results were compared to a previous analysis which included the actuator pair's distributed mass, but excluded the accelerometer mass. These results are given in Table 3.5.

Because the accelerometer was modeled as a point mass applied to an infinitesimally small area, the finite element model predicts a change in natural frequency only in those modes which do not have nodal lines located at the center node -- the (1,1), (1,3), and (3,1) modes. However, since the accelerometer mass is actually distributed over a nonzero, although small, surface area rather than concentrated at the (1,1) antinode, the mass will have some effect on all the modes, and the magnitude of the effect on the (1,1) mode can be expected to be smaller than that predicted here. Table 3.3 illustrates the effect on natural frequency when a mass is modelled as a distributed rather than a point mass.

Based on these results, it can be assumed that the effect of accelerometer mass on (1,1) natural frequency is small (less than 7% for the simply supported case) and could probably be neglected in an experimental modal analysis. However, the effect of the accelerometer on the panel's displacement and hence its acoustic characteristics, cannot be assumed negligible and will be further discussed in another section.

The natural frequencies of the panel model, including spring element boundaries and actuator mass, are given in Table 3.6. The normal modes results used in the initial forced response analysis include the accelerometer mass to provide for comparison to experimental results obtained using an accelerometer. The normal modes results which exclude the accelerometer mass were used to obtain panel velocities to be used as

Table 3.5 -- Effect of accelerometer mass on undamped natural frequency, a) simply supported, and b) clamped

	a) simply supported			b) clamped		
mode	without accelerometer	with accelerometer	% chg	without accelerometer	with accelerometer	% chg
1,1	1019	949	-7	2841	2509	-12
1,2	2285	2285	0	3575	3575	0
2,1	2684	2684	0	3921	3919	0
2,2	3848	3848	0	5181	5181	0
1,3	4035	3694	-8	5161	4762	-8
2,3	5750	5749	0	7125	7124	0
3,1	5883	5543	-6	7821	7273	-7
1,4	6334	6334	0	7691	7692	0
3,2	7069	7069	0	8950	8950	0
2,4	8248	-	-	9805	-	-

Table 3.6 -- Natural frequencies used in forced response calculations

mode	accelerometer mass included	accelerometer mass excluded	experimental results
1,1	1601	1753	1708
1,2	3089	3089	3196
2,1	3353	3363	2324
1,3	4309	-	-
2,2	4613	4613	-

SYSNOISE input data. Both sets of results are given in Table 3.6, along with experimental results for the first three modes.

Figures 3.6 and 3.7 show the corresponding frequency response functions (FRF) of velocity versus force predicted by the finite element model. Figure 3.6 includes the effect of the accelerometer mass while Figure 3.7 does not. In both cases, only those modes which do not contain nodal lines beneath the center node appear in the FRF. This is consistent with analytical prediction [38] and can be explained by noting that the actuator pair is symmetrically located about the nodal lines of the (1,2), (2,1), and (2,2) modes. Because points on opposite sides of these three modes are 180° out of phase, these modes do not couple into the motion of the actuator, for which all points on its surface are in-phase. This phenomenon is explained in greater detail in Dimitriadis, et al [38].

In performing a forced response calculation, it is necessary to specify the damping ratio, ζ, for each mode. This damping ratio includes both the internal damping of the material and the external damping created by the constraints, or boundary conditions, on the structure. Some estimates of internal damping are available in the literature [42]; external damping is generally more difficult to characterize.

For this analysis, viscous damping was assumed, and the damping ratio, ζ, was estimated experimentally using a 3 dB-down method described in the literature [43]. For the (1,1) mode, the damping ratio measured was 5.0%. Because the next two modes were not clearly excited due to the location of the actuators, damping ratios for these modes could not be experimentally determined, and so a value of 5.0% was used for all modes. In general, however, the damping ratio can be expected to vary with mode. The damped natural frequencies were then calculated. These are given in Table 3.7.

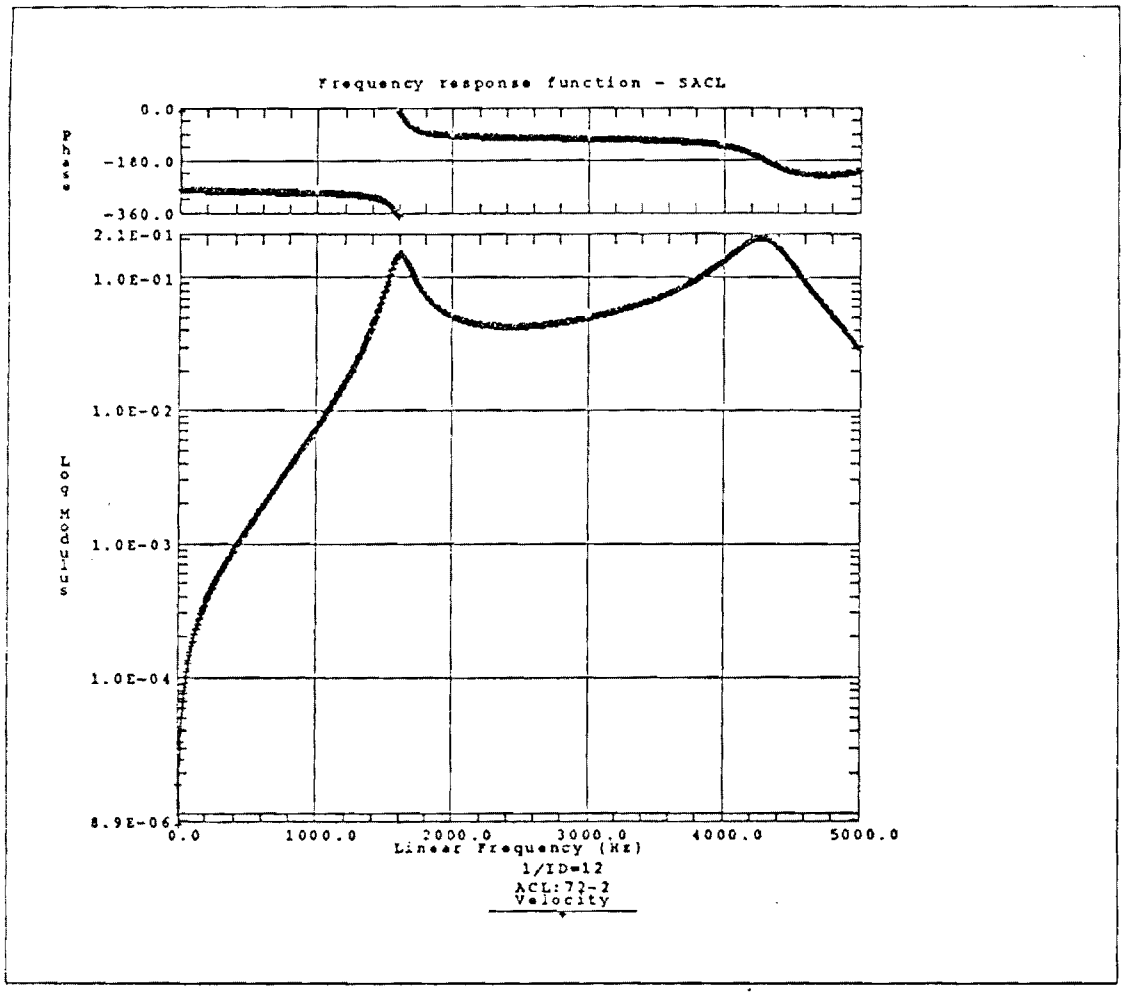

Figure 3.6 -- Frequency response function with accelerometer mass included (FEM prediction).

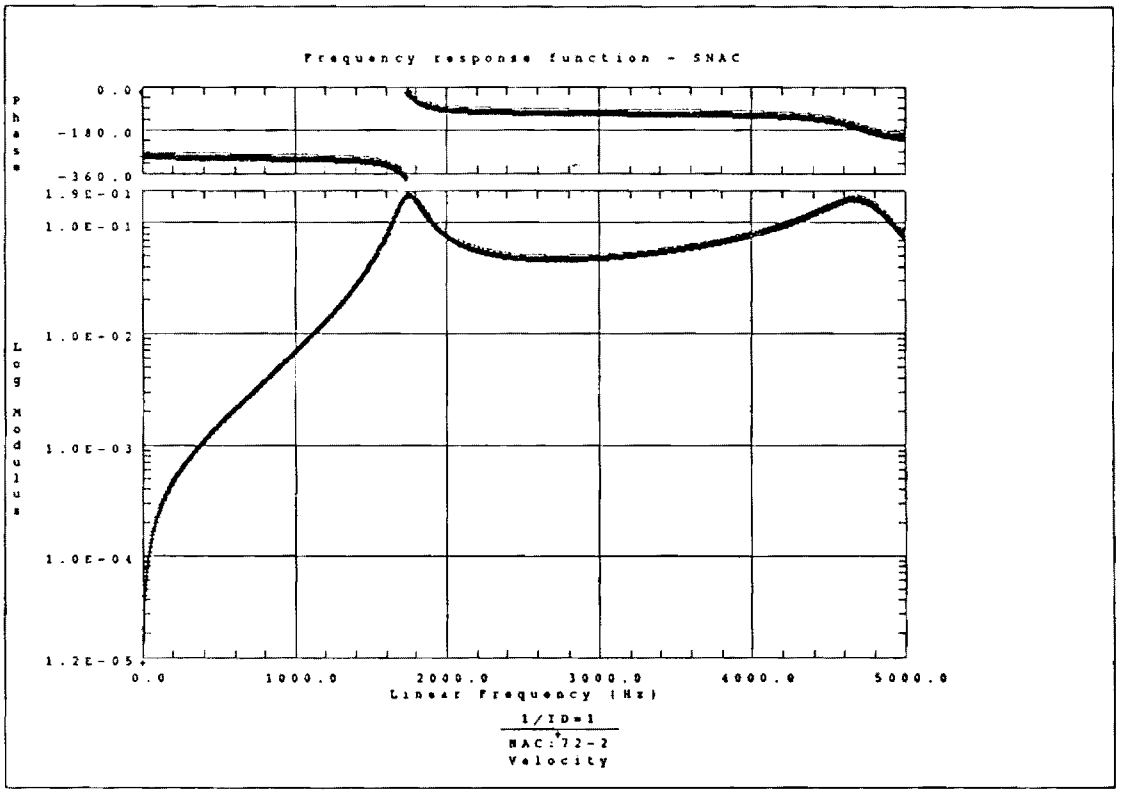

Figure 3.7 -- Frequency response function excluding the accelerometer mass (FEM prediction).

Table 3.7 -- Damped and undamped natural frequencies (accelerometer mass excluded).

mode	undamped	damped
1,1	1753	1751
1,2	3089	3085
2,1	3363	3359

As previously discussed, an analytical model derived from flat plate theory was used to predict the loads on the panel induced by the actuator. The case of one actuator was chosen (configuration 3 in Table 3.4) based on experimental observation and aerodynamic considerations. The equivalent forces and moments were modelled as distributed loads applied to those nodes corresponding to the actuator edges. Anexcitation voltage of 100 V_{rms} was used in the loads calculations, as this was the voltage level at which experimental velocity measurements were taken.

The excitations were defined such that the loads on opposite sides of the actuator are applied in opposing directions. The excitations were defined in the frequency domain so that the panel response could be calculated over a range of frequencies for the given voltage input.

The next step in the finite element analysis is the calculation of the panel displacements at various excitation frequencies. These displacements were first calculated for the case including the accelerometer mass, and the results were compared to experimental results obtained at an input frequency of 1800 Hz and an excitation voltage of 100 V_{rms}. The displacements were then calculated for the case of no accelerometer. These results for the center node are summarized in Table 3.8.

The effect of the accelerometer mass on the panel displacements is apparent. For the case of 1800 Hz, at which the experimental data was taken, the finite element model predicts a 69% decrease in displacement at the center node due to the mass of the accelerometer. In general, the effect of accelerometer mass on panel response is frequency dependent. For instance, at an excitation frequency of 1601 Hz, the finite element model predicts an *increase* in response with accelerometer mass. This results can be explained by referring to the FRF's of Figures 3.3 and 3.4. For the case including the accelerometer, 1601 Hz corresponds to the panel's (1,1) resonance, whereas for the

Table 3.8 -- Predicted displacement, δ, of the center node at input voltage of 100 V_{rms}.

frequency, Hz	δ, accelerometer mass included	δ, accelerometer mass excluded
1601	*1.41 x 10^{-5}	8.05 x 10^{-6}
1644	1.21 x 10^{-5}	1.04 x 10^{-5}
1708	7.92 x 10^{-6}	1.51 x 10^{-5}
1753	6.08 x 10^{-6}	*1.73 x10^{-5}
1800	4.76 x 10^{-6}	1.55 x10^{-5}

* denotes resonance condition

case excluding the accelerometer, 1601 Hz is about 150 Hz removed from the (1,1) resonance and so excites a relatively weaker response. Thus, the accelerometer affects the panel response in two ways: 1) by adding a lumped mass to the structure that, in general, decreased the magnitude of the response, and 2) by altering the panel's frequency response function. In comparing the finite element results to experimental results, the finite element prediction is 1.6 times greater than experimental, or well within an order of magnitude. This difference can be attributed to the following factors:

1) the assumption of perfect bonding in the actuator analytical model,

2) the fact that the analytical model was developed for a flat plate, not a curved panel,

3) error in the estimate of damping,

4) error in the specification of the boundary conditions,

5) neglecting the effect of the cylinder's motion on the panel's response, and

6) variance in the panel's material properties.

Any of these factors could significantly alter the predicted displacements of the FEM model.

By comparing experimental displacement measurements to the analagous finite element model prediction in this manner, it is possible to scale the finite element model prediction for the case excluding the accelerometer by the same factor, and to use the scaled results as velocity boundary conditions for an acoustic radiation analysis. This was the approach taken in this study.

The forced response analysis was repeated, using an input voltage of 8.75 V_{rms}, and these results were used for SYSNOISE input (corresponding to the experiments done) so that they could be directly compared to experimental acoustic pressure measurements. (The SYSNOISE analysis is detailed in Chapter 5.)

3.2.5 Validation of the Model

In any finite element analysis, it is necessary to validate the model results. In this analysis, the model was validated by two means: 1) convergence check and 2) comparison to known analytical solutions. As in any numerical method, the solutions obtained using finite element analysis are approximate, and thus contain some error due to discretization of the problem. The amount of error for a given analysis depends in part on the size and type of the mesh generated. For this analysis, thin shell quadrilateral elements were used. To determine the mesh size, the model was run for successively finer meshes until the change in results was negligible. These results for the first five modes are given in Table 3.9. It was found that increasing the number of elements by a factor of 2.25 resulted in less than 1% change in natural frequency. Further study with a 480-element mesh resulted in an even smaller change. Thus, based on these convergence results, a 120-element mesh was used in the analysis.

The model was also run for cases for which analytical solutions exist, and the results further validate the model. Analytical results for a curved panel with either simply supported edges or clamped edges were used [44]. The finite element model was run for these same boundary conditions, and the results are shown in Table 3.10. As a further check, analytical and numerical solutions to the analagous flat plate problem were determined, using the solutions of Leissa [40], and a flat plate finite element model, respectively. These results are presented in Table 3.11.

For the curved panel, the largest error occurs for the (1,1) mode with simply supported boundaries. Here, the model underpredicts the natural frequency by almost 25%. However, these analytical solutions are approximations and so contain some error themselves. The flat plate results are much closer to analytical prediction, within 2%, for the first five modes. These analytical results are exact. The flat plate results were

Table 3.9 -- Convergence of model.

	120-element model		270-element model		% change	
mode	simply supported	clamped	simply supported	clamped	simply supported	clamped
1,1	1245	3594	1237	3606	-0.6	+0.3
1,2	2698	4436	2683	4478	-0.6	+0.9
2,1	3066	4700	3058	4684	-0.2	-0.3
2,2	4304	6111	4286	6115	-0.4	0.0
1,3	4623	6205	4632	6269	+0.2	+1.0

Table 3.10 -- Curved panel, comparison of FEM to analytical solution.

	simply supported			clamped		
mode	analytical	FEM	% error	analytical	FEM	% error
1,1	1650	1245	-24.5	3703	3594	-2.9
1,2	3278	2698	-17.7	4597	4436	-3.5
2,1	3070	3066	-0.1	5294	4700	-11.2
2,2	4363	4304	-0.1	6417	6111	-4.8
1,3	5024	4623	-8.0	6396	6205	-3.0

Table 3.11 -- Flat plate, comparison of FEM to analytical solution.

	simply supported			clamped		
mode	analytical	FEM	% error	analytical	FEM	% error
1,1	1043	1048	+0.5	1963	1963	0.0
1,2	2176	2187	+0.5	3298	3310	+0.4
2,1	3038	3069	+1.0	4588	4634	+1.0
1,3	4171	4227	+1.3	5810	5917	+1.8
2,2	4064	4088	+0.6	5495	5522	+0.5

obtained in order to determinine where the error in the curved panel results originates. The curved panel analytical solution contains two terms, one representing the natural frequency of the analagous flat plate, and one representing the effect of curvature. From the results of Tables 3.10 and 3.11, it may be concluded that the curvature effect makes the largest contribution to the error in the FEM results.

In summary, one basic procedure for developing the finite element model is this:

1. Using the analytical solutions, choose a geometry that yields a fundamental frequency in the range of interest.

2. Create a finite element model with this geometry, check for convergence, and calculate the normal modes.

3. If the mass of the actuators relative to the panel cannot be assumed negligible, add the mass of the actuators to the model as a distributed mass and recalculate the normal modes.

4. Modify the boundary conditions as appropriate. Spring elements may be used to model boundaries that are somewhat less than completely rigid. Spring constants may be determined by analytical estimates, e g. from beam theory, or by trial and error.

5. When comparing FEM results to experimental results, include the mass of any added components such as accelerometers in the FEM model. For non-contacting measurement methods such as laser doppler velocimeter, this step is not necessary.

6. Adjust the model parameters -- geometry, material, boundary conditions -- as required to produce a model with the desired characteristics.

7. Model the excitation loads on the structure and calculate the forced response -- displacements, stresses, strains, etc.

3.3 Preliminary Experiments

Several experiments were performed to establish the mechanical characteristics of the curved panel sound source, including an experimental modal analysis, testing of the panel's acoustic output, and measurement of the panel's response to excitation of the actuators. For all the experimental work undertaken, the sound source was fitted in a test duct representative of an engine inlet (see Section 3.3.1). The results of these experiments were used primarily in the development of the finite element model, but also provided some insight into the structural and acoustic characteristics of the sound source.

3.3.1 Description of Test Duct and Panel Assembly

The source panel was comprised of one aluminum panel and two identical piezoelectric patches. The patches (actuators) were applied to the panel in the following manner. First, the panel surface was cleaned thoroughly. A thin layer of M-Bond 200 strain-gauge adhesive was then applied over the area where the actuator was to be mounted. This adhesive layer was covered with a strip of teflon film and allowed to cure. This first adhesive layer electrically insulates the actuator from the panel. The actuator patch was then cleaned, and a 1-mil brass lead was attached using silver paint. The teflon strip was removed from the panel and a second thin layer of adhesive was applied. The actuator was positioned on this adhesive layer, and the adhesive was again allowed to cure. In order to force the actuator to conform to the curvature of the panel, a second panel, identical to the first, was placed over the actuator, with a 1/2" (0.0127 m) layer of foam between the two. A weight was then placed on the second panel to apply pressure. Once the adhesive cured, the actuator was inspected for cracks and also to ensure no gaps existed in the adhesive layer. If the actuator had cracked, or the bond was unacceptable, the actuator was removed with a razor blade, the adhesive layer was

removed with a belt sander, and the whole procedure was repeated. Actuators were applied to both the inside and the outside surfaces of the panel in this manner.

Other methods of applying the actuator to the panel were tried, with varying degrees of success. The problem is in obtaining the required curvature without fracturing the actuator. In an attempt to utilize smaller patches, portions of the actuator patch were cut using a razor blade, and the edges filed smooth. However, the filed edges were always rougher than the uncut edges, despite the filing, and these portions of patches fractured in every attempt to apply them to the panel. The cracks typically originated either at stress concentrations along the edges or in the region where the brass lead was attached. To avoid this problem, it was decided to use the full-size patch. It was found that attaching the brass lead with silver paint rather than solder further improved the process yield.

The source panel was mounted in a duct representative of an engine inlet. Two ducts were used, one 12" (0.3048 m) long and one 36" (0.9144 m) long, each made of PVC (polyvinyl chloride) pipe with 18" (0.4572 m) outer diameter and 17" (0.4318 m) inner diameter. These two ducts are referred to throughout this thesis as the short and the long duct, respectively. A 4" by 3" (0.1016 by 0.0762 m) window was cut from the wall of the duct, over which the source panel was mounted using M-bond 200 adhesive. Because the source panel's dimensions are larger than the window, an overlap of approximately 1.25" (0.0318 m) resulted on all four sides of the window. The adhesive was applied under this entire area of overlap in order to maximize the bond area. Next, a bead of RTV silicone rubber was applied around the outside edges of the panel to seal off any leaks and to prevent the air inside the duct from communicating with the air outside the duct. This has the effect of increasing the radiation efficiency of the source by creating a baffled mounting configuration. The duct was suspended from the ceiling of

an anechoic chamber using nylon rope. One end was left open, and the other was terminated with a finite impedance. The finite impedance terminating one end of the pipe was either a 4" (0.1016 m) thick conical layer of open-cell foam, representing an anechoic termination, or a 3/4" (0.0191 m) - thick plywood panel, representing a rigid termination. Both terminations were used in the various experiments run. The entire outside surface of the pipe was wrapped in a 3" (0.0762 m) layer of open-cell foam to absorb the sound radiating from the outside surface of the pipe. The experimental setup is shown in Figures 3.8 - 3.10.

3.3.2 Equipment Used

For most of the experiments conducted, the function generator used was a B&K Type 2032 signal generator. The function generator output was connected to a gain box, through which the signal was passed and then input to a Proton power amplifier. The amplifier output was connected to a 17.5:1 power transformer, which stepped up the voltage. The output signal from the transformer was used to drive the piezoactuators.

The interior response was measured using 1/4" (0.0064 m) Radio Shack omnidirectional microphones mounted in an array (see Figure 3.6). The array was constructed such that the microphones could be rotated about the duct axis a full 360°. Translation along the duct axis was allowed via a traversing mechanism. A total of five microphones were mounted in the array, equally spaced and all oriented along the duct axis, pointing toward the source panel. Although the microphones used were omnidirectional, care was taken to mount the microphones in such a manner as to minimize the chance of distortion due to reflections from the array structure itself. Exterior measurements were taken with one 1/2" (0.0127 m) B&K omnidirectional microphone mounted on a rotating mechanism. Its position was controlled by a stepper

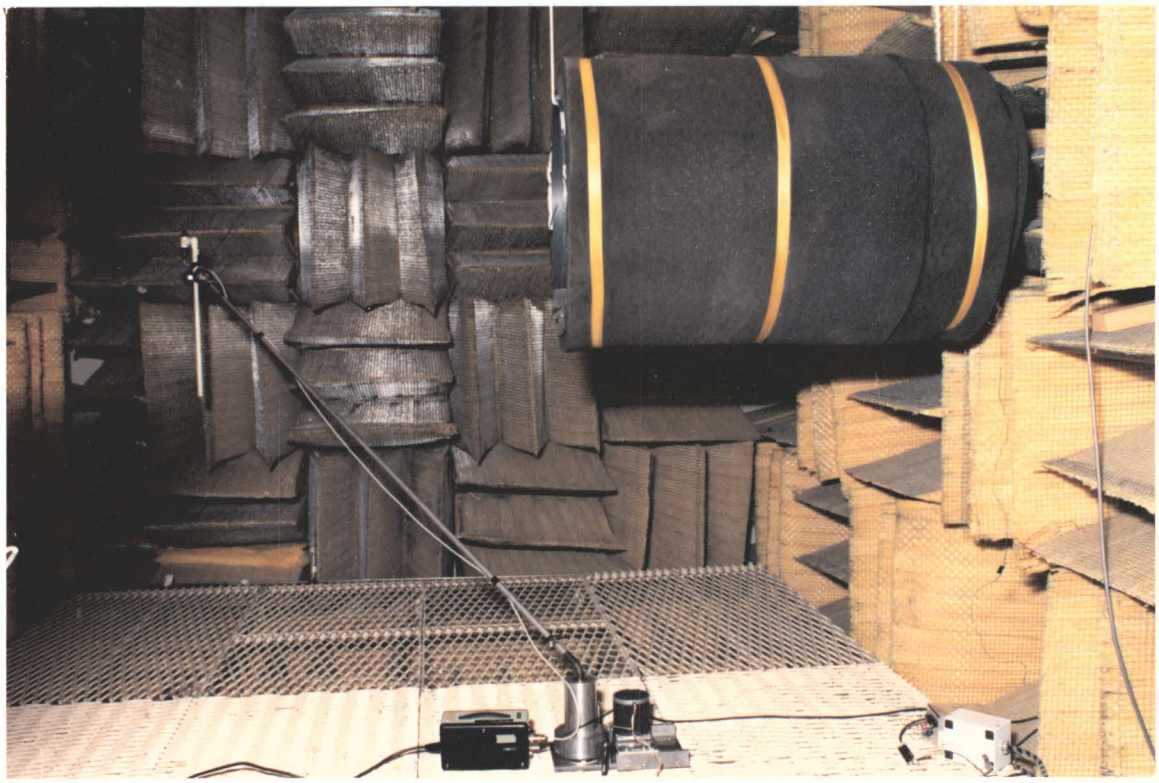

Figure 3.8 -- Experimental set-up, including long duct wrapped in foam and exterior microphone.

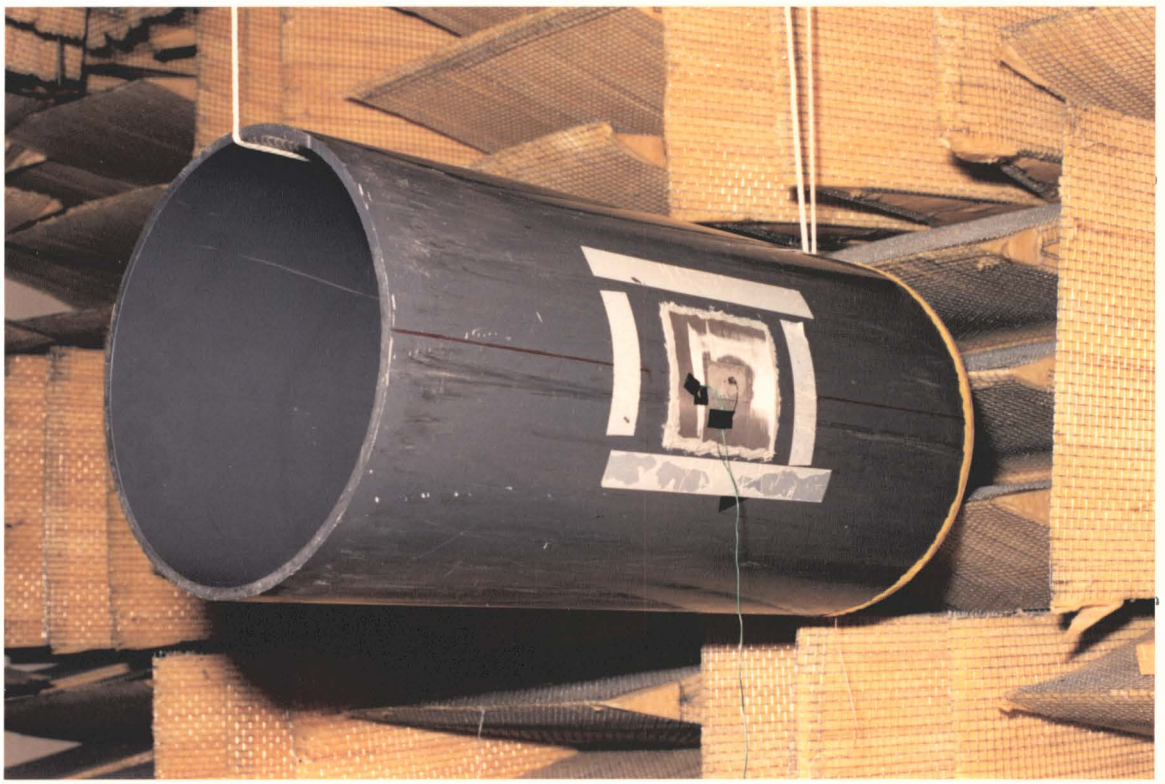

Figure 3.9 -- Long duct and source panel.

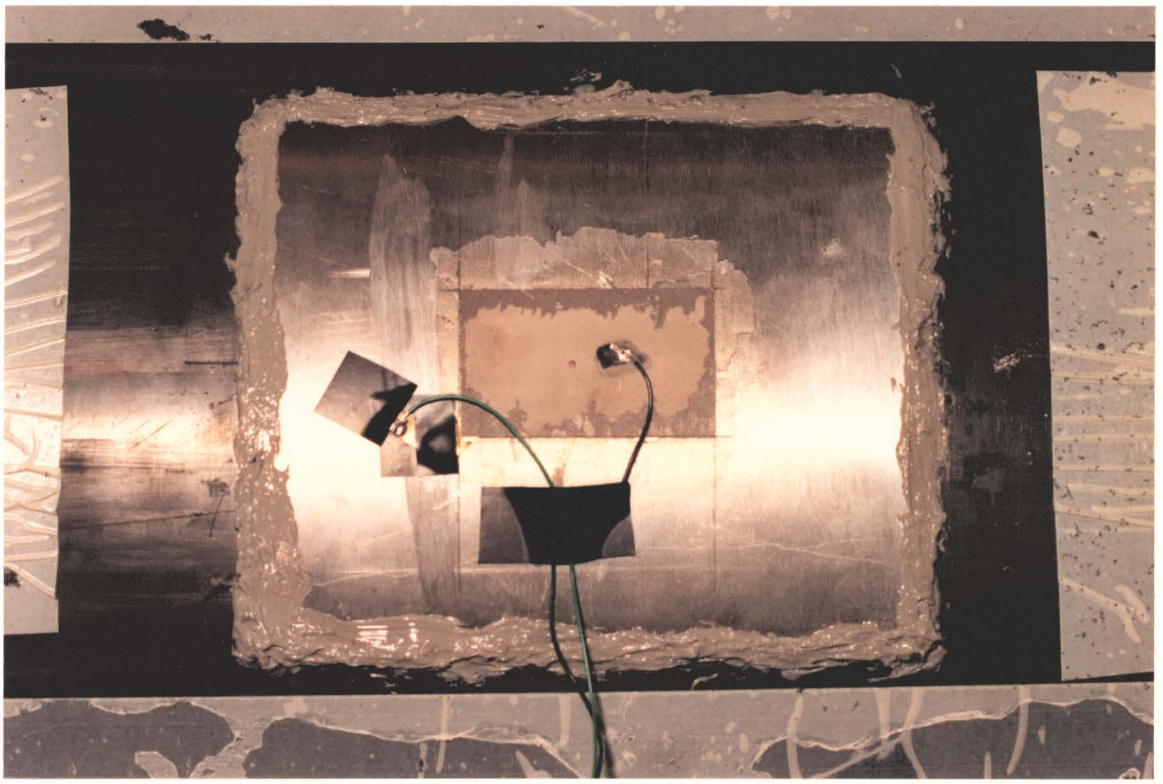

Figure 3.10 -- Source panel used in experiments.

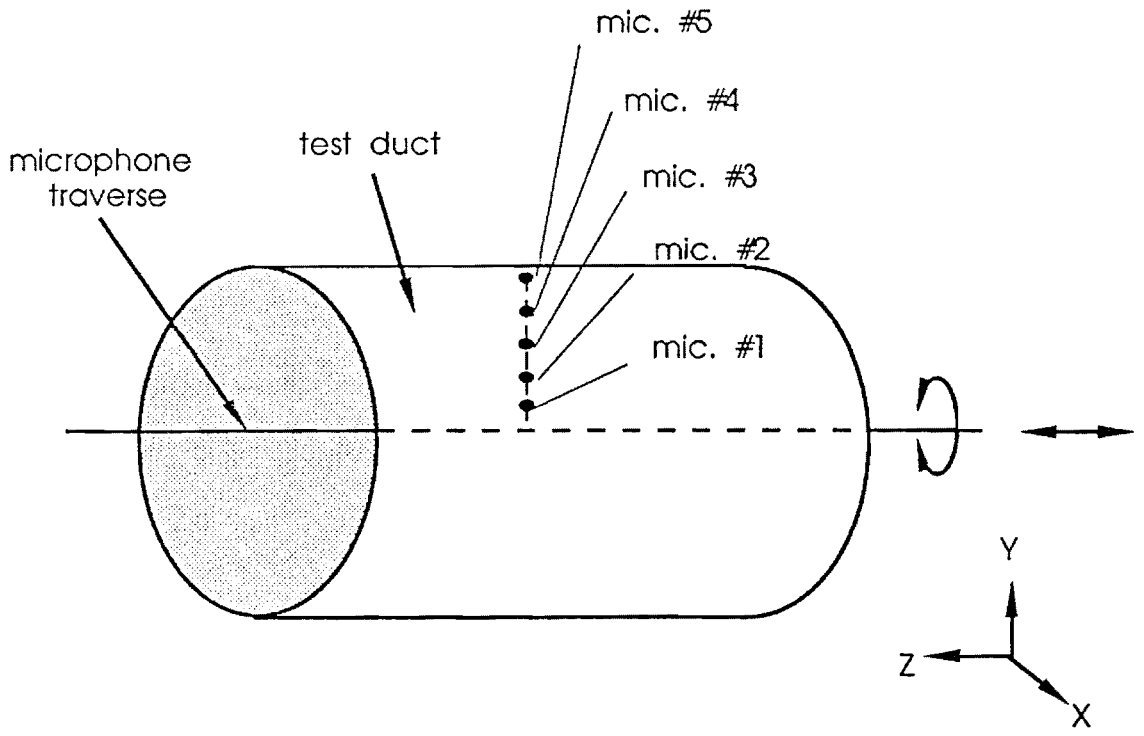

Figure 3.11 -- Microphone array used in interior sound level measurements. Array has both translational and rotational capability.

motor which rotates in 9° increments. Exterior measurements were taken over an area extending from -117° to +117°. Calibration of the microphones is detailed in Appendix D.

The experiments were conducted in a 9 ft by 14 ft by 8 ft (1.74 m by 4.27 m by 2.44 m) anechoic chamber located in Virginia Tech's Vibration and Acoustics Laboratory.

3.3.3 Modal Analysis

Measurement of the panel's natural frequencies and mode shapes were done using two methods -- 1) accelerometers, and 2) a laser doppler velocimeter (LDV). The results of this modal analysis were used to establish the boundary conditions on the panel and to estimate the amount of damping in the system. These results were then incorporated into the finite element model. To measure the panel's resonant frequencies using an accelerometer, the panel was driven by a white noise signal from the piezo while attached to the test duct. A 2-g B&K accelerometer was attached to the panel, and a B&K signal analyzer was used to process the results. Using the voltage into the transformer as the input signal and the signal from the accelerometer as the output signal, the frequency response function (FRF) was generated (see Figure 3.12). This was done for several accelerometer locations in order to detect as many modes as possible. The peaks in the FRF correspond to the panel's resonant frequencies and are summarized in Table 3.2. Because of the manner in which the panel is attached to the test duct, the motion of the panel is coupled to that of the cylinder. Several of the peaks on the FRF which do not correspond to panel resonances are thought to be influenced by cylinder resonances. The influence of these modes can especially be seen in the lower end of the frequency spectrum. An analytical solution was done for the cylinder's natural

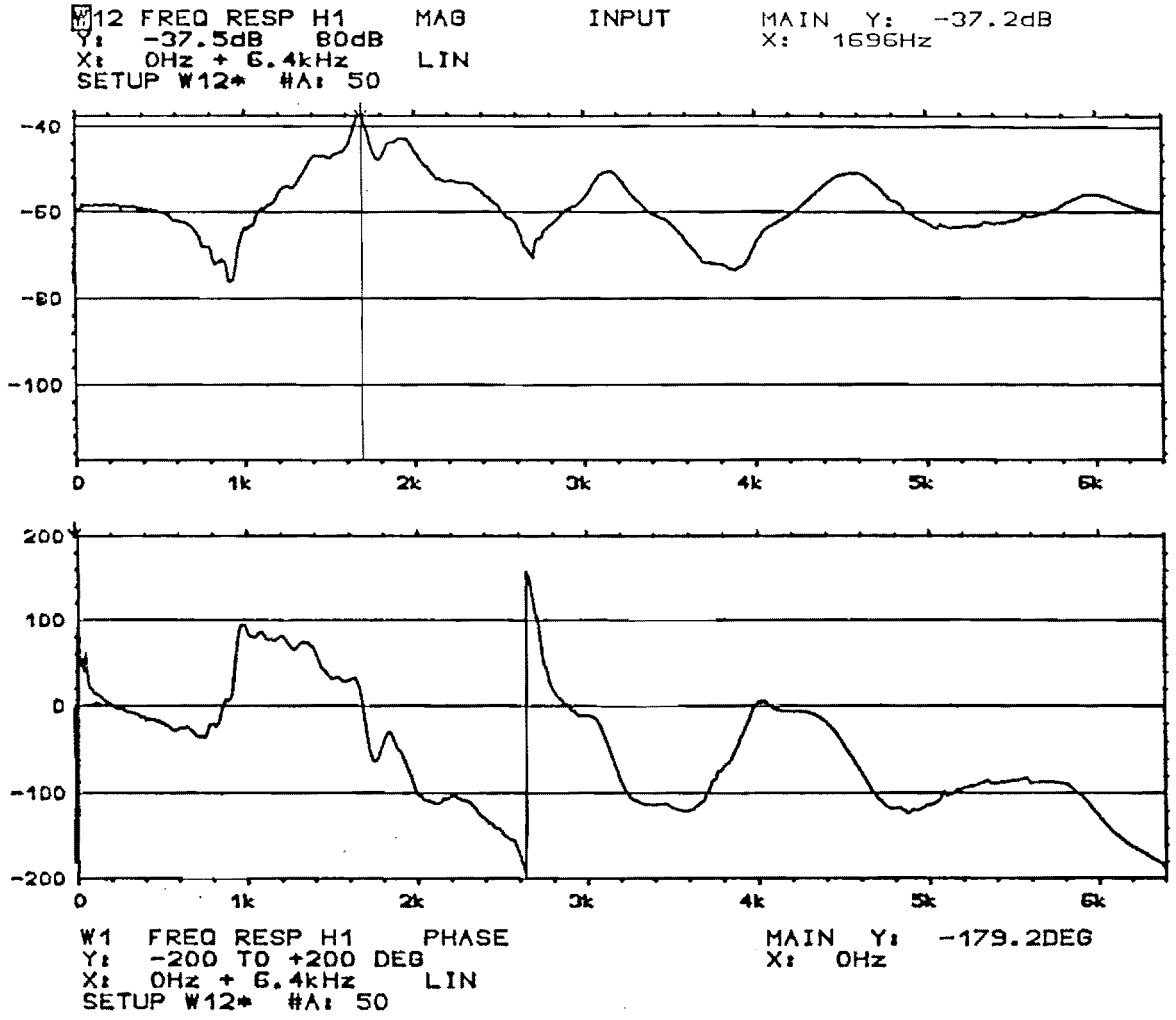

Figure 3.12 -- Frequency response function of the source panel, measured with an accelerometer.

frequencies, and this solution indicates that any cylinder modes present in the 1400 - 2000 Hz range will be of very high order and therefore of complex shape. The relative motion of the panel compared to the cylinder is discussed in a later section.

Another noteworthy feature of the FRF is the relatively high amount of damping measured. The damping was computed by measuring the frequency change over a 3 dB bandwidth, following the procedure outlined in Reference 43. For the first mode, the damping was estimated to be 5.0%. This rather high damping is thought to result from the coupling of the panel to the PVC pipe, since PVC material has high internal damping. Contributions to damping also come from the adhesive joint between panel and cylinder and from the panel's internal damping.

Next, the mode shape at 1440 Hz was measured using two accelerometers. One accelerometer was held stationary while the second accelerometer was moved over several points on the panel's surface. The FRF between the two accelerometers was measured, and the results (magnitude and phase) were used to plot the mode shape. The result was a (1,1) mode shape. Because of the time involved in plotting mode shapes by this procedure, the remaining mode shapes were generated using the laser doppler velocimeter (LDV).

Another reason for using the LDV is to evaluate the effect of the accelerometer's mass on the resulting FRF. Because no mass is added to a structure when using the LDV, it is possible to compare the two FRF's generated -- one using the LDV and one using an accelerometer -- and determine what effect, if any, the accelerometer's mass has on the FRF. The FEM analysis indicated that accelerometer mass loading is negligible, but experimental verification of this was appropriate.

The LDV used was an Ometron VPI Sensor located in the Modal Analysis Laboratory in Virginia Tech's Mechanical Engineering Department. The signal generator

used was a Hewlett-Packard 3324A, and Ometron software was used to analyze the data. All other equipment used was as previously described.

The FRF of the panel was obtained by passing a white noise signal to the piezoactuators and measuring the response -- the panel velocity -- at a given location. This location corresponds to placement of an accelerometer, and the location of the laser beam was varied several times while measuring the response in order to detect as many modes as possible. The FRF obtained using the LDV was a measurement of velocity relative to force, while the FRF obtained using the accelerometer was a measurement of acceleration relative to force. The difference between these results can be summarized as follows.

$$\omega_{dn} = \omega_n \quad \text{for } \frac{V}{F} \text{ (mobility)}, \tag{15}$$

$$\text{while} \quad \omega_{dn} = \frac{\omega_n}{\sqrt{1-\zeta^2}} \text{ for } \frac{A}{F} \text{ (accelerance)}. \tag{16}$$

Here the damping is assumed to be viscous. These results would indicate that the results obtained using the LDV (the mobility FRF) would yield resonances that are lower in frequency that those obtained using an accelerometer, all other factors being equal, because for the accelerance plot, $\omega_{dn} > \omega_n$, and ω_{dn} is what is actually measured. The difference between damped and undamped natural frequency increases with increasing damping, as can be seen in Equation 16. However, the mass of the accelerometer can be expected to lower the resonant frequencies seen on the accelerance FRF relative to those obtained using the LDV, since the LDV method introduces no mass loading effects. Because these effects counteract each other, the resonant frequencies obtained using the LDV could be either higher or lower than those obtained using the accelerometer

method, depending on which of these two effects -- damping or mass loading -- is dominant.

The FRF obtained using the LDV is shown in Figure 3.13. The resonant frequencies obtained using the LDV are slightly lower than those obtained using the accelerometer method for all but the third mode. This indicates that the damping effect more than counterbalances the mass-loading effect of the accelerometer. The magnitude of the difference between the two sets of results is less than 2% for each mode. Thus, the LDV results may be interpreted as a validation of the results obtained using the accelerometer method, and verification of the FEM's prediction of negligible accelerometer mass loading.

Several mode shapes were mapped using the LDV. The procedure followed was to excite the panel via the piezoactuator, using a pure sinusoidal input signal. The laser then scanned the entire surface of the panel, measuring the transverse velocity at numerous discrete points. This data was then processed and an image of the mode shape was generated. Two examples are given in Figures 3.14 and 3.15. First, several of the FRF's peaks in the 1400 - 2000 Hz range were investigated. In each case, the (1,1) vibrational mode was clearly displayed. In viewing these figures, it should be recalled that the outer 1.25" (0.0318 m) of the panel was joined to the cylinder surface. Therefore, a substantial portion of the mode shape shown is actually a display of the cylinder vibration rather than the panel vibration. For example, in Figure 3.14, the panel's (1,1) mode is displayed as a set of concentric elliptical rings in the center of the panel. The remainder of the panel, or about 40% of the panel's surface area, is attached to the cylinder and shows relatively little movement compared to the panel's "hot spot", or center.

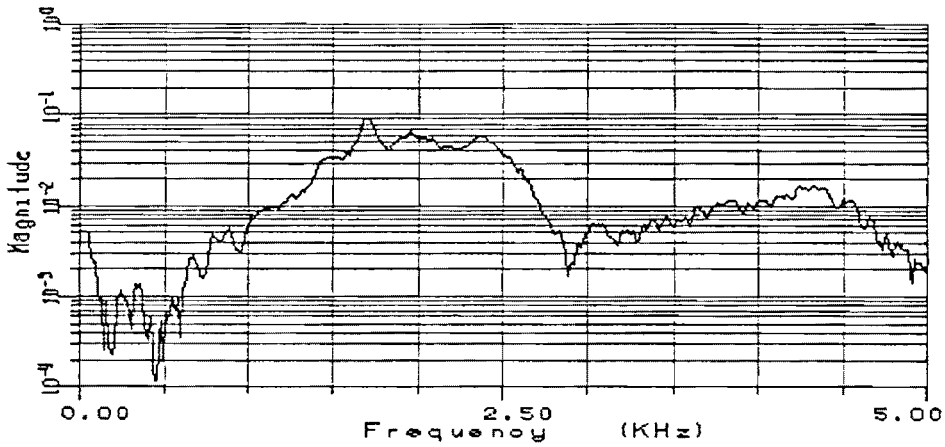

Figure 3.13 -- Frequency response function of the source panel, measured with the laser doppler velocimeter (LDV).

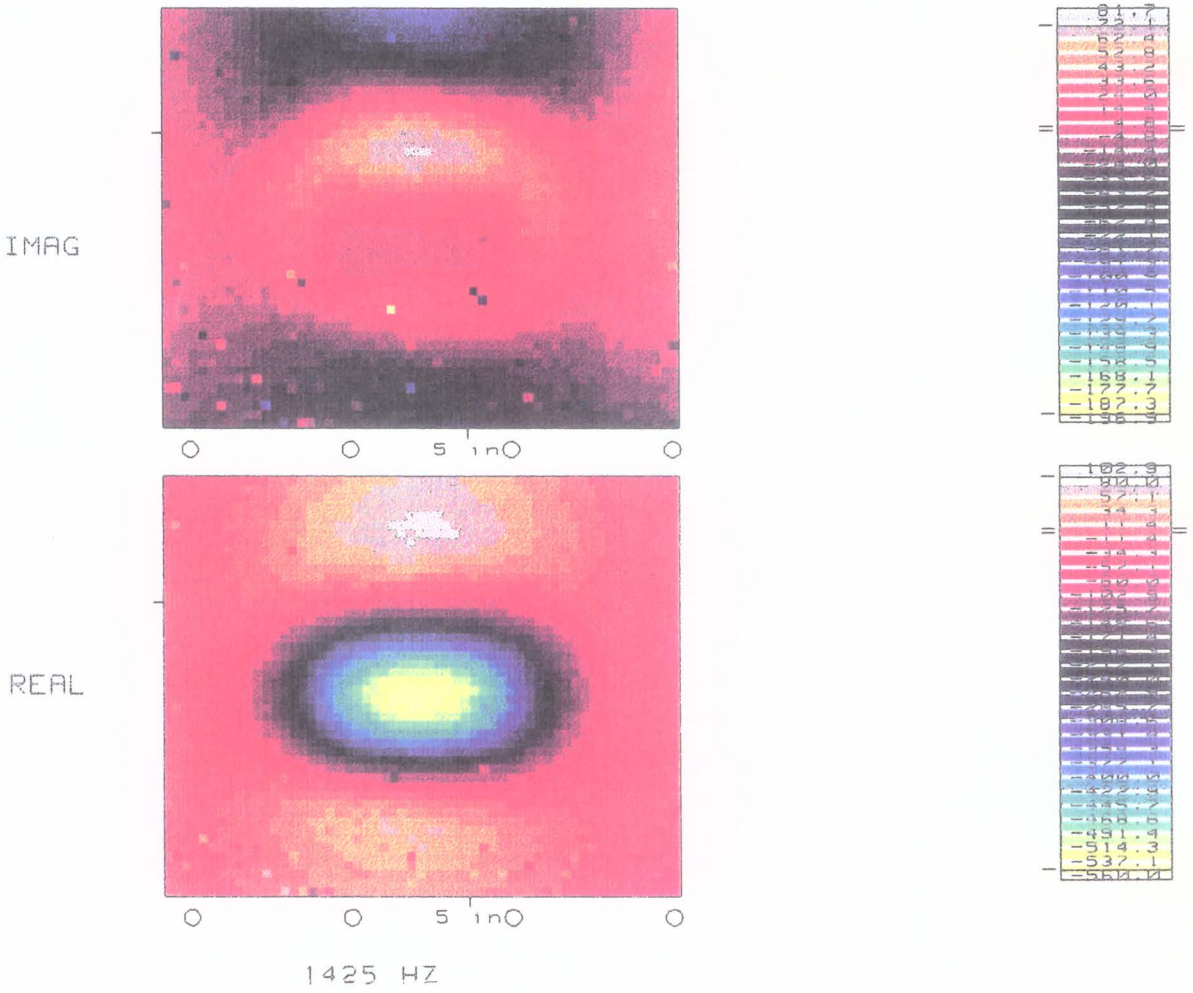

Figure 3.14 -- (1,1) mode shape, measured at 1425 Hz.

Although the (1,1) mode is excited over a frequency range of 1400-2000 Hz, the panel's fundamental frequency occurs at about 1700 Hz. Several other peaks of smaller magnitude are thought to result from superposition of the panel's (1,1) mode and various cylinder modes. Near the higher end of this frequency range, contributions could also be measured from higher-order panel modes because of the amount of damping involved. Further mapping of mode shapes indicates that the second mode, or (2,1) mode, occurs at about 2388 Hz. This mode is shown in Figure 3.15. It is apparent from both the velocity values measured and the amplitude of its peak on the FRF that this mode is much weaker in amplitude than the (1,1) mode. This is to be expected, since the piezoactuator used to drive the panel was positioned at the panel's approximate center and parallel to the panel's edges. Thus, it is not to be expected that a strong response at the (2,1) resonance would be generated, since the (2,1) mode has a nodal line centered beneath the piezoactuator.

Similarly, the next two modes, or the (1,2) and (2,2) modes, which also have nodal lines centered beneath the actuator, would not be expected to generate a large response, and this was verified in the experiments. The next mode to generate a clear mode shape was the fifth, or (3,1), mode, shown in Figure 3.16. The (3,1) mode was identified at 4300 Hz.

A comparison of experimental and FEM results was presented in Table 3.6. A rather large discrepancy in results occurs at the (2,1) mode. The experimental results for the other modes are within about 10% of the FEM prediction. The experimental result for the (1,1) mode, which is the mode of interest in this study, differs from FEM prediction by about 3%. Of course, the finite element model could be refined further in order to decrease the error, if necessary. However, for the purposes of this study the model yields satisfactory results as is.

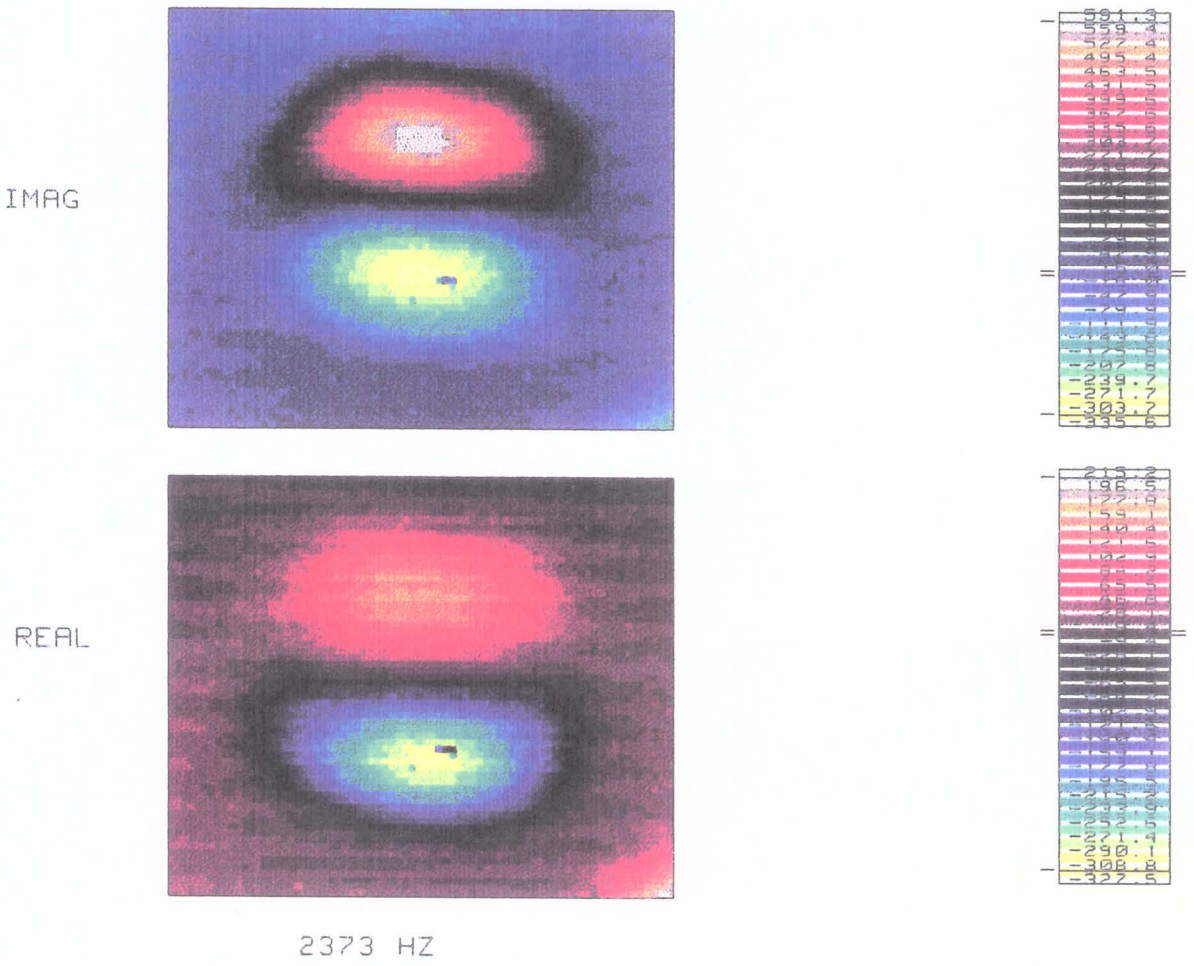

Figure 3.15 -- (2,1) mode shape, measured at 2373 Hz.

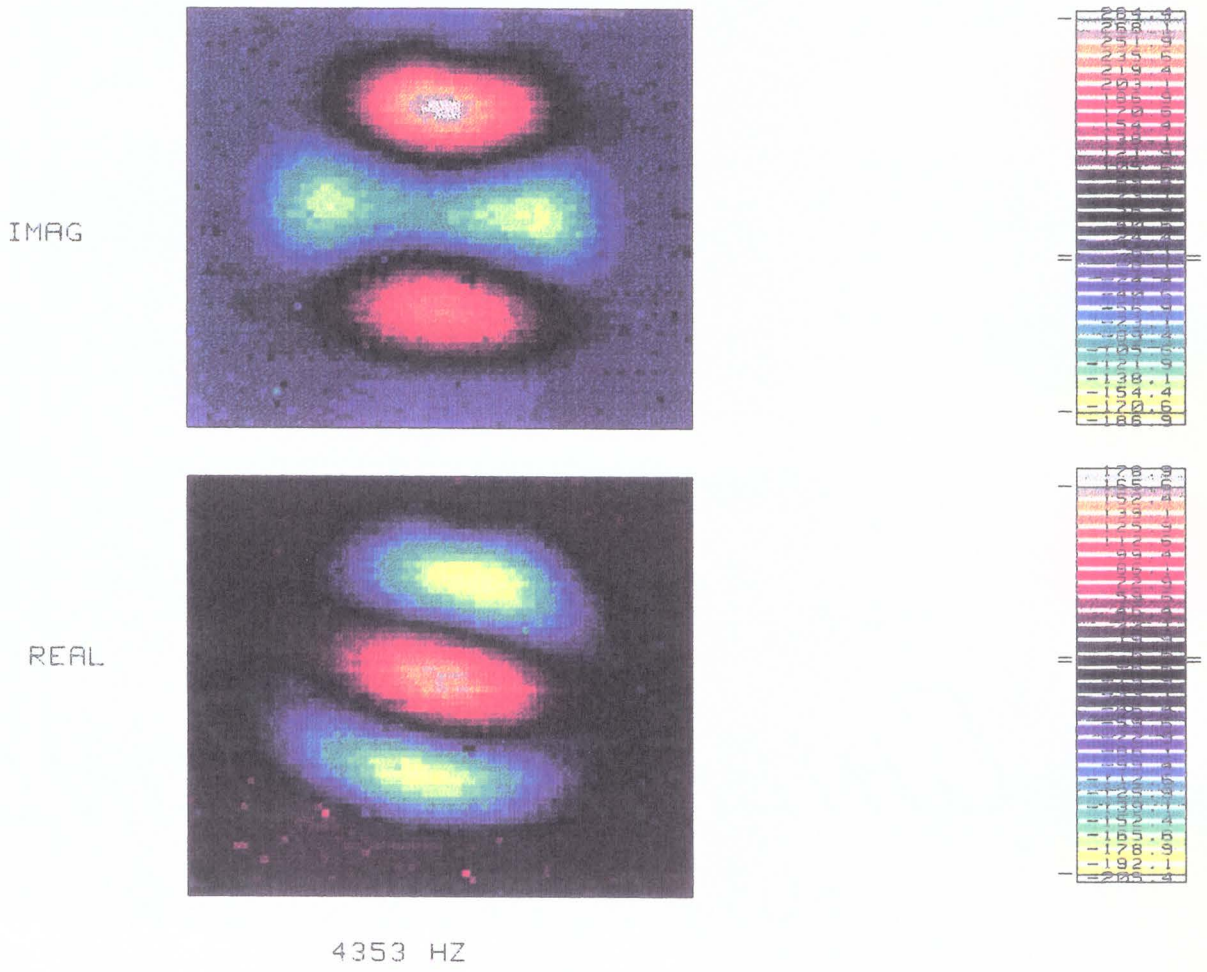

Figure 3.16 -- (3,1) mode shape, measured at 4353 Hz.

It may be beneficial here to reiterate two points: 1) why this modal analysis was done, and 2) why the FEM was developed. First, modal analysis of the panel was emphasized because it is important to know where the (1,1) mode is, and over what frequency range it can be excited. The reason for this is the (1,1) mode of vibration will yield the most efficient acoustic radiation. Second, the FEM was developed and refined so that it may be used as a design tool. Knowing how to specify the restraints, or boundary conditions, on the panel has proven to be the key to generating an FEM model capable of predicting panel resonances with reasonable accuracy. Of course, any change in the physical mounting configuration, including a change in cylinder material, will change the boundary conditions of the panel, and so will necessitate changes in the FEM to reflect the alteration in the physical system.

3.3.4 Measurement of Panel Velocity

The velocity at the center point of the panel was obtained using an accelerometer. This measurement was taken to provide a comparison for the finite element model results, as discussed in Section 3.2.4.

The velocity measurement was taken as follows. A 2-gram B&K accelerometer was attached to the center point of the panel using beeswax. Since this point is on the piezoactuator, the accelerometer was electrically insulated from the piezoactuator using electrical tape. The panel was then excited by applying a 100 V_{rms}, 1800 Hz sinusoidal signal to the actuator, and the panel's velocity was measured directly. The procedure was repeated several times, with good repeatability, and the velocity measured averaged 0.0234 m/s. The equivalent rms displacement is thus 2.07×10^{-6} m, corresponding to a maximum displacement of 2.93×10^{-6} m. The finite element model predicts a maximum displacement of 4.76×10^{-6} m for the same excitation voltage and frequency.

Chapter 4 Experimental Work

4.1 General Acoustic Characteristics

4.1.1 Panel Response vs Actuator Configuration

In addition to the structural testing of the panel, already described, some general acoustic characteristics of the sound source were investigated. The first test of the source panel's acoustic properties was to drive the panel over a range of frequencies and measure the acoustic pressure at several arbitrary microphone locations inside the test duct (the experimental rig is described in Section 3.3.1). This was done by exciting the piezoactuator(s) with a white noise signal. The panel was driven in four different modes -- 1) outside -- only the actuator on the outer surface of the panel was driven; 2) inside -- the actuator on the inside panel surface was driven alone, 3) bending -- the outside and inside actuators were driven 180° out of phase, and 4) stretching -- the outside and inside actuators were driven in-phase. In this experiment, the voltage into the transformer was held constant at 0.500 V_{rms}, and the acoustic response was measured in rms voltage also. Each measurement was taken at five arbitrary microphone locations corresponding to z = 2" (0.0508 m), θ=165°, and r = 1", 2.5", 4", 5.5", and 7" (0.0254, 0.0635, 0.1016, 0.1397, and 0.1778 meters, respectively).

The results show the same general form as the structural FRF -- relatively smooth peaks centered near f = 1700, f = 4500, and f = 6000 Hz. However, superimposed on these general curves are several sharp peaks that do not appear on the structural FRF. These are believed to correspond to acoustic resonances of the cylindrical cavity. A typical acoustic response curve is shown in Figure 4.1. In this case, the outside piezo alone was driven, and the downstream end of the duct was fitted with an anechoic

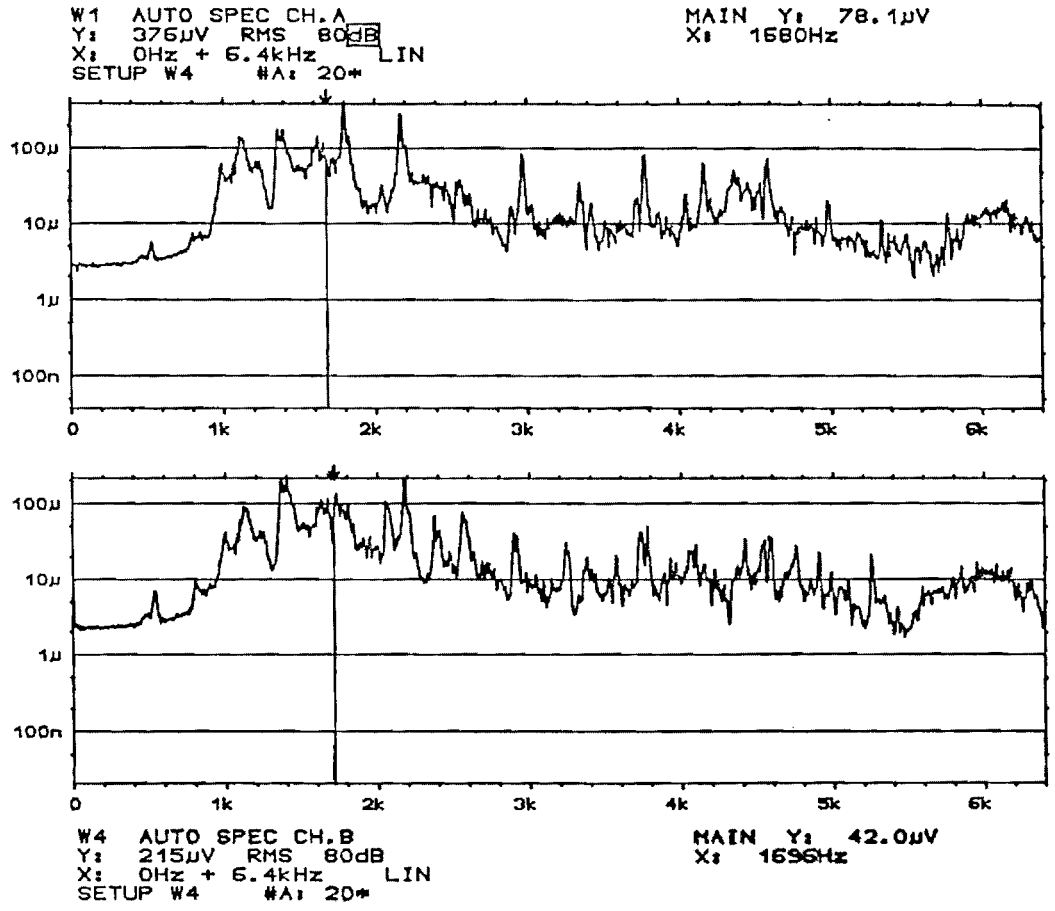

Figure 4.1 -- Response curve, measured inside the test duct.

termination. The upper and lower graphs of Figure 4.1 refer to microphone #1 and #2. The tests were repeated for rigid termination of the downstream end, as well, with the same form of the response curve resulting. In addition, all four excitation modes -- outside, inside, bending, and stretching -- produced the same general form of the response curve, although there were differences in the magnitude of the response.

It is interesting to compare the relative responses of the four excitation modes -- inside, outside, bending, and stretching. All four modes produced the same form of the response curve, as previously described. However, the amplitude of the response varies greatly from one excitation mode to another. The results, plotted in Figure 4.2 in 25-Hz increments for microphone #5, are somewhat unexpected.

It is appropriate to preface further discussion of the experimental results with a summary of theoretical principles underlying the generation of transverse vibrational modes using in-plane piezoactuators. The relationship between input voltage and induced strain may be written as follows:

$$\varepsilon = d_{31}\frac{V}{t_a} \tag{17}$$

where d_{31} is the piezoelectric strain coefficient of the actuator material, V is the applied voltage, and t_a is the thickness of the actuator. This relationship is discussed more fully in Dimitriadis, et al [38], but some important results are summarized here. The analytical model results derived for flat structures (beams and plates) are summarized in Appendix C. For a flat plate, when one actuator is driven alone, the resulting load is a combined bending moment and an axial force applied along the edges of the driven actuator at the neutral surface of the panel. The bending moment is created by application of the in-plane forces generated by the actuator to points which are off the

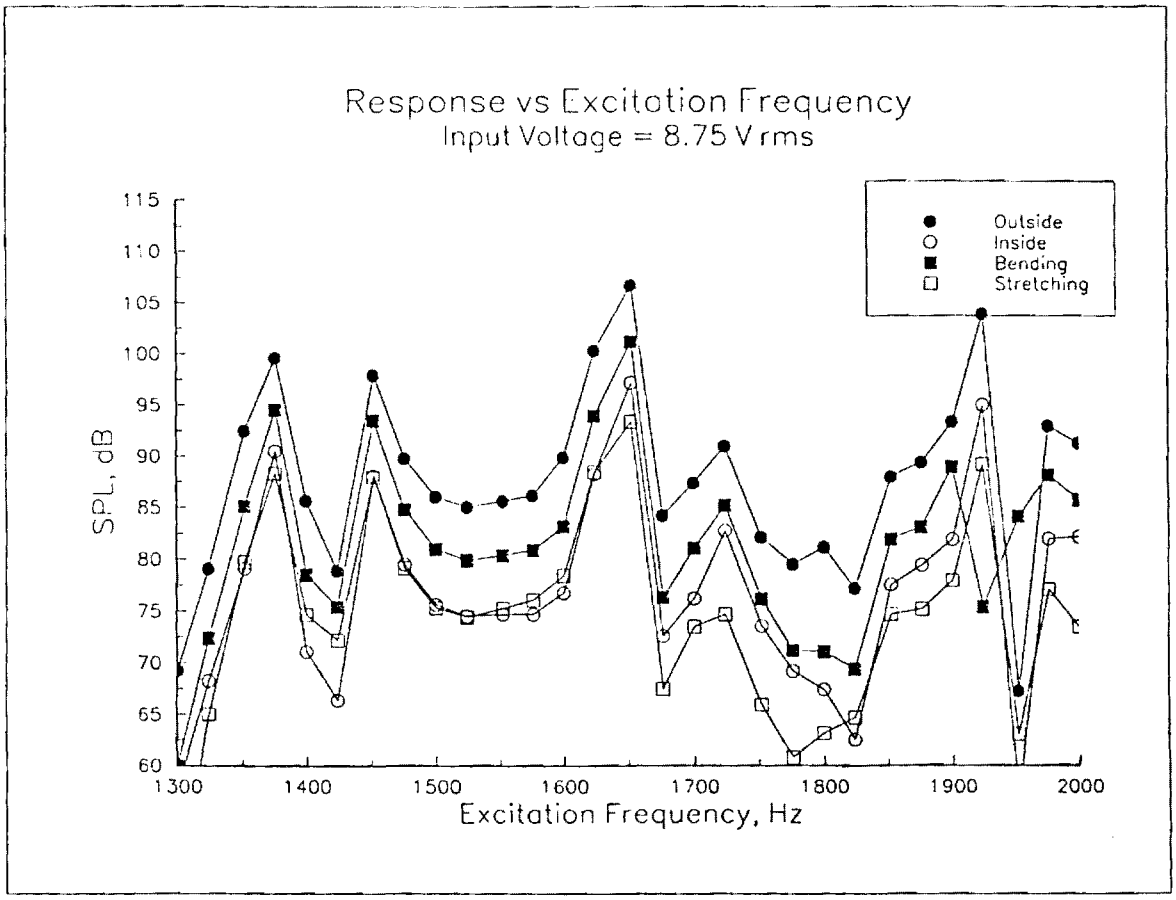

Figure 4.2 -- Acoustic response to white noise excitation: comparison of four excitation modes.

neutral surface of the panel. This bending moment will then tend to generate out-of-plane, or transverse, displacement of the panel. In a curved structure, the axial force will do the same, because in a cylindrically curved structure such as this panel, out-of-plane motion is coupled to the in-plane motion of the axial load. The amplitude of this out-of-plane displacement is a function of excitation frequency, the structure's dynamic and material properties, input voltage to the piezoactuator, actuator geometry, placement, and material properties, and the actuator's piezoelectric strain coefficient.

Since the inside and outside piezoactuators used in this experiment are of the same geometry and piezoelectric properties, and since the two actuators are symmetrically bonded to the panel, it could be expected from the flat plate model that the inside and the outside actuator, each activated alone, should generate the same response to a given excitation voltage and frequency, based on flat plate models. However, as the results in Figure 4.2 show, this was not the case in this experiment.

For a flat plate, when both actuators are driven together at the same voltage and frequency as either the outside or inside actuator driven alone, the panel can be expected to respond in a different manner, depending on whether the actuators are driven in-phase or out-of-phase. When the actuators are driven 180° out-of-phase, the resulting bending moment is theoretically twice that of one actuator driven alone.

When both actuators are driven in-phase, the resulting load in a flat plate is pure tension alternating with pure compression. Because the forces resulting from the actuators are symmetrically positioned about the neutral surface and are equal in magnitude, no bending moment results. However, because the panel is a curved structure, out-of-plane displacement is expected to result. The results of Figure 4.2 show that the acoustic response due to bending is about three times the response due to

stretching. This result is not unexpected, as flat plate theory predicts zero bending moment for the stretching mode.

Having reviewed the theory, it is now appropriate to discuss the experimental results. One interesting result of this experiment is that the largest response was generated by the outside excitation mode. Based on flat plate theory, it could be expected that the bending excitation mode would generate the largest response, since it produces a bending moment that is twice that produced by the outside mode. Moreover, flat plate models predict the inside and outside excitation modes would generate equivalent results, since the two actuators are equivalent in material and geometry. However, the experimental results show that this outside mode produced acoustic pressure of about twice the magnitude of that generated by the inside mode.

Another interesting result is that the outside excitation mode produced a greater response than the bending mode. This was quite unexpected, as theory predicts a greater response for two actuators driven out-of-phase than for one actuator driven alone. This is true even if the two actuators driven out-of-phase do not produce the same load on the panel. For instance, if due to deterioration in piezoelectric strain coefficient, one actuator produces a force, P, while the other actuator produces a force of only $\frac{P}{2}$, it can be shown that the resulting load for the excitation mode is a moment of magnitude $\frac{3Pb}{4}$, where b is the thickness of the panel. However, if only one piezoactuator producing a force, P, were driven, as in the outside or inside excitation mode, then the resulting moment would have a magnitude of only $\frac{Pb}{2}$.

These experiments were repeated several times using different panels, actuators, and varying the excitation voltage and frequency. Each time the same general results

were observed. The most plausible explanation is that the curvature effects of the panel alter the response characteristics to such an extent that the general trends predicted by the flat plate models do not hold for curved structures for all excitation modes.

4.1.2 Response vs Excitation Voltage

The next experiment was to investigate the acoustic response as a function of input voltage to the piezoactuators. The panel was driven, in each of the four excitation modes, in 8.75 V_{rms} increments from 8.75 to 175 V_{rms}. The actuators were driven with a sinusoidal input signal at a frequency of 1800 Hz in each instance. The response was measured at one arbitrary microphone location outside the duct (1.6 meters from the duct inlet at an angle of -45° relative to the duct axis). The results are given in Figure 4.3. The response varies linearly with input voltage, as expected from theoretical prediction, up to about 105 V_{rms}, when the response begins to fall off somewhat, probably due to decay of the piezoelectric properties at high voltage. These results were obtained while driving the inside actuator alone. Figure 4.4 shows the results over the linear range (up to 105 V_{rms}). These results were measured inside the duct at an arbitrary microphone location, z = 2" (0.0508 m), θ =165°. They show the response for all four modes of actuator excitation -- outside, inside, bending, and stretching. The relative magnitude of the response for each excitation mode is discussed in a previous section. However, from this experiment it can be seen that the general pattern discussed in Section 4.1.1 holds for the entire voltage range investigated here. That is, the greatest response is generated by the outside mode, followed by the bending, inside, and stretching modes. These results were utilized to advantage in further experimental work. It is known that piezoelectric properties deteriorate over time, if the applied voltage level exceeds a certain level. By

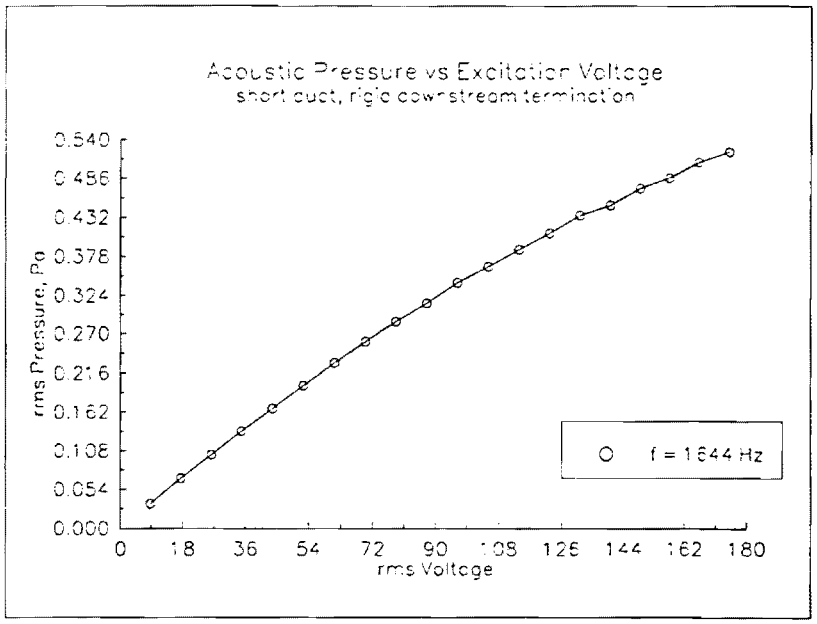

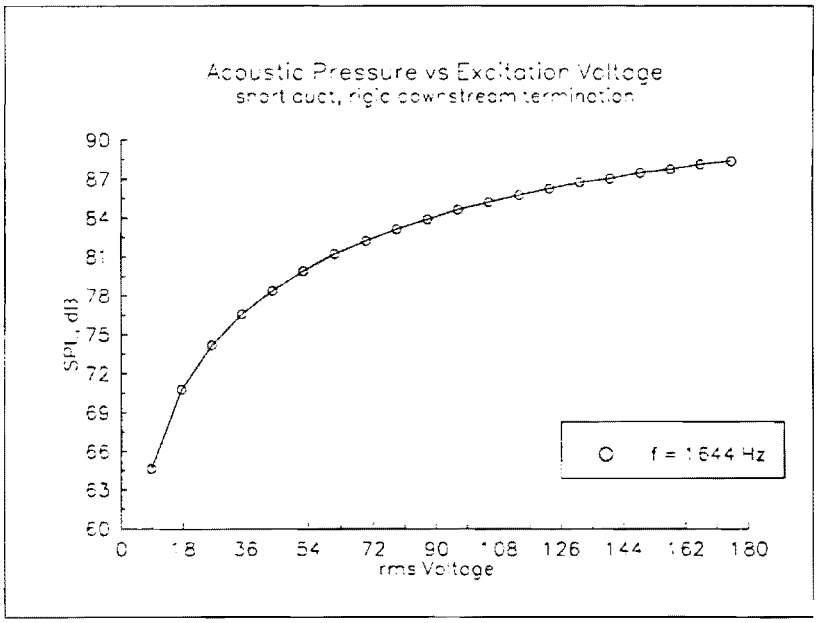

Figure 4.3 --Acoustic response as a function of piezoceramic excitation voltage: inside actuator excitation mode.

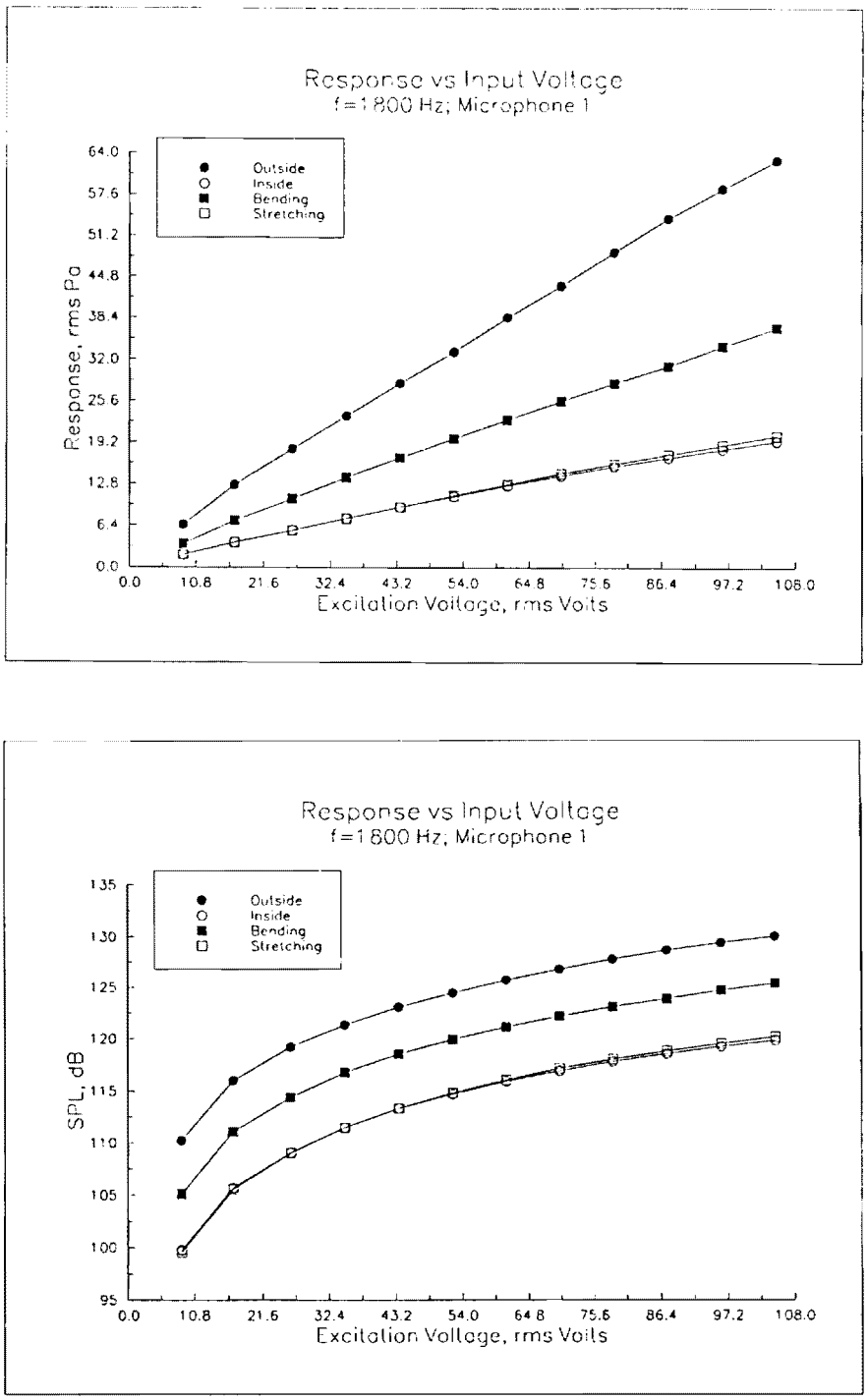

Figure 4.4 -- Acoustic response as a function of piezoceramic excitation voltage: comparison of four actuator excitation modes.

limiting the input voltage level to within the safe range, it is possible to conduct extended testing without experiencing any variation in piezoelectric properties that could contaminate the results. Also, by determining the relationship between input voltage and panel response, it is possible to scale the results from low-voltage experiments by an appropriate factor in order to ascertain the response at higher voltage levels. This was the approach taken in this work.

4.2 Interior Response Measurements

As described in Section 3.3.1, the sound field inside the pipe was mapped using an array of five 1/4" (0.0695 m) microphones. The sound field was mapped at several axial locations, and at different frequencies. For each measurement, one end of the cylinder was open while the other end was fitted with an anechoic termination (a 4" conical-shaped layer of open-cell foam). For each test, an input voltage of 8.75 V_{rms} was used, and only the outside actuator was driven. This voltage level is well within the "safe" region of voltage, ensuring that the piezoelectric properties will not change appreciably during the testing. The long pipe was used in all cases.

Two parameters were of interest in these studies -- the overall sound pressure levels generated, and the effect of axial location on the sound measurements.

4.2.1 Sound Levels Generated

Sound measurements were taken at each of the five microphone locations as the array was rotated about the test duct axis in 30° increments. Each measurement was recorded in millivolts and was converted to pressure (in Pascals) using the sensitivity factor appropriate for each microphone (see Appendix D for details). From the

computed value of pressure at each measurement location, the overall average sound pressure level for a particular plane was computed by the following formula:

$$SPL_{avg} = 10 * \log\left[\frac{\sum_{i=1}^{5} p_i^2 A_i}{A_t \rho_0 c I_{ref}}\right], \qquad (18)$$

where p_i = average rms pressure at the i^{th} microphone,

A_i = the area subtended by the i^{th} microphone,

A_t = total area of the plane ($=\sum_{i=1}^{5} A_i$), and

$I_{ref} = 10^{-12}$ W/m^2.

Results are given in Table 4.1 for the case of 1800 Hz, measured at z = 0" (the source plane) and at a location 12"(0.3048 m) from the source plane, toward the open end of the test duct. Two points are immediately obvious: 1) the variance of the results across a given plane, and 2) the decay in results with axial distance from the source. This second point will be addressed in the next section. The sound pressure level at the source plane varies from 111 dB at microphone 1 (the microphone closest to the center of the duct) to 87 dB measured at microphone 3 (located 3" away from microphone 1). This 24 dB, area-averaged variance indicated that the sound field is not a diffuse field, as might have been expected. At a plane 12" toward the open end of the pipe, the variance has decreased to 13 dB, and the region of highest pressure is still the center of the plane. The decrease in variance indicates that the sound energy is distributing itself more uniformly over the duct cross-section as the sound waves progress down the duct and reflect off the duct walls. The fact that the region of highest pressure is in the center of the duct indicates that the waves are reflecting more or less normally from the pipe walls, rather

than moving in a "spiral-tangential" manner along the duct wall. This general pattern suggests the dominant acoustic mode is of large radial order and small circumferential order [45]. Indeed, calculation of the duct cutoff frequencies does indicate that the excitation frequency of 1800 Hz will excite the (0,3) acoustic mode.

Of particular interest is the magnitude of the acoustic response generated, because the effectiveness of the secondary source in an active control system depends to a great extent on the ability of this source to generate sufficiently high acoustic levels.. These measurements were taken at a very low voltage level (8.75 V_{rms}) and the response can be expected to increase with voltage. Indeed, previous experiment shows a linear relationship between voltage and pressure over a wide range, so for example, the 95 dB average sound pressure level measured at z = 12" can be expected to translate to a 20 dB increase for a ten-fold increase in voltage. These piezoactuators are capable of withstanding voltage levels up to about 450 V_{p-p}, or 160 V_{rms}. However, the voltage-to-pressure relationship is non-linear above about 105 V_{rms}. Still, 95 dB SPL at 8.75 V_{rms} corresponds to about 119 dB at 160 V_{rms}.

The sound levels generated can be further increased by installing multiple source panels in the duct. Each doubling of the number of sources can be expected to generate a 6 dB increase in sound pressure level. Of course, the number of sources that can be installed in a particular duct will be limited by the size of the source and the duct. Still, interior pressure levels of this magnitude are very encouraging.

Table 4.1 -- Interior sound pressure measurements taken in the long pipe. Excitation frequency is 1800 Hz, and input voltage = 8.75 V_{rms}.

axial location	mic. #1	mic. #2	mic. #3	mic. #4	mic. #5	plane average
source plane	111	108	87	103	99	103
z = 12"	102	92	98	95	89	95

4.2.2 Response vs Axial Location

The plane-averaged sound pressure levels were observed to decrease from 103 dB at z = 0" to 95 dB at z = 12", or a decrease of 8 dB over a distance of less than two wavelengths. This decay can be attributed to three factors. First, the test duct walls are not completely rigid, and a portion of the sound energy is transmitted through the wall rather than reflected back into the pipe cavity. Second, some loss of acoustic energy is associated with losses in the fluid medium as the acoustic energy is degraded to thermal energy. Third, at the source plane (z = 0"), the response is composed of both propagating waves and the decaying waves of acoustic modes with cutoff frequencies above the excitation frequency (1800 Hz). This near-field effect diminishes with distance from the source until only the effects of the propagating waves remain. Thus, the 8 dB drop from the z = 0" plane to the z = 12" plane can be attributed to a combination of energy absorbed by the pipe walls and the decaying strength of the higher-order modes. This effect is further discussed in Section 5.3.

4.3 Exterior Radiation Measurements

While the interior sound pressure fields are of general interest and are very important in terms of positioning the secondary sources in an active control system, radiation of sound energy to the atmosphere external to the duct is of particular interest in aircraft engine noise studies. If the sound energy inside the duct were not radiated outward, there would be no noise problem associated with the inlet duct. It is known that ducts whose dimensions are small compared to acoustic wavelength are very inefficient radiators of acoustic energy [45]. Unfortunately, engine inlet design is such that the acoustic wavelengths are typically much smaller than the dimensions of the duct, so that almost all the acoustic energy inside the duct is radiated outward. For example, in this

study, the acoustic wavelengths are on the order of 8 in. (0.20 m), while the duct diameter is 17 in. (0.43 m), or twice as large as the wavelength. Because of these considerations, the exterior as well as the interior acoustic radiation was measured experimentally.

Sound measurements were taken around the entrance of the pipe at a radius of 1.6 meters. The measurements were taken in increments of 9°, from -117° to +117°, where 0° coincides with the axis of the test duct (see Figure 4.5). Measurements were taken not only to characterize the acoustic radiation from the open end of the pipe, but to evaluate the effects of excitation frequency, test duct end termination (anechoic vs rigid), test duct length, and input voltage. These experiments are described in the following sections.

4.3.1 Response vs Excitation Frequency

Four panel excitation frequencies were considered -- f = 1708 Hz, which is the panel's fundamental frequency; also f = 1644 Hz, an off-resonance frequency which is near an acoustic resonance, and f = 1800 Hz and f = 2056 Hz, chosen arbitrarily. For these tests, the long pipe was used, and the downstream end was fitted with an anechoic termination. The results are shown in Figure 4.6. It is interesting to note the relative magnitudes of the response. The highest response levels are those associated with f = 1708 Hz and f = 1644 Hz. Since these correspond to a structural and an acoustic resonance, respectively, this result is not surprising. The average response at these two frequencies, found by averaging the pressure at each measurement location and converting this average pressure to sound pressure level, is about 63 dB. It is interesting to note, however, that from -90° to 0°, the 1644 Hz response is greater, while from 0° to +90°, the 1708 Hz response is. Both the 1644 Hz and the 1708 Hz response exceed the off-resonance responses significantly. For the 1800 Hz case, the average difference is

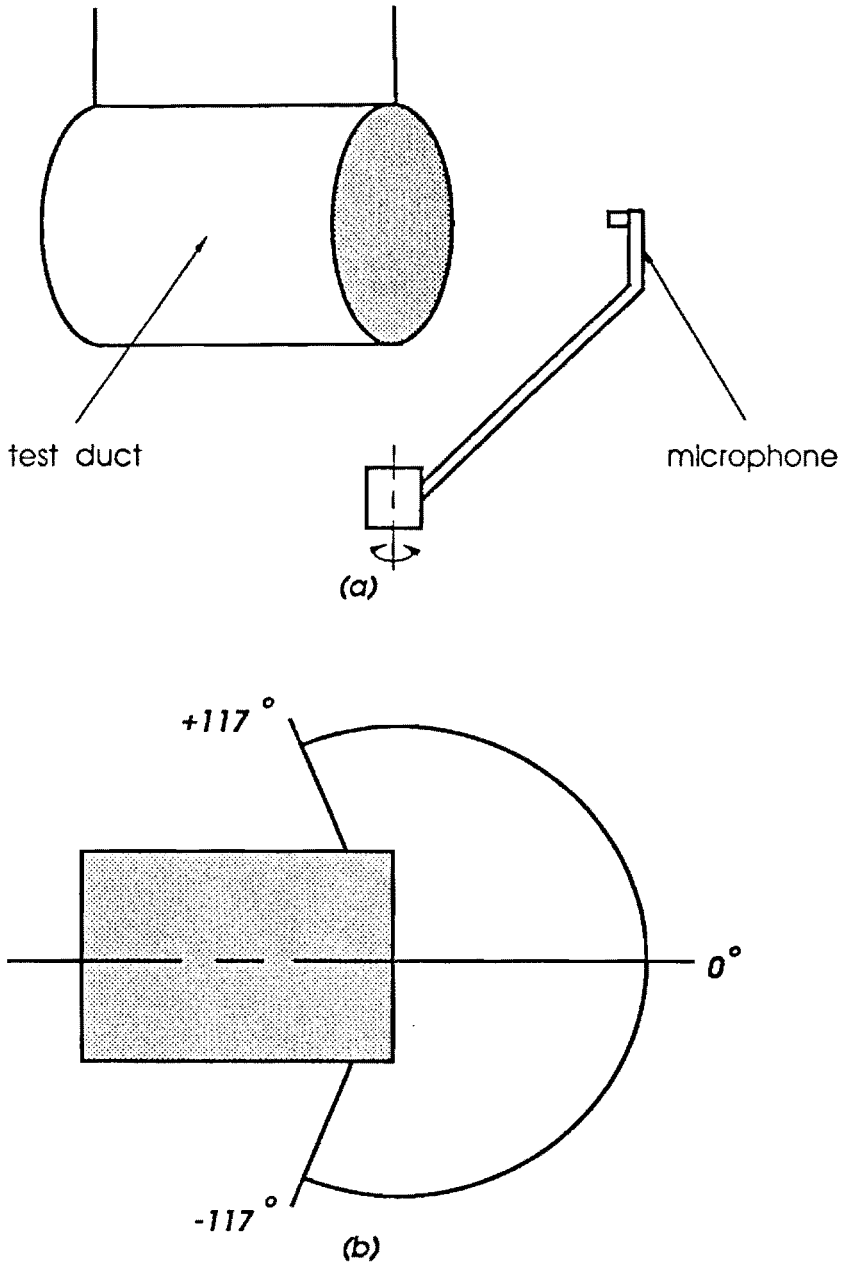

Figure 4.5 --Schematic of exterior sound level measurement setup: a) test duct and microphone; b) top view of test duct, showing the area traversed by the microphone.

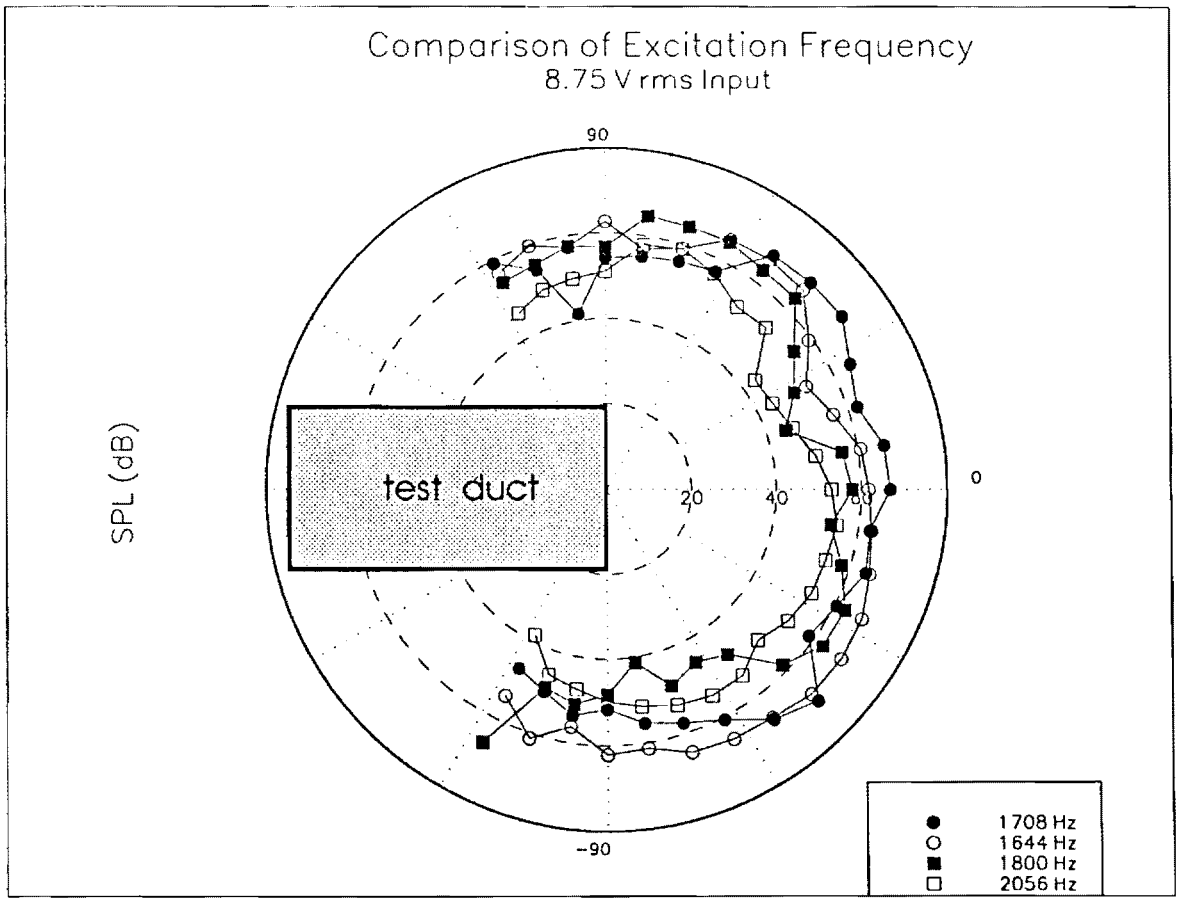

Figure 4.6 -- Sound pressure level measurements taken outside the long duct fitted with an anechoic downstream termination.

about 4 dB, while the 2056 Hz response is 10 dB weaker. These results, as well as those of other experiments run, are tabulated in Table 4.2, cases 1-4.

4.3.2 Effect of Duct End Termination

Next, the effect of the downstream termination was investigated. Experiments were run for two different terminations: 1) foam, to represent an anechoic, or semi-infinite, termination, and 2) rigid. In the rigid case, a 3/4" thick plywood end cap was bolted to the end of the pipe, and the interface was sealed with modelling clay. Two excitation frequencies were considered -- 1708 Hz (structural resonance) and 1644 Hz (acoustic resonance).The results are shown in Figure 4.7 for the 1644 Hz case. The overall increase in sound pressure level is apparent. The average increase due to the rigid end cap is about 6 dB. This is in agreement with theory. Since the end cap causes the sound waves to reflect from the downstream end, the pressure level doubles, corresponding to a 6 dB increase.

4.3.3 Effect of Test Duct Length

The short test duct was used to evaluate the effect of pipe length on acoustic pressure. For these experiments, the rigid end cap was used, as the short pipe was too short to accomodate the conical foam end cap. The excitation voltage was again 8.75 V_{rms}, and the excitation frequencies studied were 1644 Hz and 1708 Hz.

The results show a slight decrease in average sound pressure level for the 1644 Hz case (1.9 dB), and, surprisingly, a significant decrease (9.2 dB) for the 1708 Hz case. This result is perhaps due to the fact that the 1644 Hz case, since it is not a structural resonance, is not appreciably affected by the change in duct length. Instead of its

Table 4.2 --Averaged results of exterior sound pressure level measurements. Results are in dB.

Case	duct	Plane Mapped	Downstream Termination	V_{rms} Input	frequency	average SPL (dB)
1	long	0°	anechoic	8.75	1708	63.3
2	long	0°	anechoic	8.75	1644	63.3
3	long	0°	anechoic	8.75	1800	59.0
4	long	0°	anechoic	8.75	2056	52.7
5	long	0°	rigid	8.75	1708	67.8
6	long	0°	rigid	8.75	1644	71.0
7	short	0°	rigid	8.75	1708	58.6
8	short	0°	rigid	8.75	1644	69.1

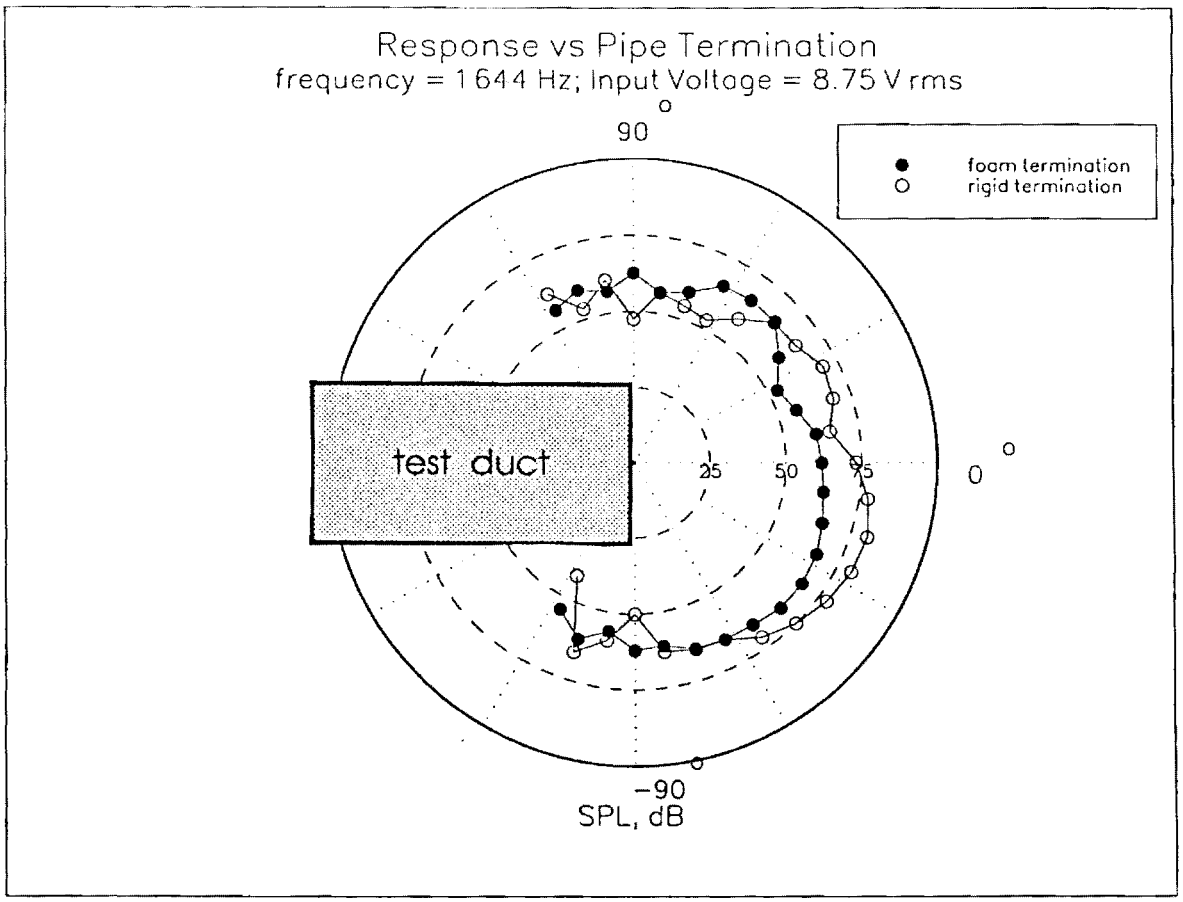

Figure 4.7 -- Effect of downstream termination on sound pressure measurements.

acoustic output being generated directly from the panel surface, the acoustic output at 1644 Hz consists of the contributions from various acoustic modes having cutoff frequencies below the excitation frequency. These cutoff frequencies are dependent only on duct radius, not length, so that the change in length does not affect the excitation of these acoustic modes. The panel excites these acoustic modes inside the duct, and they in turn excite the medium outside the duct. However, in the 1708 Hz case, corresponding to the panel's structural resonance, the change in pipe length effectively moves the panel much closer to the open end of the pipe (4" from the inlet edge to the panel's forward edge, vs 16" for the long pipe) and so alters the acoustic medium that the panel "sees". In the long pipe case, the panel radiates into a space effectively constrained by the pipe geometry. However, in the short pipe case, because the panel is so close to the open end of the pipe, the panel is effectively radiating into not only the pipe cavity but the open area beyond as well. The resulting decrease in specific acoustic impedance would have the effect of decreasing the pressure levels generated for a given panel velocity distribution. These results are shown in Figures 4.8 and 4.9.

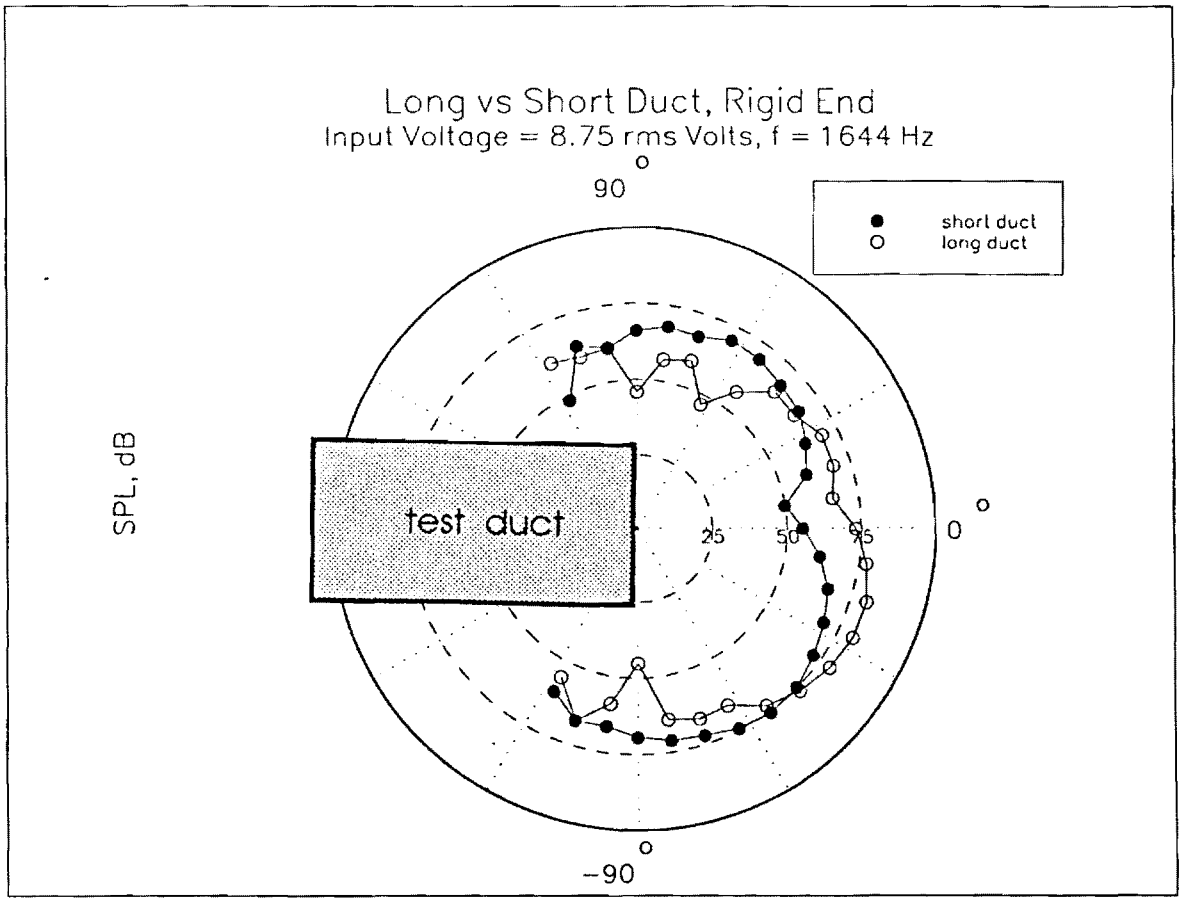

Figure 4.8 -- Effect of duct length on exterior sound pressure radiation. Excitation frequency = 1644 Hz.

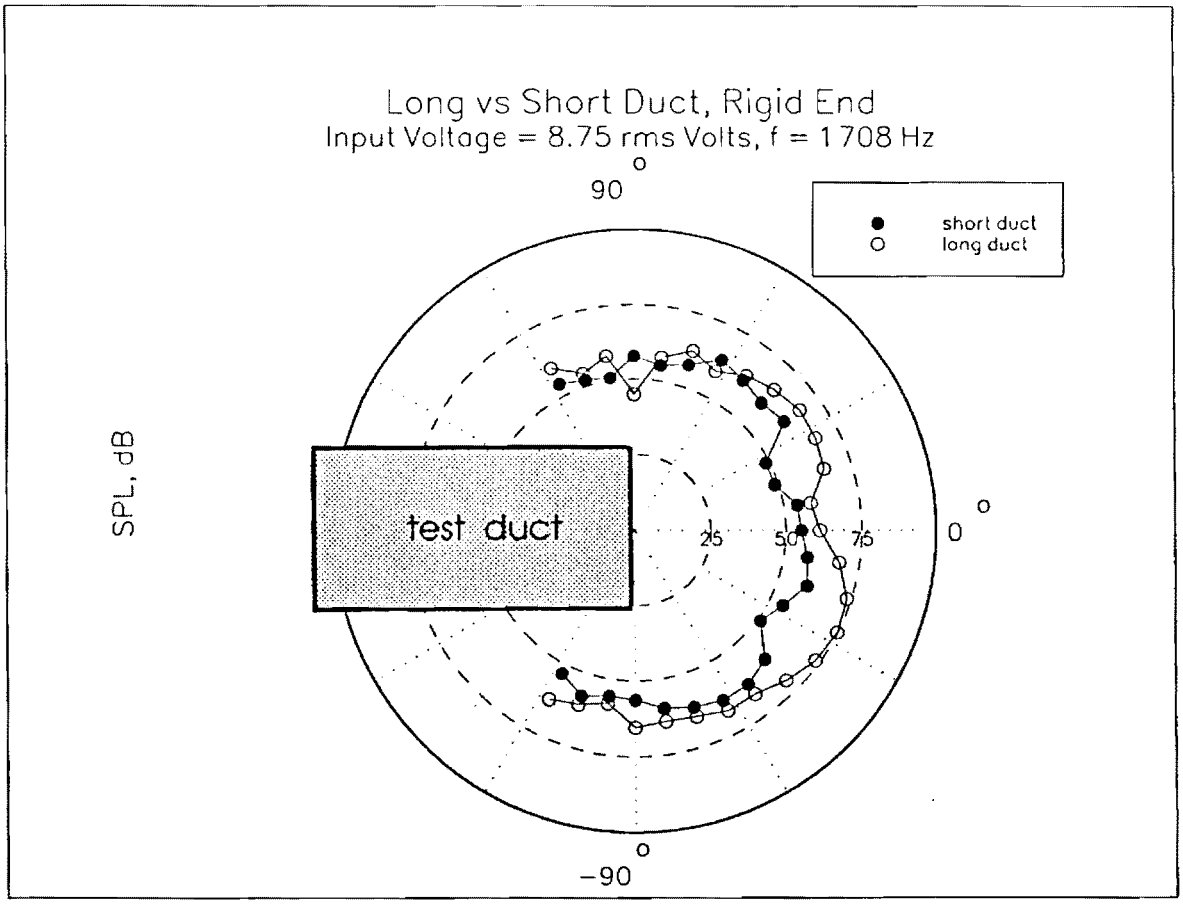

Figure 4.9 -- Effect of duct length on exterior sound pressure radiation. Excitation frequency = 1708 Hz.

Chapter 5 Numerical Analysis Using SYSNOISE

Because of the time and expense involved in designing and building experimental rigs, it is desirable to develop analytical or numerical tools for predicting the acoustic radiation generated by a vibrating structure such as the panel considered in this study. One such commercially available code is SYSNOISE, which utilizes the boundary element and finite element methods of analysis. In this study, SYSNOISE was used to model some of the experiments performed in order to assess its performance as a prediction tool for this application. A method of modelling the test duct and source was developed and utilized in this analysis. This method involves three basic steps: 1) modelling of the physical system (panel and duct), 2) specification of boundary conditions, and 3) specifying the points (locations) for which the acoustic response is to be calculated.

The boundary element solution method (BEM) was utilized for this study. This method is formulated by applying Green's theorem to the Helmholtz equation. Through Green's theorem, a three-dimensional problem with a volume integral is reduced to a two-dimensional surface integral, and it becomes necessary to discretize only the radiating surface rather than the radiating surface and surrounding medium [46]. All the analyses performed for this study were uncoupled, that is, the structural behavior of the panel and cylinder were assumed independent of the surrounding fluid. This assumption is justified when the density of the fluid is small compared to the density of the structure.

5.1 Modelling of Test Duct and Source

The short duct was modelled in I-DEAS and transferred to SYSNOISE. This model includes nodes representing the source panel. The maximum element size

imposed by SYSNOISE (a maximum of six elements per wavelength) dictates the mesh size of the I-DEAS input file. Consequently, because of limitations in computing capability, only a portion of the pipe was modelled, and symmetry conditions were utilized to keep the model to a manageable (and solvable) size. With this limitation in computing capability, it was not possible to model the long duct, so only the short duct was considered in the SYSNOISE analysis.

Instead of modelling the pipe and the source panel separately, the panel was modelled as an integral part of the pipe. That is, the pipe mesh was constructed so that the nodes in the area where the panel is mounted are of the same geometry as the panel's finite element mesh. Velocity data extracted from the source panel finite element model could then be directly transferred to SYSNOISE.

The short pipe was modelled using one symmetry plane. The entire 12" (0.3048 m) of length and 180° of circumference was modeled, including a mesh representing the downstream exit plane of the duct. The symmetry plane was used to model the additional 180° of circumference. The exit plane was included in the model so that the impedance boundary conditions for the downstream end could be specified. In this manner, the rigid end cap used in the experiments could be included in the model. The model size is 684 nodes and 643 elements and requires about six hours of VAX run time. The I-DEAS model used as SYSNOISE input is shown in Figure 5.1

5.2 Determination of Boundary Conditions

For this analysis, the appropriate boundary conditions include velocity and specific acoustic impedance. The amplitude of the velocity at each node corresponding to a panel node was obtained from the I-DEAS forced response analysis using an 8.75 V_{rms} excitation. Because SYSNOISE requires the normal component of velocity as

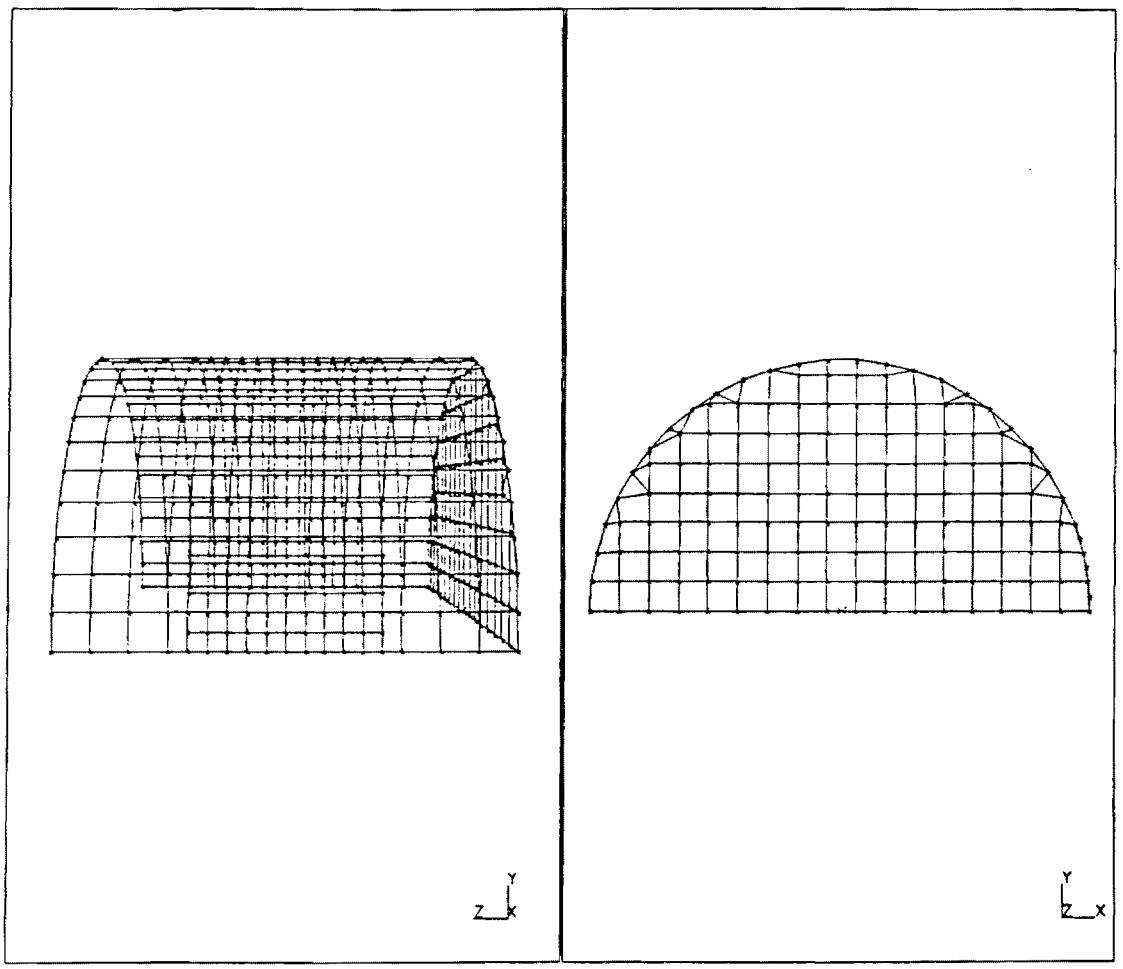

Figure 5.1 -- Finite element mesh representing the short duct used in the experiments.

input data, it is necessary to extract this information from the I-DEAS source model, using the results of the forced response analysis. One method of doing this for a curved structure such as the panel is to create a local coordinate system for each node, and orient it such that one axis is normal to the panel surface at that node. The velocity data can then be extracted in terms of the local coordinate system. This was the approach taken in this study.

For all nodes on the cylinder surface other than those corresponding to the panel, the velocity boundary condition was assumed zero (the default value). This implies two things -- 1) the cylinder is a perfectly reflecting surface, and 2) the cylinder itself makes no contribution to the acoustic output of the system. These implications will be discussed further in the next section.

5.3 Comparison to Experimental Results

Selected experiments were modelled in SYSNOISE in order to assess its performance as a predictor of acoustic radiation for this application. The displacement values calculated in the I-DEAS forced response analysis formed the basis of the SYSNOISE analysis, and the importance of obtaining a good FEM model of the source cannot be overemphasized. The particular experiments modelled in SYSNOISE included exterior measurements using the short duct with a rigid end cap. Both the overall sound pressure levels generated and the acoustic radiation patterns were compared with the analagous experimental cases. In addition, interior mapping of the short duct with a rigid end cap was modelled, although this was not done experimentally. The results of these SYSNOISE analyses are presented in Table 5.1. The analyses represent the acoustic response to the panel vibrating at 1708 Hz with a 8.75 V_{rms} input voltage.

Table 5.1 -- Results of SYSNOISE analyses of the interior pressure levels (f = 1708 Hz for borh cases). Results are in dB.

Case	duct	downstream termination	response plane	maximum SPL	minimum SPL	average SPL
1	short	rigid	z=0"	92	66	79
2	short	rigid	z=6"	79	70	77

One of the experimental results noted in Section 4.2.2 is that the average sound pressure level inside the duct decays with axial distance from the source. This effect was also observed in the SYSNOISE analyses. For the short pipe, for example, the average sound pressure level decays from 79 to 77 dB over a distance of 6" (0..1524 m). In Section 4.2.2, it was noted that this decay in sound pressure level could be attributed to three factors: 1) absorption of sound energy into the duct walls, 2) losses in the fluid medium, and 3) the diminishing influence of near-field effects with distance. However, because the SYSNOISE analysis models the duct walls as completely rigid, absorption of sound energy is not a factor in the SYSNOISE analysis. Therefore, the 2 dB drop in average sound pressure level can be attributed to a combination of losses in the fluid medium and the diminishing effect of the evanescent, or decaying, modes.

Contour plots of the interior results for the case of a rigid downstream terminations are given in Figure 5.2. This plot represents results at the duct inlet plane.

Also of interest is the acoustic radiation from the inlet end of the duct. This was calculated for several points located 1.6 meters around the inlet plane of the pipe, similar to the experiments in which a microphone, located on a boom 1.6 meters from the inlet plane, was rotated about the inlet face. These SYSNOISE calculations were done for two planes, as were the experiments: 1) the 0° plane, for which the axial center line of the panel lies in the same plane as the response points, and 2) the 90° plane, or the plane normal to the plane formed by two points on the panel axial centerline and any point on the duct axis. These results are plotted in Figures 5.3 and 5.4, and both sets of results are for the rigid termination case. For the 90° plane, the results are symmetric about the z-axis, while the 0° plane results show an asymmetric radiation pattern. In Figure 5.5, superimposed on the 0° plane plot are the experimental results for the same case (0° plane, rigid end, short pipe, f = 1708 Hz). Two features are noteworthy: 1) the

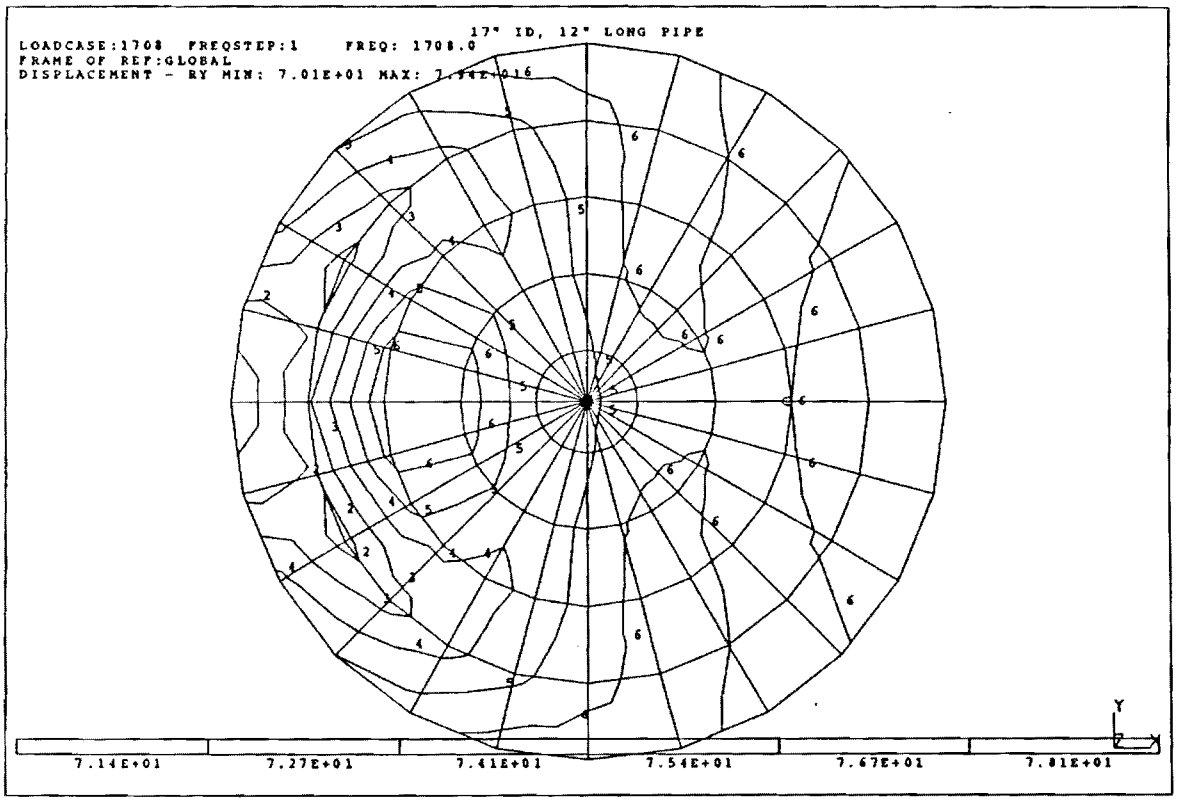

Figure 5.2 -- SYSNOISE interior results for the short pipe with a rigid downstream termination.

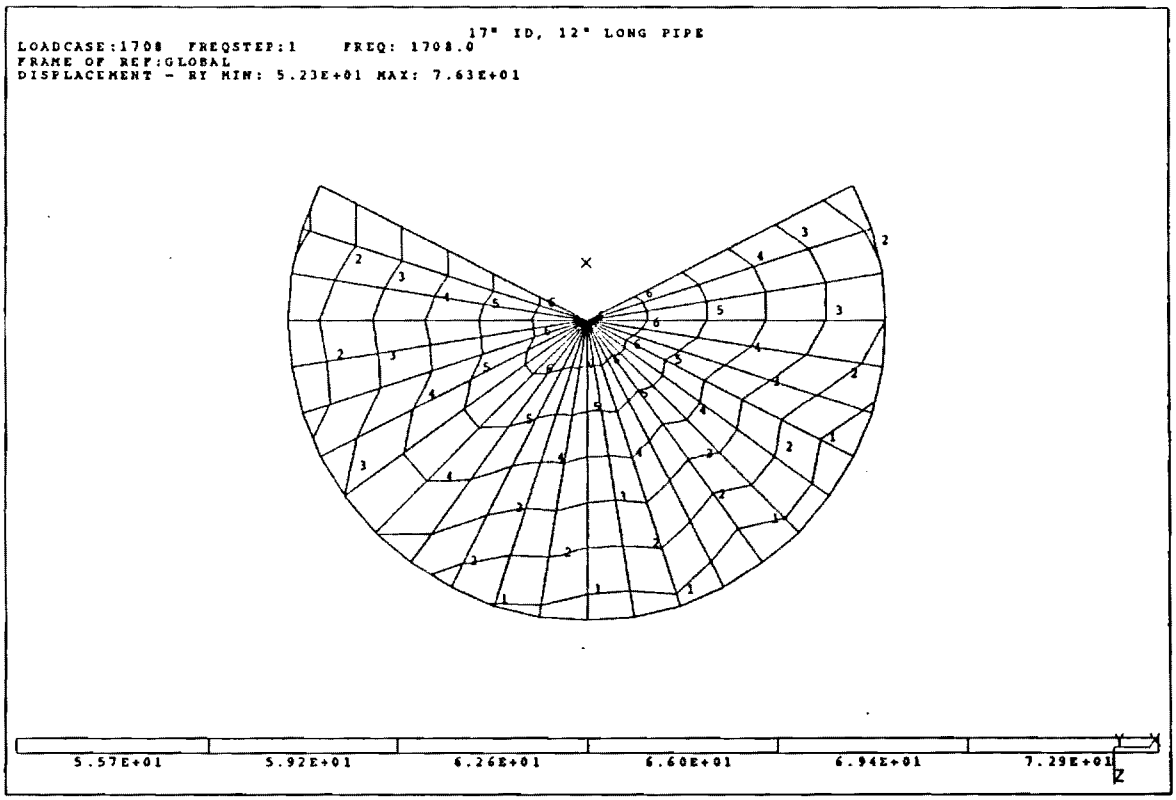

Figure 5.3 -- SYSNOISE exterior sound level results for the short duct with a rigid downstream termination (plane position = 0°).

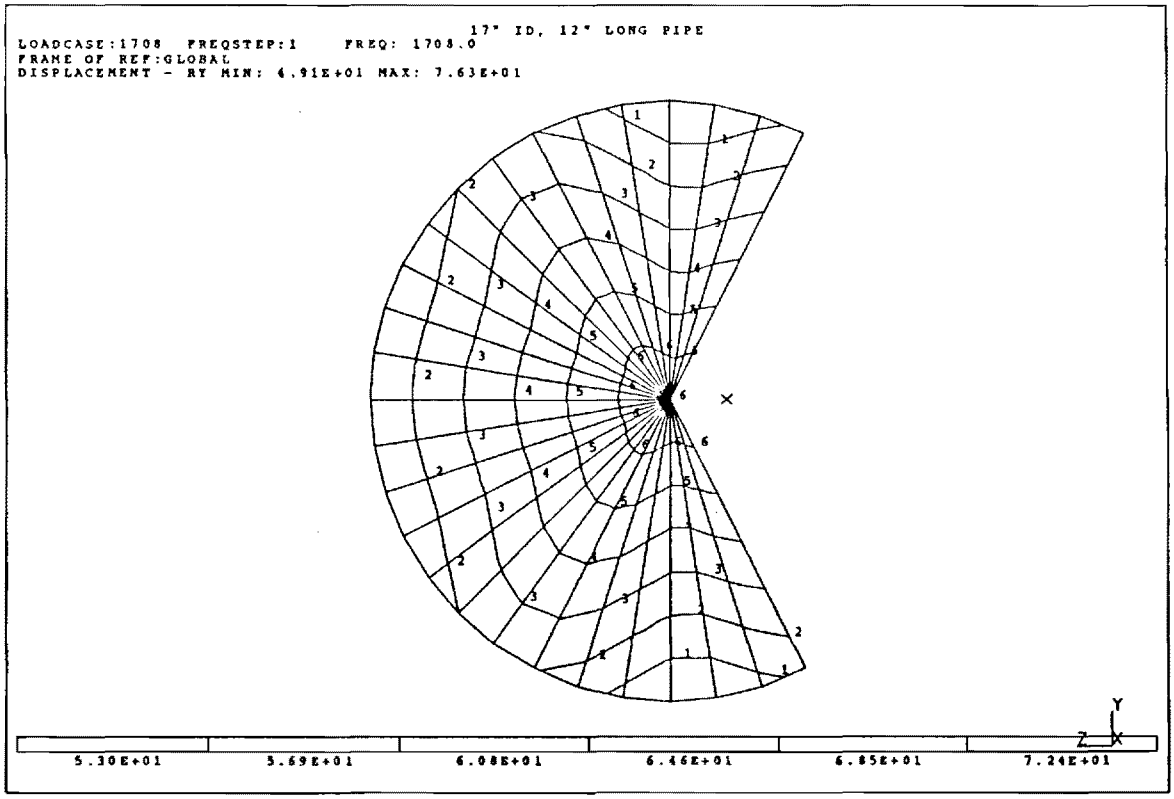

Figure 5.4 -- SYSNOISE exterior sound level results for the short duct with a rigid downstream termination (plane position = 90°).

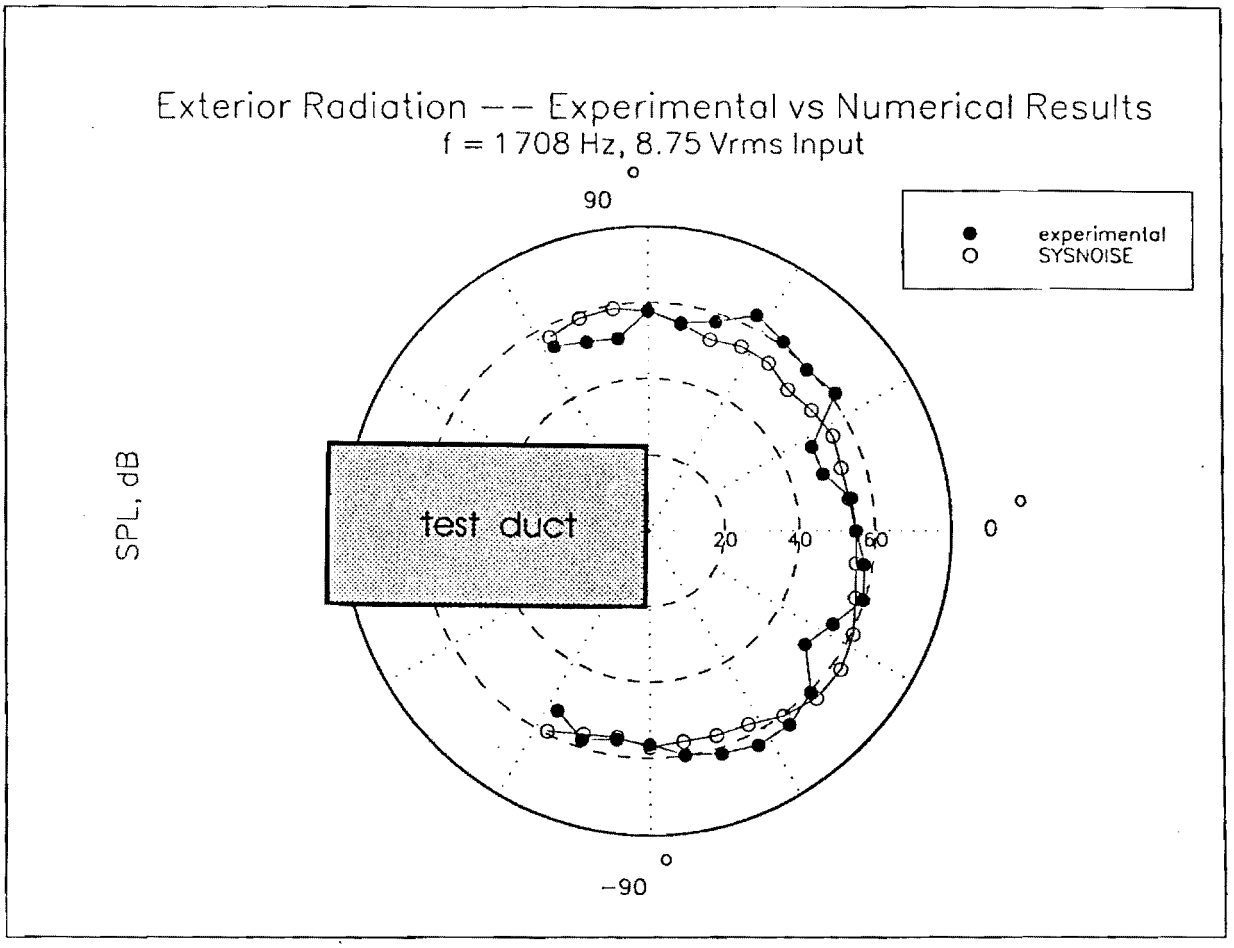

Figure 5.5 -- Comparison of experimental and SYSNOISE results for the short duct with a rigid downstream termination.

directivity pattern is somewhat similar, as the maximum level occurs around 30° to 60°, and 2) the average magnitude differs by only 0.5 dB. From this second point, it can be inferred that the acoustic output of the pipe structure itself, measured in the far field, is indeed negligible, as was assumed in the SYSNOISE modelling, and makes no substantial contribution to the overall acoustic output of the system for the short pipe case.

In order to characterize the contribution from the cylinder walls, it is necessary to determine the velocity at each node in terms of magnitude and phase and add this information to the SYSNOISE model. This was not done for this study. However, it may be expected that the long pipe, with a surface area of 2030 $in.^2$, would make a much greater contribution to overall sound level for a given cylinder velocity distribution than would the short pipe, with a surface area of 673 $in.^2$., since total acoustic power can be expressed as the acoustic intensity integrated over surface area.

5.4 Design Modifications Using SYSNOISE

Once the appropriate modelling techniques have been determined, it is possible to alter the panel design and use SYSNOISE to predict the acoustic response. Such design changes could include changes in panel material, geometry, actuator size or location, or input voltage. In each case, the appropriate finite element model is developed, velocity data are obtained, scaled as needed, and transferred to SYSNOISE, and the model is then solved. Specifically, the steps needed to execute a design evaluation in SYSNOISE are as follows.

1. Develop an appropriate finite element model of the sound source. Solve for displacement and convert to velocity (see section 3.2.5).

2. Develop an appropriate finite element model of the inlet duct. Include nodes that physically correspond to the nodes of the sound source model.

3. Specify the boundary conditions for the inlet duct mode. Such boundary conditions can include pressure, velocity, and impedance requirements.

4. Using the RESPONSE command in SYSNOISE, calculate the acoustic response at a particular frequency or range of frequencies for each node in the inlet duct mode.

5. Define the point or points for which the acoustic response is to be calculated for post-processing. This step is the equivalent of selecting the microphone locations in an experiment.

6. Using the POSTPROCESS command, compute the acoustic pressure, velocity, and intensity at these points.

7. Convert the results to a format suitable for graphical postprocessing (e.g.,I-DEAS), and extract the results.

Chapter 6 Summary, Conclusions, and Recommendations

6.1 Summary

In this work, a compact sound source was developed and tested experimentally. This source was designed as an acoustic control source for an active control noise cancellation system and was developed specifically for the reduction of single-frequency noise components such as those typically found in the inlet ducts of aircraft engines. The source was fitted in a cylindrical duct representative of an aircraft engine inlet, and the source's dynamic properties and acoustic output were experimentally investigated. In addition, a numerical boundary element code was employed to model the source-duct system.

The source, consisting of a curved aluminum panel and two piezoceramic actuators, was designed to have a fundamental resonant frequency near 2000 Hz, as this is the lower limit of the fundamental blade passage frequency range typically encountered in existing turbofan engines. The source has a radius of curvature corresponding to that of the test duct. Flat piezoceramic actuators were used, and were applied to the panel in such a manner as to force them to conform to the panel's curvature. Various methods of applying the actuators were attempted, with varying degress of success. An assembly process was developed which makes it possible to obtain a satisfactory bond without fracturing the ceramic. Still, yield is relatively poor, and further work is needed in this area.

A finite element software package, SDRC I-DEAS, was used to design the sound source. However, it was found that experimental data was needed to adequately

represent the boundary conditions on the model. With the addition of spring elements representing the interface between the source and test cylinder, a model was developed which yields acceptable agreement with experimental data in terms of natural frequency, mode shape, and displacement amplitude.

It was found that the mass loading of the piezoceramic actuator pair does alter the natural frequencies of the panel by a significant amount. This is an important result, as piezoceramic actuator mass loading is usually assumed negligible [34]. For this reason, the model included the piezoactuator pair's mass, modelled as distributed lumped mass elements. It was also found that the mass of the accelerometer used to measure velocity had only a small (7% maximum) effect on the resonant frequency, but had a significant effect on the amplitude of the displacement. This effect must be considered when comparing experimental data with FEM results. The effect was quantified over a range of frequencies and the experimental velocity data were modified accordingly.

The induced loading of the panel by the actuator was calculated using a two-dimensional analytical model derived from plate theory. For the case of one actuator driven alone, the model shows remarkably good agreement with experimental measurement, despite the fact that the panel is a portion of a cylinder, not a flat plate. Cases involving two actuators driven together were not considered in the FEM analysis.

Modal analysis of the panel shows that the (1,1) mode is clearly excited over a frequency range of 1400-2000 Hz. This is a significant result, as it indicates that the panel can produce relatively high acoustic levels over a 600-Hz range. Acoustic measurement does show some variation in output over this range, as expected, but generally confirms that the greatest acoustic output occurs over this range. This result is important in terms of driving the source at varying frequency to correspond to varying engine operating speed.

Testing of the mode of actuator excitation and its effect on acoustic output revealed that the maximum acoustic output is achieved by driving the outside actuator alone. This is an important result, as it directly contradicts the flat plate analytical models, which predict that driving the pair 180° out of phase maximizes acoustic output. Moreover, it was found that the outside and inside piezoactuators produce significantly different levels of acoustic output. This is again a contradiction of the flat plate analytical models. These results are believed to stem from the panel's curvature coupling the in-plane to the out-of-plane motion. For further study, it may be necessary to develop an analytical model from shell theory.

Testing of the source's acoustic output as a function of excitation voltage shows that the response varies linearly throughout most of the recommended voltage range. The response was observed to fall off somewhat above 105 V_{rms}. Still, it is possible to scale results of a test or an analysis done at a particular voltage level to infer the response at a different voltage level, based on the experimental data.

The sound source was fitted in a length of PVC pipe representative of an aircraft engine inlet, and the acoustic field was mapped both inside and outside the test duct in an anechoic chamber. The parameters investigated include excitation frequency, excitation voltage, duct length, termination of the downstream duct exit (anechoic vs rigid), and distance from the source. It was found that maximum acoustic output is achieved when the panel is driven at its fundamental frequency, as expected. However, it was also found that equally high acoustic levels can be generated by driving the panel at an acoustic resonant frequency near the structural resonance. Thus, in designing a sound source of this type, it may be advantageous to consider the resonant frequencies of the cylindrical cavity as well as the panel's structural resonance. Interior sound pressure levels as high as 102 dB at 8.75 V_{rms} were measured. This corresponds to 125 dB at maximum

voltage input (450 V_{p-p}). This measurement included a downstream anechoic termination.

It was found that terminating the downstream pipe exit with a rigid obstruction increases the acoustic measurements by about 6 dB compared to terminating the downstream end anechoically, increasing the maximum interior level to 131 dB. This is an important result, because the rigid case is much more representative of the actual aircraft engine inlet duct, which is terminated by the fan blading. Sound pressure level can be further increased by increasing the number of sources installed in the duct. The exact amount of acoustic pressure needed to cancel the primary field will depend upon the specific application. However, generating over 130 dB with only one panel is a very encouraging result.

It was found that duct length had little effect on acoustic pressure for the case of excitation of an acoustic resonance. However, for excitation at the panel's structural fundamental frequency, a significant decrease (10 dB) in acoustic output was noted for the short duct. This is thought to be caused by the panel's proximity to the inlet opening altering the acoustic impedance that the panel "sees", thereby decreasing its acoustic output. This effect was not observed in the non-resonance case, possibly because duct cutoff frequencies are independent of duct length, and so the same excitation of acoustic modes occurs regardless of duct length. These results must be assessed in terms of a specific application, as duct lengths can vary greatly with engine design. However, it may be concluded that it is desirable to locate the sources as close to the fan as possible to increase the acoustic levels generated by the source. This is desirable, too, from the standpoint of control [25].

Finally, it was desired to develop an analytical tool for predicting acoustic radiation from a vibrating structure such as the panel so that this tool could be used in

further design work. A commercial software package for predicting acoustic radiation, SYSNOISE, was used for this purpose. The requirements for modelling the panel-duct system were developed and implemented. The finite element model used to design the sound source plays a crucial role in modelling the source-duct system, as the velocity data required as input by SYSNOISE is extracted from the I-DEAS model. Alternatively, velocity data could be obtained experimentally, but it is much more desirable to have an analytical means of obtaining the velocity data.

For the short duct, the SYSNOISE model was found to give generally good predictions of exterior radiation patterns, and remarkably good agreement of exterior sound pressure levels. The size of the SYSNOISE model does present problems in terms of the computing capability required to solve larger models. Because of a limitation in computational capability, it was necessary to utilize symmetry in modelling the short pipe. It was also necessary to restrict the analysis to low frequencies, and it was not possible to adequately model the long pipe. However, this problem with model size of the long pipe should not adversely affect further work, as engine inlets are typically much shorter than 36" (0.9144 m). The JT15D, for example, has a 21" (0.5344 m) inlet. Model size will become more of a concern as the frequencies studied increase and the wavelengths and maximum element size decrease. The problem is not in the model size itself but rather in the computational time and storage requirements for processing large models. Thus, these restrictions in modelling capability are due to limitations in the computer system used rather than the software itself.

The design methodology developed in this study is briefly summarized as follows.

1. Select the panel material.

2. Determine the panel inner radius, which should correspond to the duct inner radius at the location where the panel will be installed.
3. Using analytical solutions as a guide, select dimensions which will yield the fundamental frequency required for the particular application and will meet requirements such as actuator size. The actual fundamental frequency of the panel will be slightly higher than the analytical solution for simply supported boundary conditions, yet lower than the analytical solution for clamped boundary conditions.
4. Model the geometry using finite element method software, including actuator mass, and represent the actual boundary conditions with spring elements. Experimental data may be needed to properly characterize the boundary conditions.
5. Iterate as needed, changing panel length, width, or thickness as needed to obtain the desired fundamental frequency, f_{11}. In general, f_{11} increases with increasing panel thickness and decreases with increasing panel length or width.
6. Calculate the actuator loads for a given voltage, and apply these loads to those nodes lying beneath the actuator edges.
7. Calculate the FEM forced response to the actuator loads, extract displacement data, and convert to velocity. This velocity data serves as input to the SYSNOISE model.

The analysis done in this study can be summarized as follows.

1. Develop and validate the finite element model of the source, using experimental data to properly characterize the boundary conditions.
2. Extract displacement data from the source model and convert to velocity data.

3. Model the inlet duct and sound source in I-DEAS and transfer the model to SYSNOISE.
4. Apply the appropriate boundary conditions to the SYSNOISE model and solve for acoustic pressure.

This process is shown schematically in Figure 6.1.

6.2 Conclusions

The conclusions of this study can be summarized as follows.

1. Flat piezoceramics can be effectively used to excite a curved panel.
2. Mass loading effects of the piezoactuators are not negligible for this study.
3. Mass loading of the accelerometer has a significant effect on panel displacement but not on resonant frequency.
4. An analytical actuator model based on plate theory provided results that compared well to experimental results, for the case of the outside actuator.
5. Acoustic test results indicate that the outside actuator provides significantly more acoustic output than the other excitation modes. This does not agree with theory.
6. Acoustic response varies linearly with excitation voltage up to about 105 V_{rms}.
7. The (1,1) mode is clearly excited over a 600-Hz range. Acoustic output is maximized at the (1,1) resonant frequency, but equally high levels can be excited at frequencies corresponding to acoustic resonances.
8. The maximum average interior sound pressure level obtained exceeded 130 dB at the panel's fundamental frequency using one source, indicating that sources of this type are capable of generating very high acoustic levels.
9. A rigid downstream termination increases the sound pressure level by 6 dB over the anechoic wedge case.

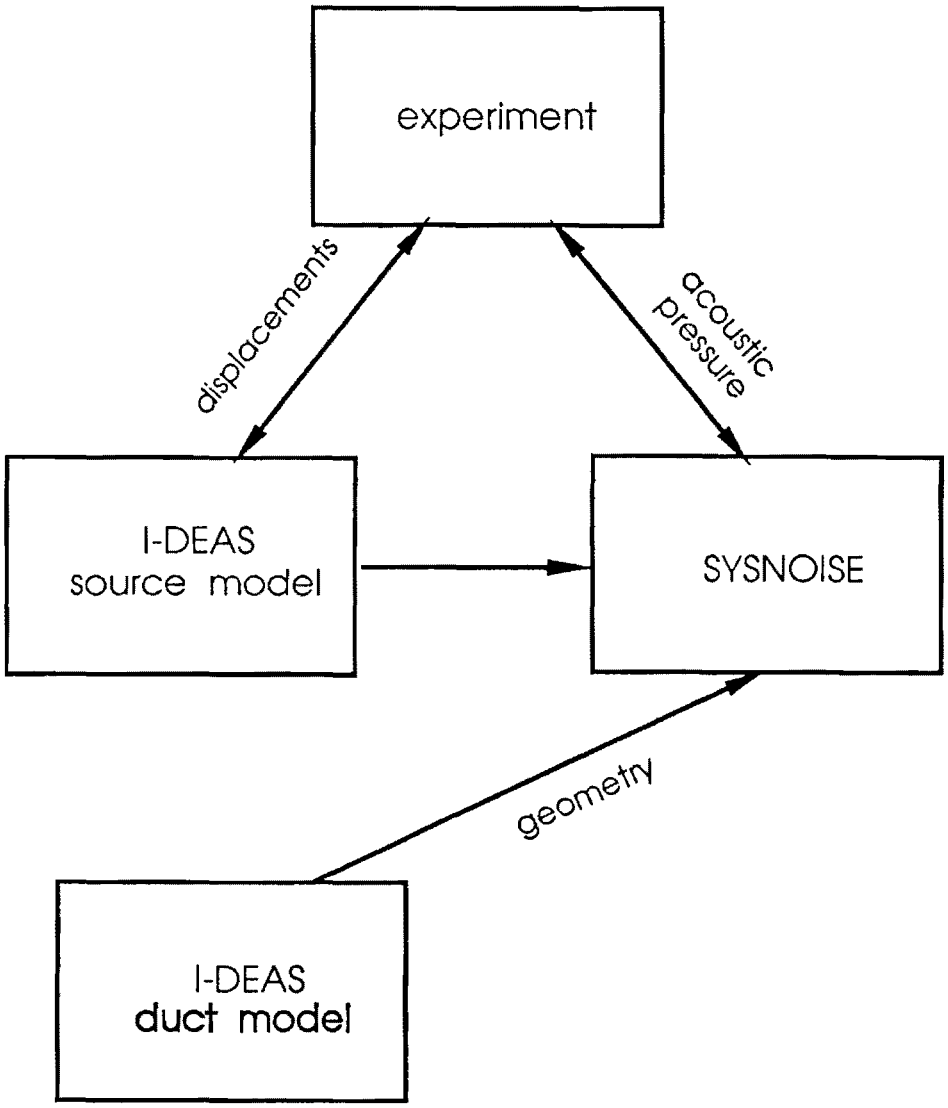

Figure 6.1 -- Schematic of analysis methodology.

10. Duct length has little effect on sound level for off-resonance excitation, but has a significant effect (9 dB) on the structural resonance excitation case.
11. The SYSNOISE model results show very good agreement with experimental results for the short duct case (0.5 dB error).

6.3 Recommendations

Recommendations for future work are as follows.

1. Because of the difficulty in attaching the flat piezoactuators to a curved surface, an alternative configuration should be considered, including 1) using curved piezoceramics, or 2) machining flats on the panel surface.
2. For more detailed analysis, an actuator model derived from curved panel theory would be useful. Such a model would then account for the in-plane and out-of-plane coupling effects observed in this study and could be used to determine, for example, the optimal actuator thickness.
3. For longer ducts where the cylinder walls can be expected to contribute to the sound levels generated, the finite element analysis must be expanded to account for panel-cylinder interaction and cylinder contribution to the acoustic field generated. Alternatively, the cylinder velocity data can be determined experimentally, but this would be a very lengthy procedure, as the mode shape is of very high order at the frequency range of interest.
4. For further work, it would be advantageous to develop analytical models for estimating the effective stiffness of the boundary conditions on the panel. This model could then be used to determine the appropriate spring stiffnesses in the finite element model and eliminate the need to obtain this information experimentally.

5. Since blade passage frequency typically varies significantly with RPM over the engine operating range, it would be advantageous to adaptively change the panel's fundamental frequency to correspond to a range of engine operating speeds. Further work should include development of this capability. One possibility is to apply a DC load to the actuator, thereby changing the stiffness and thus the dynamic characteristics of the panel.

Chapter 7 References

1. Cumpsty, N.A., Aerothermodynamics of Aircraft Engine Components, Coates, G.C., editor, AIAA Publishing, 1985.

2. Tyler, J.M. and Sofrin, T.G. "Axial Flow Compressor Noise Studies," *SAE Transactions*, Vol. 70, pp. 309-332, 1962.

3. Mugridge, B.D. and Morfey, C.L. "Sources of Noise in Axial Flow Fans," *Journal of the Acoustical Society of America*, Vol. 5, No. 5, Pt. I, 1975.

4. Cumpsty, N.A., "A Critical Review of Turbofan Noise," *Journal of Fluids Engineering, Transactions of the ASME*, Vol. 99, Ser. I. No. 2, pp.278-293, 1977.

5. Chamberlain, G., "Good Cancels Bad in Auto Noise", *Design News*, pp. 128-132, October 1991.

6. Lefebvre, S., "Active Control of Interior Noise Using Piezoceramic Actuators in a Large-Scale Composite Fuselage Model," M.S. Thesis, Virginia Polytechnic Institute and State University, 1991.

7. Thomas, R.H., Burdisso, R.A., Fuller, C.R., and O'Brien, W.F., "Preliminary Experiments on Active Control of Fan Noise from a JT15D Turbofan Engine," Letter to the Editor, *Journal of Sound and Vibration*, submitted April 1992.

8. Thomas, R.H., Burdisso, R.A., Fuller, C.R., and O'Brien, W.F., "Experiments on the Active Control of Inlet Fan Noise from a JT15D Engine,", paper presented at the 122nd meeting of the Acoustical Society of America, Nov. 4-8 1991, Houston, Texas.

9. Morfey, C.L., "Rotating Pressure Patterns in Ducts: Their Generation and Transmission," *Journal of Sound and Vibration*, Vol. 1, pp. 60-87, 1964.

10. Sofrin, T.G. and McCann, J.C., "Pratt and Whitney Experience in Compressor Noise Reduction," paper presented at the 72nd meeting of the Acoustical Society of America, 1966.

11. Nayfeh, A.H., Kaiser, J,E., and Telionis, D.P., "The Acoustics of Aircraft Engine Duct Systems," *AIAA Journal*, Vol. 13, pp. 130-153, February 1975.

12. Morfey, C.L., "The Acoustics of Axial Flow Machines," *Journal of Sound and Vibration*, Vol. 22, No. 4, pp. 445-466, 1972.

13. Lansing, D.L., "Exact Solution for Radiation of Sound from a Semi-Infinite Circular Duct with Application to Fan and Compressor Noise," NASA SP-228, 1970.

14. Lowson, M.V., "Theoretical Analysis of Compressor Noise," *Journal of the Acoustical Society of America*, Vol. 47, No. 1, pp. 371-385, 1970.

15. Candel, S., "Acoustic Radiation from the End of a Two-Dimensional Duct, Effects of Uniform Flow and Duct Lining," *Journal of Sound and Vibration*, Vol. 28, No. 1, pp. 1-13, 1973.

16. Metzger, F.B., "Strategies for Aircraft Interior Noise Reduction in Existing and Future Propeller Aircraft,", SAE Technical Paper No. 810560, 1981.

17. Sofrin, T.G. and Pickett, G.F., "Multiple Pure Tone Noise Generated by Fane at Supersonic Tip speeds,: International Symposium on the Fluid Mechanics and Design of Turbomachinery, NASA SP-304, Pt. II, 1970.

18. Morfey, C.L., and Fisher, M.J., "Shock-Wve Radiation from a Supersonic Ducted Rotor," *Aeronautical Journal*, Vol. 74, pp. 579-585, 1970.

19. Smith, M.J.T. and House, M.E., "Internally Generated Noise From Gas Turbine Engines: Measurement and Prediction," *Journal of Engineering and Power, Transactions of the ASME*, Series A, Vol. 89, pp.177-190, 1967.

20. Bushell, "A Survey of Low Velocity and Axial Jet Noise with Application to Prediction," *Journal of Sound and Vibration*, Vol. 17, No. 2, pp. 271-282, 1971.

21. Kazi, S. and Okazaki, T., "Propagation of Sound Waves Through a Blade Row," *Journal of Sound and Vibration*, Vol. 11, No. 3, pp. 355-375, 1970."

22. Facey, J.R., "Return of the Turboprops," *Aerospace America*, October 1988.

23 Whitlow, Jr., J.B., and Sievers, G.K., "Building the Foundation," *Aerospace America*, October 1988.

24. Groeneweg, J., Shepherd, K., and Henderson, W., "Toward the Future," *Aerospace America*, October 1988.

25. Elliott, S.J. and Nelson, P.A., "The Active Control of Sound," *Electronics and Communications Engineering Journal*, pp. 127-136, August, 1990.

26. Olson, H.F., and May, E.G., "Electronic Sound Absorber," *Journal of the Acoustical Society of America*, Vol. 25, No. 6, pp. 1130-1136, 1953.

27. Olson, H.F., "Electronic Control of Noise, Vibration, and Reverberation," Journal of the Acoustical Society of America," Vol. 28, No. 5, pp. 966-972, 1956.

28. Conover, W.B., "Fighting Noise with Noise," *Noise Control*, Vol. 2, No. 1, pp. 78-92, 1956.

29. Frampton, K.D., "Active Control of Acoustic Radiation Due To Discontinuities on Thin Beams," M.S. Thesis, Virginia Polytechnic Institute and State University, April 1991.

30. Trinder, C.J. and Nelson, P.A., "Active Noise Control in Finite-Length Ducts," *Journal of Sound and Vibration*, Vol. 89, pp. 95-105, 1983.

31. Swinbanks, M.A., "The Active Control of Sound Propagation in Long Ducts," *Journal of Sound and Vibration*, Vol. 27, pp. 411-436, 1973.

32. Curtis, A.R.D., Nelson, P.A., Elliott, S.J., and Bullmore, A.J., "Active Suppression of Acoustic Resonance," *Journal of the Acoustical Society of America*, Vol. 81, pp. 624-6731, 1987.

33. Snyder, S.D., and Hansen, C.H., "Active Noise Control in Ducts: Some Physical Insights," *Journal of the Acoustical Society of America*, Vol. 86, No. 1, July 1989.

34. Fleming, M.R., "An Experimental Investigation of the Harmonic Excitation of Simply Supported Plates With Multiple Surface-Bonded Piezoceramic Actuators," M.S. Thesis, Virginia Polytechnic Institute and State University, November 1990.

35. Crawley, E.F., and de Luis, J., "Use of Piezoelectric Actuators as Elements of Intelligent Structures," *AIAA Journal*, Vol. 25, No. 10, pp. 1373-1385.

36. Lazarus, K.B., and Crawley, E.F.,"Induced Strain Actuation of Composite Plates," GTL Report No. 197, Massachusetts Institute of Technology, Cambridge, Massachusetts, 1989.

37. Wang, B. and Rogers, C.A., "Modelling of Finite-Length Spatially Distributed Induced Strain Actuators for Laminate Beams and Plates", *Proceedings of the*

AIAA/ASME/ASCE/AHS/ACS 32nd Structures, Structural Dynamics, and Materials Conference, Maryland, pp. 1511-1520.

38. Dimitriadis, E.K., Fuller, C.R., and Rogers, C.A., "Piezoelectric Actuators for Distributed Vibration Excitation of Thin Plates," *ASME Journal of Vibration and Acoustics,* Vol. 113, pp.100-107, January, 1991.

39. Kim, S.J., and Jones, J.D., "Optimization of Piezo-Actuator/Substructure Coupling for Active Noise and Vibation Control," paper presented at *Recent Advances in Active Control of Sound and Vibtation* conference, April 15-17., 1991, Blacksburg, Virginia.

40. Leissa, A.W., Vibration of Shells, NASA SP-288, 1973.

41. S.D.R.C., I-DEAS User's Guide, Structural Dynamics Research Corporation, 1988.

42. Lazan, B.J., Damping of Materials and Members in Structural Mechanics, Pergimon Press, 1968.

43. Instruction Manual, Brüel & Kjær Dual Channel Signal Analyzer Type 2032, August, 1983.

44. Blevins, R.D., Formulas for Natural Frequency and Mode Shape, Robert E. Krieger Publishing, 1979.

45. Morse, P.M., and Ingard, K.U., Theoretical Acoustics, McGraw-Hill, 1968.

46. Fyfe, K.R., Coyette, J.G., and van Vooren, P.A., "Acoustic and Elasto-Acoustic Analysis Using Finite Element and Boundary Element Methods", *Sound and Vibration,* December, 1991, pp. 16-22.

47. Pearsons, K.S. and Bennett, R., "Handbook of Noise Ratings," NASA CR-2376, 1974.

48. Park, S., Liang, C., and Rogers, C.A., "Vibration Analysis of Cylindrical Structures with Piezoelectric Actuators," research report submitted to Westinghouse, February 1991.

Appendix A -- Wave Propagation for an Ideal Fluid at Rest in a Cylindrical Duct

For a rigid-walled circular duct with no mean flow, the homogeneous wave equation can be written as

$$\frac{\partial^2 p}{\partial r^2}+\frac{1}{r}\frac{\partial p}{\partial r}+\frac{1}{r^2}\frac{\partial^2 p}{\partial \theta^2}+\frac{\partial^2 p}{\partial z^2}-\frac{1}{c^2}\frac{\partial^2 p}{\partial t^2}=0 \qquad \text{(A1)}$$

The pressure, $p = p(r,\theta,x,t)$ is found as a solution to this equation, subject to the following boundary conditions:

1) p is a continuous function.

2) $\frac{\partial p}{\partial r}=0$ at $r=r_0$.

3) At one end of the cylinder, the pressure at the plane normal to the cylinder axis is specified as some function of r, satisfying conditions 1) and 2) and is a periodic function of time.

Equation A1 can be solved by separation of variables, and the pressure fluctuation, p, can be written as

$$p = \Theta(\theta)\, R(r)\, X(x)\, T(t)\,, \qquad \text{(A2)}$$

where each function acts only on the variable shown. These four functions are defined as follows.

1) $$\Theta(\theta) = \cos(m\theta + \phi_m), \qquad \text{(A3)}$$

where m is any integer including zero and ϕ_m is the phase of the mth mode

2) $$T(t) = \cos(\omega t + \alpha), \qquad \text{(A4)}$$

3) $$R(r) = J_m(k_{m\mu} r) + Q_{m\mu} Y_m(k_{m\mu} r) \qquad \text{(A5)}$$

where J_m and Y_m are Bessel functions of the first and second kind of order m, respectively, and $k_{m\mu}$ and $Q_{m\mu}$ are eigenvalues for the particular mode and hub-tip ratio, α (when the hub-tip ratio is zero, $Q_{m\mu}$ is zero also), and

4) $$X(x) = \exp\left(-\sqrt{\left(k_{m\mu}^{\sigma}\right)^2 - \left(\frac{\omega}{c}\right)^2}\, x\right) \qquad \text{(A6)}$$

The solutions are formed from these four equations to satisfy boundary condition 3. These solutions are discussed in detail in Reference [1].

Appendix B -- Noise Rating Scales

Because acoustic signals vary greatly, sound levels are typically expressed in terms of a logarighmic scale. Sound levels, expressed in decibels (dB), may refer to either the local pressure flucturation, the acoustic power generated, or the acoustic intensity. In this study, sound level was expressed in terms of sound pressure level (SPL) as

$$SPL = 20 \log_{10}\left(\frac{p}{p_{ref}}\right) \tag{B1}$$

where p is the rms pressure, and p_{ref} is the reference rms pressure equal to 20 μPa.

In the study of aircraft noise, noise levels are often descibed in terms of perceived noise level (PNL), tone-corrected perceived noise level (PNLT), and effective perceived noise level (EPNL). The PNL rating scale is somewhat subjective in nature. It is intended to represent the sound level of the octave band of white noise, centered at 1 kHz, that a listener would judge "equally noisy" as the sound being rated. Calculation of PNL is complicated and is explained in detail in reference [47]. Because the PNL is a less reliable indicator in annoyance when the noise rated has a strong tone component, the tone-corrected perceived noise level rating (PNLT) was developed. This PNLT rating adds a correction factor to the PNL to account for the tone.

Because aircraft noise is often of short duration, the EPNL rating scale was developed to account for the duration of the noise as well as its sound level. The PNLT is calculated at 0.5-second intervals over the duration of the noise, and the EPNL is calculated as

$$EPNL = 10 \log \sum_{i=0}^{d} \log^{-1} \frac{PNLT_i}{10} - 13 \tag{B2}$$

where d = the number of 0.5-second intervals into which the noise duration is divided, and

$PNLT_i$ = the tone-corrected perceived noise level after the i^{th} time interval.

The effective perceived noise level is the rating scale referenced in FAR Part 36 and ICAO/FAA regulations.

Appendix C -- Piezoelectric Analytical Models

There are several analytical models in the literature describing the loading of a substructure induced by the actuation of surface-bonded piezoelectric transducers. The results of three of these models are considered in this study. Of these, the model of Dimitriadis, et al [38] was used to calculate the loads at a given voltage level. These loads were then used as input to a finite element model which calculated the structure's displacement. The Dimitriadis model is derived from plate theory, whereas several of the other published models are derived from beam theory. The other two models considered are those of Wang and Rogers [37], derived from laminate plate theory, and of Lazarus and Crawley [36], derived from beam theory. These models were considered because they have been used previously in studies involving cylinders [48].

The derivation of these three models is fully described in the literature. The results for the cases of pure bending (both actuators driven 180° out of phase), pure extension (both actuators driven in-phase), and combined bending and extension (one actuator driven alone) are summarized in Table C.1

Table C.1 -- Summary of analytical actuator load models

Case	Dimitriadis, et al	Wang and Rogers	Lazarus and Crawley
pure bending	$M_{eq} = C_0 \varepsilon b$	$M_{eq} = \frac{t_b^2 E_b}{6+\psi} b\varepsilon$	$M_{eq} = \frac{t_b^2 E_b}{6+\psi} b\varepsilon$
pure extension	$P_{eq} = \frac{2C_0 \varepsilon b}{t_b}$	$P_{eq} = \frac{2t_b E_b}{6+\psi} b\varepsilon$	$P_{eq} = \frac{2t_b E_b}{2+\psi} b\varepsilon$
combined bending and extension	$P_{eq} = \frac{C_0 \varepsilon b}{t_b}$ $M_{eq} = \frac{C_0 \varepsilon b}{2}$	$P_{eq} = \frac{t_b E_b}{6+\psi} b\varepsilon$ $M_{eq} = \frac{t_b^2 E_b}{2(6+\psi)} b\varepsilon$	$P_{eq} = \frac{t_b E_b}{1+\psi} b\varepsilon$ $M_{eq} = \frac{t_b^2 E_b}{2(1+\psi)} b\varepsilon$

where
$$C_0 = -E_p \frac{1+\upsilon_a}{1-\upsilon_b} \frac{C}{1+\upsilon_b-(1+\upsilon_a)C} \frac{2}{3} \frac{t_b^2}{4} \tag{C1}$$

$$C = -\frac{E_a}{E_b} \frac{1-\upsilon_b^2}{1-\upsilon_a^2} K \tag{C2}$$

$$K = \frac{3t_a \frac{t_b}{2}(t_b + t_a)}{2\left(\frac{t_b^3}{8} + t_a^3\right) + \frac{3t_b t_a^2}{2}} \tag{C3}$$

$$\psi = \frac{t_b E_b}{t_a E_a} \tag{C4}$$

and
$$\varepsilon = \frac{d_{31} V}{t_a} . \tag{C5}$$

Appendix D -- Calibration of Microphones

The 1/2" B&K microphone was calibrated using a single-tone (1000 Hz) calibrator rated at 94 dB sound pressure level. The corresponding rms pressure was calculated using the relationship

$$94\text{dB} = 20\log\left(\frac{p}{p_{ref}}\right) \tag{D1}$$

for which p is calculated as 1.0024 Pa.

The voltage level induced in the microphone was measured several times, and the average voltage reading was 44.53 mV. Thus, the ratio of 1.0024 Pa per 44.53 mV was established. This sensitivity factor was used to convert voltages measured by the microphone to pressure levels.

The five 1/4" Radio Shack microphones were all calibrated using the 1/2" B&K microphone as a reference. Each of the 1/4" microphones was positioned adjacent to the 1/2" microphone in turn, and the measured voltage level of each was recorded. The average ratio $R_{i,f}$ of the two voltage levels was computed for each microphone over a frequency range of 1000 - 2000 Hz in 100-Hz increments. The results are plotted in Figure D.1.

The sensitivity factor for the i^{th} microphone at a frequency of f Hz was then calculated in units of Pa/mV as

$$s_{i,f} = R_{i,f}\frac{1.0024\text{Pa}}{44.53\text{mV}} \tag{D2}$$

where $$R_{i,f} = \frac{V_{B\&K}}{V_i}$$

The equivalent pressure was then calculated by multiplying the measured voltage (in millivolts) by the sensitivity factor.

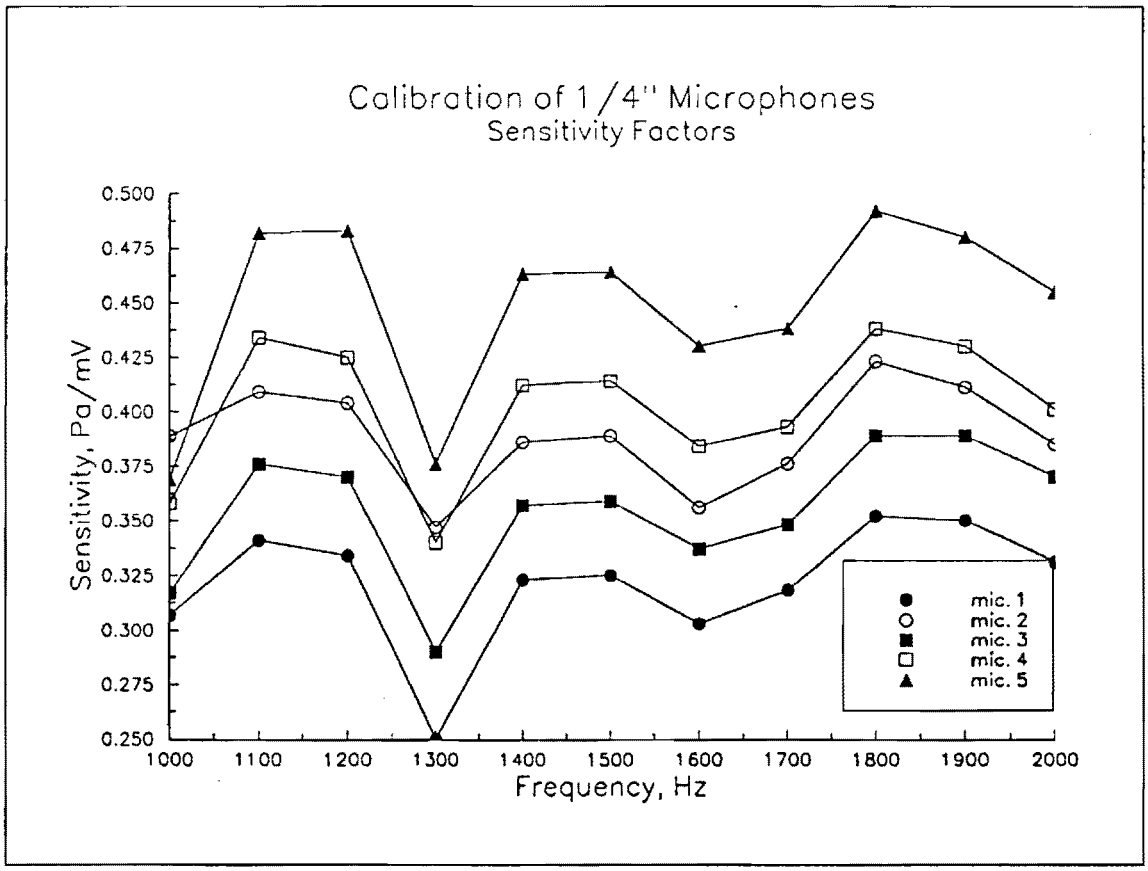

Figure C.1 -- Calibration curves for the 1/4" Radio Shack microphones.

Vita

The author was born in 1964 and grew up in Montross, Virginia, a small town in Virginia's Northern Neck. She enrolled at Virginia Tech in 1982, and while an undergraduate, worked as a co-op engineer for R.J. Reynolds Tobacco Company in Winston-Salem, North Carolina. She received her Bachelor of Science degree in Industrial Engineering and Operations Research in 1987. She then worked for Westinghouse Electric Corporation for three years prior to returning to Virginia Tech in 1990 for her M.S. degree in Mechanical Engineering. Upon completing her Master's Degree, the author will work for Michelin Tire Corporation in Greenville, South Carolina.